

# Rotating massive stars through the ages, with applications to WR stars, Pop III stars and Gamma Ray Bursts

André Maeder\* and Georges Meynet†

*Geneva Observatory, University of Geneva*

This article first reviews the basic physics of rotating stars and their evolution. We examine in particular the changes of the mechanical and thermal equilibrium of rotating stars. An important (predicted and observed) effect is that rotating stars are hotter at the poles and cooler at the equator. We briefly discuss the mass loss by stellar winds, which are influenced by the anisotropic temperature distribution. These anisotropies in the interior are also driving circulation currents, which transports the chemical elements and the angular momentum in stars. Internal differential rotation, if present, creates instabilities and mixing, in particular the shear mixing, the horizontal turbulence and their interactions.

A major check of the model predictions concerns the changes of the surface abundances, which are modified by mass loss in the very massive stars and by rotational mixing in O- and B-type stars. We show that the observations confirm the existence of rotational mixing, with much larger effects at lower metallicities.

We discuss the predictions of stellar models concerning the evolution of the surface velocities, the evolutionary tracks in the HR diagram and lifetimes, the populations of blue, red supergiants and Wolf-Rayet stars, and the progenitors of type Ibc supernovae. We show, that in many aspects, rotating models provide a much better fit than non-rotating ones. Using the same physical ingredients as those which fit the best the observations of stars at near solar metallicities, we explore the consequences of rotating models for the status of Be stars, the progenitors of Gamma Ray Bursts, the evolution of Pop III stars and of very metal poor stars, the early chemical evolution of galaxies, the origin of the C-enhanced Metal Poor stars (CEMP) and of the chemical anomalies in globular clusters.

Rotation, together with mass loss are two key physical ingredients shaping the evolution of massive stars during the whole cosmic history.

## Contents

<b>I. INTRODUCTION</b>	2
<b>II. THE MECHANICAL AND THERMAL EQUILIBRIUM OF ROTATING STARS</b>	3
A. The mechanical equilibrium for uniform rotation	3
B. Differential rotation: the case of shellular rotation	4
C. The critical velocities	5
D. The breakdown of thermal equilibrium in rotating stars	5
E. The von Zeipel Theorem and observations	6
<b>III. MASS LOSS FROM MASSIVE STARS</b>	6
<b>IV. THE CIRCULATION AND MAIN INSTABILITIES IN ROTATING STARS</b>	7
A. The transports of elements and angular momentum	7
B. The meridional circulation	8
C. The horizontal turbulence in differentially rotating stars	9
D. Shear mixing and other instabilities	10
<b>V. ROTATION AND MAGNETIC FIELDS</b>	11
A. Some properties of a dynamo in a radiative zone	11
B. The basic equations	13
C. The case of Tayler–Spruit dynamo	13
<b>VI. RECENT GRIDS OF MODELS OF MASSIVE ROTATING STARS</b>	14
<b>VII. THE ELEMENT ABUNDANCES IN MASSIVE STARS</b>	14
A. Model effects of mass loss on abundances	15

---

\*Electronic address: Andre.Maeder@unige.ch

†Electronic address: Georges.Meynet@unige.ch

B. The effects of rotation on the surface abundances	15
C. The observed N/H excesses	15
D. The observed He excesses	16
<b>VIII. EVOLUTION OF ROTATION AT THE SURFACE AND IN THE INTERIOR</b>	17
A. Initial conditions for rotating models	17
B. Evolution of the surface velocities	18
C. The Be stars and the evolution towards the critical velocity	18
D. Evolution of the interior angular momentum content	19
<b>IX. EVOLUTIONARY TRACKS AND LIFETIMES</b>	20
A. The Main-Sequence phase	20
B. The post- Main-Sequence evolution	21
C. Lifetimes	21
<b>X. MASSIVE STAR POPULATIONS AND THE CASE OF FIRST STARS</b>	22
A. The ratio of blue to red supergiants	22
B. Current problems with Wolf-Rayet stars	22
C. Solutions of WR problems in terms of rotation?	23
D. Pop III star models with rotation	24
E. Strong mass loss in Pop III stars?	26
<b>XI. SUPERNOVAE AND GAMMA RAY BURSTS</b>	27
A. The type Ib and Ic supernovae	27
B. The progenitors of long soft Gamma Ray Bursts	28
<b>XII. STELLAR NUCLEOSYNTHESIS</b>	29
A. Rotation and stellar yields at $Z=0.020$	29
B. Impact on the early chemical evolution of galaxies	30
C. The Carbon-Enhanced- Metal- Poor stars	31
D. The chemical anomalies in globular clusters	32
<b>XIII. CONCLUSIONS</b>	33
<b>References</b>	34
<b>Figures</b>	37
<b>Tables</b>	54

## I. INTRODUCTION

It may be surprising that we emphasize the need of accounting for the effects of rotation in stellar evolution, since in practice all stars are rotating around their axis. However, it must be recalled that the so-called "standard theory" of stellar evolution generally ignores the effects of stellar rotation and treats the stars as non-rotating bodies, despite the fact that stars more massive than about  $1.5 M_{\odot}$  rotate fast on the average (Fig. 1).

The recent progresses in astrophysical observations, particularly in high resolution spectroscopy and in asteroseismology, have shown many significant deviations from the standard models, for example the many large nitrogen enrichments resulting from mixing in massive stars (Sect. VII). These observations show the need to also account for the various effects of rotation in stellar modeling. All model outputs are finally modified by the proper account of rotation: the stellar luminosities and radii, the lifetimes, the chemical abundances at the surface, the helio- and asteroseismology responses, the nature of supernova explosions, the amounts of nucleosynthetic products, the nature of the final remnants, ...

For practical purpose, it is often convenient to distinguish 4 main groups of rotational effects in stellar physics.

1.- *The equilibrium configuration of rotating stars:* it results from the centrifugal force on the stellar equilibrium. The equipotentials are modified and in particular the shape of the stellar surface, which affects the surface  $T_{\text{eff}}$  and gravity distributions.

2.- *The effects of rotation on mass loss or accretion:* in fast rotating stars, the isotropy of mass loss (or accretion when present) is destroyed and anisotropies appear and are effectively observed.

3.- *The rotational mixing:* the internal distortion induces circulation currents which transport the elements and angular momentum, while differential rotation may produce several instabilities which also contribute to the transport processes.

4.- *The interactions with magnetic field:* the presence of an internal magnetic field may produce an internal coupling of rotation, leading to solid body rotation, while external fields produce some magnetic braking. A major uncertainty

concerns the existence of a dynamo in radiative regions with differential rotation. We examine some properties of such a dynamo.

The above distinction is evidently a simplification since the various effects are related. For example, it is the modification of the internal equilibrium structure which drives the mixing. In turn, the mixing modifies the internal distribution of the elements and this also influences the equilibrium structure.

In this review, we focus on the rotational effects in the Main-Sequence (MS) and post-MS phases, i.e. in the nuclear phases. The effects of rotation in star formation are also a most important chapter of astrophysics, but they would deserve another specific review. We consider here the case of single stars, the many effects of rotation in relation with tidal interactions in binaries are also beyond the scope of this review. Most of the effects discussed here in the case of single stars evidently have their counterparts in binaries, however their modeling is still in its infancy.

Recent reviews on the observational and theoretical aspects of stellar rotation are given in IAU symposium 215 (Maeder & Eenens, 2004) and the theoretical aspects have recently extensively been reviewed (Maeder, 2009).

## II. THE MECHANICAL AND THERMAL EQUILIBRIUM OF ROTATING STARS

The equilibrium and stability configurations of rotating stars have been reviewed long ago (Lebovitz, 1967). In practice, except for stars with little internal density contrast, like white dwarfs or neutron stars, the approximation of the Roche model is acceptable. It assumes that the effective gravity results from the matter centrally condensed, with in addition the effect of the centrifugal force. For all stellar masses, the rotational energy of the Roche model represents at most about 1% of the absolute value of the potential energy.

The properties of rotating stars depend on the distribution of the angular velocity  $\Omega(r)$  inside the stars. The simplest case is that of solid body rotation, i.e.  $\Omega = \text{const.}$ , while more elaborate models include differential rotation.

### A. The mechanical equilibrium for uniform rotation

Let us first consider the case of a constant angular velocity  $\Omega$  in the Roche model in hydrostatic equilibrium. The gradient of pressure  $P$  is given by

$$\frac{1}{\varrho} \vec{\nabla} P = -\vec{\nabla} \Phi + \frac{1}{2} \Omega^2 \vec{\nabla} (r \sin \vartheta)^2, \quad (1)$$

$\varrho$  is the local density,  $\Phi$  is the gravitational potential, which is unmodified by rotation in the Roche approximation and which gives the gravitational acceleration  $\vec{g} = -\vec{\nabla} \Phi = -\frac{G M_r}{r^2} \vec{e}_r$ ,  $r$  being the distance to the center. The components of  $\vec{g}$  are  $(-g, 0, 0)$  and  $g = \frac{\partial \Phi}{\partial r}$ . If  $\Omega$  is constant or has a cylindrical symmetry, the centrifugal acceleration can also be derived from a potential, say  $V$ . In case of constant  $\Omega$ , one has

$$-\vec{\nabla} V = \Omega^2 \vec{\varpi} \quad \text{and thus} \quad V = -\frac{1}{2} \Omega^2 \varpi^2. \quad (2)$$

$\varpi = r \sin \vartheta$  is the distance to the rotation axis. The total potential  $\Psi$  is  $\Psi = \Phi + V$  and with the usual Poisson equation one has  $\nabla^2 \Psi = \nabla^2 \Phi + \nabla^2 V$  with  $\nabla^2 \Phi = 4\pi G \varrho$ . In a uniformly (or cylindrically) rotating star, the centrifugal force derives from a potential and one has  $(\nabla^2 V)_\varpi = \frac{1}{\varpi} \frac{\partial}{\partial \varpi} (-\varpi^2 \Omega^2) = -2\Omega^2$ . The Poisson equation becomes

$$\nabla^2 \Psi = 4\pi G \varrho - 2\Omega^2. \quad (3)$$

and the equation of hydrostatic equilibrium

$$\frac{1}{\varrho} \vec{\nabla} P = -\vec{\nabla} \Psi = \vec{g}_{\text{eff}}. \quad (4)$$

The effective gravity  $\vec{g}_{\text{eff}}$  results from both gravitation and centrifugal acceleration (take care of the sign of  $\Phi$  and  $\Psi$ ). These expressions imply that the pressure is constant on an equipotential, i.e.  $P = P(\Psi)$ . The equipotentials and isobars coincide and the star is said *barotropic*, otherwise it is said *baroclinic*. Eq.(4) shows that the density is also a function of  $\Psi$  only. Through the equation of state  $P = P(\varrho, T)$ , one also has  $T = T(\Psi)$ . The quantities  $\varrho$ ,  $P$ ,  $T$  are constant on the equipotentials  $\Psi = \text{const.}$

The stellar surface is an equipotential. The total potential at a level  $r$  and at colatitude  $\vartheta$  ( $\vartheta = 0$  at the pole) is

$$\Psi(r, \vartheta) = -\frac{G M_r}{r} - \frac{1}{2} \Omega^2 r^2 \sin^2 \vartheta. \quad (5)$$

For a star of total mass  $M$ , let us call  $R(\vartheta)$  the stellar radius at colatitude  $\vartheta$ . Since the centrifugal force is zero at the pole, the potential at the stellar pole is just  $G M/R_p$ , where  $R_p$  is the polar radius. This fixes the constant value of the equipotential at the stellar surface, which is given by

$$\frac{G M}{R} + \frac{1}{2} \Omega^2 R^2 \sin^2 \vartheta = \frac{G M}{R_p} . \quad (6)$$

This equation also applies to moderate differential rotation, if  $\Omega$  can be considered as constant on an equipotential surface.

The shape of a Roche model is illustrated in Fig. 2 for different rotation velocities. The effective gravity resulting from the gravitational potential and from the centrifugal force is given by (4). If  $\vec{e}_r$  and  $\vec{e}_\vartheta$  are the unity vectors in the radial and latitudinal directions, one has

$$\vec{g}_{\text{eff}} = \left[ -\frac{GM}{R^2(\vartheta)} + \Omega^2 R(\vartheta) \sin^2 \vartheta \right] \vec{e}_r + [\Omega^2 R(\vartheta) \sin \vartheta \cos \vartheta] \vec{e}_\vartheta . \quad (7)$$

Care has to be given for many applications that the gravity vector is not parallel to the vector radius, with an angle  $\epsilon$  given by  $\cos \epsilon = -\vec{g}_{\text{eff}} \cdot \vec{r} / (|\vec{g}_{\text{eff}}| \cdot |\vec{r}|)$  between the two vectors.

## B. Differential rotation: the case of shellular rotation

The most studied case of differential rotation is that of the so-called "shellular" rotation (Zahn, 1992), i.e. with a rotation law  $\Omega$  constant on isobaric shells and depending to the first order on the distance  $r$  to the stellar center,

$$\Omega(r, \vartheta) = \bar{\Omega}(r) + \Omega_2(r) P_2(\cos \vartheta) , \quad (8)$$

where  $P_2$  is the second Legendre polynomial. This rotation law results from the strong horizontal turbulence in differentially rotating stars, which imposes a constancy of  $\Omega$  on isobars, while in the vertical direction, the turbulence is weaker due to the stable density stratification. The above writing of  $\Omega(r, \vartheta)$  implies some limitations, since isobars are not identical to spherical surfaces, in particular it only applies to low or moderate rotation velocities. This case is non-conservative. The surfaces defined by  $\Psi = \text{const.}$  are isobars (Meynet & Maeder, 1997), but they are not equipotentials and the star is baroclinic.

The equations of stellar structure for a star in shellular rotation can be written in a form close to that of the non-rotating case in order to minimize the necessary modifications (Meynet & Maeder, 1997). One associates a radius  $r_P$  to an isobar, it is defined by  $V_P \equiv (4\pi/3) r_P^3$ , where  $V_P$  is the volume inside the isobar. For any quantity like  $g_{\text{eff}}$ , which is not constant over an isobaric surface, a mean value is defined by

$$\langle g_{\text{eff}} \rangle \equiv \frac{1}{S_P} \oint_{\Psi=\text{const}} g_{\text{eff}} d\sigma , \quad (9)$$

where  $S_P$  is the total surface of the isobar and  $d\sigma$  is an element  $d\sigma = r^2 \sin \vartheta d\varphi d\vartheta / \cos \epsilon$  of this surface. In Lagrangian coordinates (where  $M_P$  is the mass internal to an isobar), the equations of hydrostatic equilibrium, of mass conservation, of energy production and of energy transport can be written (Meynet & Maeder, 1997),

$$\frac{dP}{dM_P} = -\frac{G M_P}{4\pi r_P^4} f_P , \quad (10)$$

$$\frac{dr_P}{dM_P} = \frac{1}{4\pi r_P^2 \bar{\rho}} \quad (11)$$

$$\frac{dL_P}{dM_P} = \varepsilon_{\text{nucl}} - \varepsilon_\nu + \varepsilon_{\text{grav}} , \quad (12)$$

$$\frac{d \ln T}{dM_P} = -\frac{G M_P}{4\pi r_P^4} f_P \min \left[ \nabla_{\text{ad}}, \nabla_{\text{rad}} \frac{f_T}{f_P} \right] , \quad (13)$$

$$\text{whith } f_P = \frac{4\pi r_P^4}{GM_P S_P} \frac{1}{<g_{\text{eff}}^{-1}>} \quad \text{and} \quad f_T = \left( \frac{4\pi r_P^2}{S_P} \right)^2 \frac{1}{<g_{\text{eff}}^{-1}>}. \quad (14)$$

where  $\varepsilon_{\text{nucl}}$ ,  $\varepsilon_\nu$  and  $\varepsilon_{\text{grav}}$  are respectively the rate of nuclear energy production, of neutrino losses and of gravitational energy production or absorption by mass unit.  $\nabla_{\text{ad}}$  and  $\nabla_{\text{rad}}$  are the adiabatic and radiative temperature  $T$  gradients ( $d \ln T / d \ln P$ ).  $\bar{\rho}$  is formally here the average density between two isobars. The above set of equations allows one to construct models of stars in differential rotation (shellular case) with little modifications with respect to the usual set of standard equations. The results are obtained as a function of  $M_P$  the mass of an isobar of average coordinate  $r_P$ . In practice,  $r_P$  is the radius of the isobar at a colatitude  $\vartheta$  such that  $P_2(\cos \vartheta) = 0$ , i.e.  $\vartheta \approx 54$  degrees.

### C. The critical velocities

The critical or break-up velocity is reached when the centrifugal force becomes equal to the gravitational attraction at the equator, i.e. when

$$\Omega_{\text{crit}}^2 = \frac{G M}{R_{\text{e,crit}}^3}, \quad (15)$$

where  $R_{\text{e,crit}}$  is the equatorial radius at break-up. With  $\Omega_{\text{crit}}$  in the equation of the surface (6) at break-up, one gets for the ratio of the equatorial to the polar radius at critical velocity,  $\frac{R_{\text{e,crit}}}{R_{\text{p,crit}}} = \frac{3}{2}$ . The equatorial break-up velocity is thus

$$v_{\text{crit}}^2 = \Omega_{\text{crit}}^2 R_{\text{e,crit}}^2 = \frac{G M}{R_{\text{e,crit}}} = \frac{2 G M}{3 R_{\text{p,crit}}}. \quad (16)$$

Introducing a non-dimensional rotation parameter  $\omega$ , defined as the ratio of the angular velocity to the angular velocity at break-up,  $\omega = \frac{\Omega}{\Omega_{\text{crit}}}$  i.e.  $\omega^2 = \frac{\Omega^2 R_{\text{e,crit}}^3}{G M}$ ,  $\Omega^2 = \frac{8}{27} \frac{G M \omega^2}{R_{\text{p,crit}}^3}$  and the equation of the surface (6) becomes with  $x = R/R_{\text{p,crit}}$

$$\frac{1}{x} + \frac{4}{27} \omega^2 x^2 \sin^2 \vartheta = \frac{R_{\text{p,crit}}}{R_{\text{p}}(\omega)}. \quad (17)$$

If the polar radius would not change with  $\omega$ , the second term would be equal to 1; Eq. (17) is thus an algebraic equation of the 3<sup>rd</sup> degree, which gives the values of the radius as a function of  $\omega$  and  $\vartheta$ . For low rotation ( $\omega < 0.5$ ), a linear approximation of  $v$  in term of  $\omega$  is valid

$$v^2 = \frac{8}{27} \frac{G M \omega^2}{R_{\text{p,crit}}^3} R_{\text{e}}^2 \approx \frac{8}{27} \frac{G M \omega^2}{R_{\text{p,crit}}} = \frac{4}{9} \omega^2 v_{\text{crit}}^2. \quad (18)$$

Fig. 3 shows the critical velocities  $v_{\text{crit}}$  for stars of various masses and metallicities. The critical velocities grow with stellar masses, because the stellar radii increase only slowly with stellar masses. The critical velocities are very large for low metallicity stars, since their radii are much smaller as a result of their lower opacities. In the most massive stars, where radiation pressure nearly compensates gravity, the effects of radiation modify the expressions of the critical velocity making them lower. In this case, one speaks of the  $\Omega\Gamma$  limit, since the stars reach their critical velocity, due to the combined effects of high radiation (the Eddington limit) and of centrifugal force (Maeder & Meynet, 2000a).

### D. The breakdown of thermal equilibrium in rotating stars

Rotation deeply affects the internal thermal equilibrium. As seen above, the equipotentials are differently spaced as a function of the colatitude  $\vartheta$ , since the star is distorted. The equipotentials are closer in polar regions and more separated near the equator. The radiative flux at some latitude is proportional to the local gradient between the equipotentials (the effective gravity, Sect. II.E). If there is no local energy source or sink, the total energy through an equipotential is conserved. Thus, there is (in a simple picture of uniformly rotating stars) an excess of flux along the polar axis and a deficiency near the equatorial plane. This thermal imbalance generates global circulation motions in the meridian plane. These currents then contribute to the mixing of chemical elements and transport of angular momentum (Sect. IV).

### E. The von Zeipel Theorem and observations

The von Zeipel theorem relates the radiative flux at some colatitude  $\vartheta$  on the surface of a rotating star and the local effective gravity  $g_{\text{eff}}(\Omega, \vartheta)$ , function of the angular velocity  $\Omega$  and  $\vartheta$ . The flux is  $\vec{F}(\Omega, \vartheta) = -\chi \vec{\nabla} T(\Omega, \vartheta)$  with  $\chi = \frac{4acT^3}{3\kappa\varrho}$ . We consider the case of a uniformly rotating star. The equipotentials and isobars coincide, they are also surface of constant  $T$  and  $\varrho$ . Thus, one has with (4)

$$\vec{F}(\Omega, \vartheta) = -\chi \frac{dT}{dP} \vec{\nabla} P(\Omega, \vartheta) = -\varrho \chi \frac{dT}{dP} \vec{g}_{\text{eff}}(\Omega, \vartheta). \quad (19)$$

The pressure gradient and effective gravity are parallel. The term  $(\varrho \chi dT/dP)$  is constant on a given equipotential, thus the flux is proportional to the effective gravity on the equipotential. This coefficient of proportionality can easily be estimated and one obtains

$$\vec{F}(\Omega, \vartheta) = -\frac{L}{4\pi G M^*} \vec{g}_{\text{eff}}(\Omega, \vartheta) \quad (20)$$

$$\text{with} \quad M^* = M \left( 1 - \frac{\Omega^2}{2\pi G \bar{\varrho}_M} \right), \quad (21)$$

where  $\bar{\varrho}_M$  is the average internal density. The above relation applies to any equipotential, but in general the von Zeipel theorem is considered at the surface of a star of total mass  $M$  and luminosity  $L$ . Eq. (20) is the von Zeipel theorem: it says that the radiative flux at the surface of a rotating star is proportional to the local effective gravity at the considered colatitude. From  $g_{\text{eff}}$ , one obtains the radiative flux locally and thus  $T_{\text{eff}}$

$$T_{\text{eff}}(\Omega, \vartheta) = \left( \frac{L}{4\pi \sigma G M^*} \right)^{\frac{1}{4}} [g_{\text{eff}}(\Omega, \vartheta)]^{\frac{1}{4}}. \quad (22)$$

Both  $g_{\text{eff}}$  and  $T_{\text{eff}}$  vary over the surface of a rotating star and influence the emergent spectrum. The equatorial regions are fainter and cooler than the polar ones, which are brighter and hotter (the differences of  $T_{\text{eff}}$  may reach a factor of 2). This effect is called the gravity-darkening. The von Zeipel theorem in a star with shellular rotation shows only minor differences (Maeder, 1999) with respect to (20). The differences, which essentially depend on the  $\Omega$  gradient close to the surface, may slightly increase the contrast between the pole and equator. 2-D models have tested the validity of the von Zeipel relation (Lovekin et al., 2006). Depending on the rotation laws, there are some small differences.

Interferometric observations with the VLTI of the Be star Achernar indicate a ratio  $R_e/R_p \approx 1.5$  (Domiciano de Souza et al., 2003). A recent analysis of the data by Carciofi et al. (2008) confirms that the observations well agree with a rigidly rotating star at  $\omega = 0.992$  in the Roche model, provided it is surrounded by a small disk. VLTI observations (Domiciano de Souza et al., 2005) of the fast rotating star Altair ( $M \approx 1.8 M_\odot$ , A7IV-V) confirm a gravity-darkening as predicted by the von Zeipel theorem. This is also supported by further studies for Altair (Peterson et al., 2008, 2006), which rotates at 90% of its breakup angular velocity. The effect of gravity-darkening receives further support (Monnier et al., 2007), but instead of an exponent 0.25 as in Eq. (22), an exponent  $\beta = 0.19$  is favored. Also, these authors notice an equatorial darkening stronger than predicted, which might result from faster equatorial rotation, of differences due to convection or opacity effects, etc. A value of  $\beta$  as small as  $\beta = 0.08$  is also found (van Belle et al., 2006) in the case of Alderamin ( $\alpha$  Cep, type A7IV-V), which rotates at 83% of its breakup velocity. Thus, the von Zeipel relation is confirmed, but there are some possible deviations.

### III. MASS LOSS FROM MASSIVE STARS

Massive stars above  $10 M_\odot$  lose, at solar metallicity, a significant amount of mass during their evolution. As an example, a star with an initial mass of  $60 M_\odot$  loses about the half of its mass during its MS evolution. Due to mass loss in further stages, it is left with only about  $10 M_\odot$  at the time of supernova explosion. The mass loss rates  $\dot{M}$  of OB stars reach about  $10^{-5} M_\odot \text{ yr}^{-1}$  with wind velocities up to  $3000 \text{ km s}^{-1}$ . For these stars  $\dot{M}$  is a billion times larger than for the Sun, for which  $\dot{M}$  is about  $10^{-14} M_\odot \text{ yr}^{-1}$ . The mass loss results from the stellar winds driven by the strong radiation pressure of luminous stars, which pushes the mass outside. The absorption of radiation by the spectral lines is the main effect transferring momentum from radiation to matter. In red supergiants, mass loss also occurs due to the absorption and diffusion of radiation by dust. On the whole, mass loss is a dominant effect influencing all the outputs of stellar evolution and nucleosynthesis.

The physics of stellar winds has been reviewed in several studies (Kudritzki & Puls, 2000; Lamers & Cassinelli, 1999). Owing to the many uncertainties, stellar model makers generally apply expressions of  $\dot{M}$  based on observations, which are also not free from problems. A major one is due to the clumping effects of matter in the wind, This has already lead to a reduction of the  $\dot{M}$  by a factor 2 or 3 over recent years and questions arise about a further reduction. For hot stars, there are several parametrizations of the  $\dot{M}$  rates deduced from theoretical models (Kudritzki & Puls, 2000; Vink et al., 2000, 2001) for different  $M$ ,  $L$ ,  $T_{\text{eff}}$  and metallicities  $Z$ . For O stars,  $\dot{M}$  (taken positive) behaves globally like

$$\dot{M} \sim L^{1.6} \quad \text{and} \quad \dot{M} \sim Z^{0.7}. \quad (23)$$

Let us note that Mokiem et al. (2006) find that for stars with  $\log L/L_{\odot}$  superior to about 5.4, the wind strengths are in excellent agreement with the theoretical predictions of Vink et al. (2001).

Dust–enshrouded red giants and supergiants have strong mass loss rates due to the high dust opacity. (van Loon et al., 2005) suggest the following empirical formula:

$$\log \dot{M} = -5.65 + 1.05 \log \left( \frac{L}{10^4 L_{\odot}} \right) - 6.3 \log \left( \frac{T_{\text{eff}}}{3500 \text{ K}} \right). \quad (24)$$

Wolf–Rayet (WR) stars are bare cores left over by mass loss from massive stars. Their  $\dot{M}$  are very high, due mostly to their high  $L/M$  ratios. Models indicate that the  $\dot{M}$  values scale with the actual WR masses like (Nugis & Lamers, 2000, 2002),

$$\log \dot{M} = A + B \log \frac{M}{M_{\odot}}, \quad (25)$$

with average values  $A = -5.73$ ,  $B = 0.88 \pm 0.14$  for WR stars in general. All these parametrizations are continuously revised (Gräfener & Hamann, 2008).

Rotation affects the mass loss in two ways (Maeder & Meynet, 2000b): - 1. it makes the stellar winds anisotropic because the polar regions are hotter so that the radiation pressure is stronger, - 2. for given luminosity  $L$  and  $T_{\text{eff}}$  the average mass loss rates are increased. Fig. 4 illustrates the distribution of the mass loss around a very massive stars. The higher  $T$  in polar regions drives a stronger mass flux than in the equatorial regions. This characteristic peanut shape has been observed in several nebulae around very massive stars (Nota, 1999). For stars with an equatorial  $T_{\text{eff}}$  lower than about 23000 K, the equatorial opacity increases enough to allow the radiative acceleration to push (despite the lower flux) the matter outward and to produce an equatorial ring. Some stars, the so-called B[e] stars, simultaneously show a peanut–shaped nebula and an equatorial ring.

The anisotropic mass loss rates may be integrated over the stellar surface to give the overall  $\dot{M}$  value. The result is that if we consider two stars with the same  $L$  and  $T_{\text{eff}}$ , but one with rotation velocity  $v$  and the other one with  $v = 0$ , the ratio of their  $\dot{M}$ –rates may reach very high values (Maeder & Meynet, 2000b), especially for stars close to the Eddington limit (i. e. for the brightest stars where the radiation pressure gradient becomes close to gravity). For hot stars far enough from the Eddington limit, the effects are limited, amounting to an increase of at most 70 %.

#### IV. THE CIRCULATION AND MAIN INSTABILITIES IN ROTATING STARS

Rotation drives internal circulation currents and several kinds of turbulent motions may arise from differential rotation. All these motions may contribute to the internal transport of matter and angular momentum.

##### A. The transports of elements and angular momentum

Many effects of element transport in stars can be considered as a diffusion process characterized by a diffusion coefficient  $D$ . The kinetic theory of gases indicates that in an isotropic turbulent medium with an average velocity  $v$  and a mean free path  $\ell$  the diffusion coefficient is  $D = (1/3) \ell v$ . Let us call  $X_i$ , the abundance in mass fraction of particles  $i$ . If there is a gradient of composition  $\vec{\nabla} X_i$ , the diffusion velocity of particles  $i$  is  $\vec{v}_i = -(D/X_i) \vec{\nabla} X_i$ . The diffusion equation of the chemical elements can be derived from the continuity equation, this gives at a Lagrangian mass coordinate  $M_r$ ,

$$\varrho \frac{\partial X_i}{\partial t} \Big|_{M_r} = \frac{1}{r^2} \frac{\partial}{\partial r} \left( \varrho r^2 D \frac{\partial X_i}{\partial r} \right). \quad (26)$$

The boundary conditions at the center and surface are  $\left. \frac{\partial X_*}{\partial r} \right|_{M_r=0} = \left. \frac{\partial X_*}{\partial r} \right|_{M_r=M} = 0$ , where  $M$  is the total mass. The diffusion coefficients may vary a lot and great care has to be given to their interpolation, if necessary (Meynet et al., 2004).

In a differentially rotating star, the evolution of the angular velocity  $\Omega$  has to be followed at each level  $r$  (for shellular rotation), so that a full description of  $\Omega(r, t)$  is available. The values of  $\Omega(r, t)$  influence the mixing of elements and in turn the evolution of  $\Omega(r, t)$  also depends on the mixing processes and on the distribution of the elements. The derivation of the equation for the transport of angular momentum is not straightforward. In the case of shellular rotation, the equation in the Lagrangian form becomes (Maeder, 2009; Zahn, 1992)

$$\varrho \frac{\partial}{\partial t} (r^2 \bar{\Omega})_{M_r} = \frac{1}{5} \frac{\partial}{\partial r} (r^4 \bar{\Omega} U_2(r)) + \frac{1}{r^2} \frac{\partial}{\partial r} \left( \varrho D r^4 \frac{\partial \bar{\Omega}}{\partial r} \right). \quad (27)$$

There,  $\bar{\Omega}$  is the average value of  $\Omega$  on an isobar, or in approximation (8) the value at  $P_2(\cos \vartheta) = 0$ .  $U_2$  is the radial component of the meridional circulation velocity (see next subsection). The second term on the right is a diffusion term, similar in its form to (26), while the first term on the right is an *advective term*, i.e. the transport by a velocity current. We notice that Eq. (26) does not contain such an advective term. It could contain a term of that kind, however in general it is considered that the combined effect of turbulence and circulation currents is equivalent to a diffusion *for the element transport* (see Eq. 34).

Great care has to be brought to the solution of this equation, since  $U_2$  given in the next subsection contains terms up to the third derivative of  $\bar{\Omega}$ , so that this equation is of the fourth order. If there is no viscous momentum at the edges, one has two boundary conditions given by  $\frac{\partial \bar{\Omega}}{\partial r} = 0$  at the limits. The two other conditions are given by integrating the transport equations at the bottom and top limits  $r_b$  and  $r_t$ ,

$$\begin{aligned} \frac{1}{5} \varrho r^4 \bar{\Omega} U_2 \Big|_{r_b} &= \frac{d}{dt} \left[ \bar{\Omega} \int_0^{r_b} r^4 \varrho dr \right] \quad \text{in } r = r_b, \\ -\frac{1}{5} \varrho r^4 \bar{\Omega} U_2 \Big|_{r_t} &= \frac{d}{dt} \left[ \bar{\Omega} \int_{r_t}^R r^4 \varrho dr \right] + \mathcal{M}_\Omega \quad \text{in } r = r_t. \end{aligned} \quad (28)$$

The radial components  $U_2$  of the velocity at the surface and center are zero.  $\mathcal{M}_\Omega$  represents the momentum of force applied at the stellar surface, typically by magnetic field in solar type stars or by tidal effects in binary systems.

## B. The meridional circulation

The breakdown of the thermal stability in rotating stars (Sect. II.D) drives some circulation currents. For long there was a severe physical problem: the solutions for meridional circulation were not conserving the angular momentum. Thus the reality of the circulation was often questioned and solutions without circulation were envisaged. Zahn has made a great step forward by showing that one must treat simultaneously the equation for energy conservation which expresses the thermal imbalance, the Poisson equation and the conservation of angular momentum, in order to have a self-consistent solution (Zahn, 1992).

The derivation of the circulation velocity for shellular rotation is rather lengthy (Maeder & Zahn, 1998; Zahn, 1992). The starting point is the equation of energy conservation,

$$\rho T \frac{dS}{dt} = \vec{\nabla} \cdot (\chi \vec{\nabla} T) + \varrho \varepsilon - \vec{\nabla} \cdot \vec{F}_h, \quad (29)$$

where  $S$  is the entropy per unit of mass and  $\chi$  the thermal conductivity (Sect. II.E). The term  $\varepsilon$  refers to the nuclear energy production rate only.  $\vec{F}_h = -D_h \varrho C_P \vec{\nabla}_h T$  is the flux of thermal energy due to the horizontal turbulence with a diffusion coefficient  $D_h$  (Sect. IV.C).  $C_P$  is the specific heat at constant pressure  $P$  and  $\vec{\nabla}_h$  expresses the horizontal gradient. On an isobar, the variables are expanded around their average up to the second Legendre polynomials  $P_2(\cos \vartheta)$ , where  $\vartheta$  is the colatitude, for example  $T(P, \vartheta) = \bar{T}(P) + \tilde{T}(P) P_2(\cos \vartheta)$ .

The velocity of meridional circulation is the main quantity characterizing this effect, it is expanded into 2 components

$$\vec{U} = U_2(r) P_2(\cos \vartheta) \vec{e}_r + V_2(r) \frac{dP_2(\cos \vartheta)}{d\vartheta} \vec{e}_\vartheta, \quad (30)$$



$U_2(r)$  is the amplitude of the radial component of the meridional circulation velocity,  $V_2(r)$  is the amplitude of the horizontal component. The general expression of  $U_2(r)$  in a stationary situation is

$$U_2(r) = \frac{P}{\bar{\rho} \bar{g} C_P \bar{T} (\nabla_{\text{ad}} - \nabla + \frac{\varphi}{\delta} \nabla_\mu)} \left[ \frac{L(r)}{M_*(r)} (E_\Omega + E_\mu) \right]. \quad (31)$$

$\nabla_\mu = (d \ln \mu / d \ln P)$ ,  $\varphi = (\partial \ln \varrho / \partial \ln \mu)_{P,T}$ ,  $\delta = -(\partial \ln \varrho / \partial \ln T)_{P,\mu}$ ,  $E_\Omega$  contains dozens of terms up to the third derivative of  $\Omega$  and  $E_\mu$  up to the second derivative of the mean molecular weight. An important term, also present in the case of uniform rotation in an homogeneous medium, is

$$E_\Omega \simeq \frac{8}{3} \left[ 1 - \frac{\Omega^2}{2\pi G \bar{\rho}} \right] \left( \frac{\Omega^2 r^3}{GM_r} \right). \quad (32)$$

This term is proportional to the ratio of the centrifugal to the gravitational force. The second term in the square bracket is the so-called Gratton–Öpik term. In the deep interior, it is generally negligible while it may become dominant in the outer layers, where the local average density  $\bar{\rho}$  is negligible. The sign of  $U_2$  is however not determined only by the sign of the Gratton–Öpik term and the complete expression has to be considered. Generally the inner cell is turning upward along the polar axis, while the external cell turns the opposite way (Fig. 5). This means that the inner cell is bringing angular momentum inward, while the outer cell brings it outward. However, the circulation patterns, which depends on the derivatives of  $\Omega$  and  $\mu$ , may be different according to the stellar model considered.

The circulation velocities are typically of the order of a few  $\text{cm s}^{-1}$  in upper MS stars. The velocities are larger at the beginning of the Main Sequence (MS) phase when rotation is (supposedly) uniform, then in a few percents of the MS timescale the velocities become smaller reaching an equilibrium. At the end of the MS phase, they may again become large (negatively) due to the very high Gratton–Öpik term, because of the very low density in the outer layers. The circulation timescale  $t_{\text{circ}}$ , also called the Eddington–Sweet timescale  $t_{\text{ES}}$ , is of the order of the stellar radius divided by the velocity,

$$t_{\text{ES}} \approx \frac{R}{U_2(R)} \approx \frac{GM^2}{LR} \frac{GM}{\Omega^2 R^3} \approx \frac{t_{\text{KH}}}{\Omega^2 R^3 / (GM)}. \quad (33)$$

where  $t_{\text{KH}}$  is the Kelvin–Helmholtz timescale, i.e. the thermal timescale of the star (about  $3 \times 10^7$  yr for the Sun). The circulation timescale is equal to about  $t_{\text{KH}}$  divided by the ratio of the centrifugal force to the gravity  $\Omega^2 R^3 / (GM)$ , thus  $t_{\text{ES}}$  is some multiple of  $t_{\text{KH}}$ .

Meridional circulation is important, because it transports both angular momentum and chemical elements. The presence of horizontal turbulence in differentially rotating stars affects these two kinds of transport differently. The interaction of the transport of chemical elements by meridional circulation and horizontal turbulence results in a diffusion process (Chaboyer & Zahn, 1992), with a diffusion coefficient

$$D_{\text{eff}} = \frac{(r U_2)^2}{30 D_h}. \quad (34)$$

where  $D_h$  is the diffusion coefficient by the horizontal turbulence as discussed in next Section. The above expression is valid only if  $D_h$  is large with respect to  $r U_2$  and to the coefficient of vertical diffusion.

The above reasoning does not apply to the transport of angular momentum, thus Eq. (27) contains both advective and diffusive terms. The reason is that angular momentum conservation limits the effects of horizontal motions on the transport of the angular momentum. Indeed, turbulence may be present without a net flux of angular momentum, however it maintains a shellular distribution of velocity, as shown by numerical models (Charbonneau, 1992).

### C. The horizontal turbulence in differentially rotating stars

Rotation and especially differential rotation generates turbulent motions. On the Earth, we have the example of west winds and jet streams. In a radiative zone, the turbulence is stronger (Zahn, 1992) in the horizontal than in the vertical direction, because in the vertical direction the stable thermal gradient opposes a strong force to the fluid motions. The horizontal turbulence is characterized by a diffusion coefficient  $D_h$ , which also expresses the horizontal viscosity. There are several observational indications supporting the existence of this turbulence (Maeder, 2009). The expression of  $D_h$  is uncertain and three different forms have been proposed (Maeder, 2003; Mathis et al., 2004; Zahn, 1992). That by Mathis et al. is based on the Couette–Taylor experiment, while the other two are phenomenological. The expressions by Mathis et al. and Maeder give similar results, larger by orders of magnitude with respect to those obtained with Zahn’s expression.

A diffusion coefficient behaves like  $\ell^2/t_{\text{diff}}$ , where  $\ell$  is a characteristic length (here typically  $r$ ) and  $t_{\text{diff}}$  a diffusion timescale. Thus, the question is to know which timescale is to be considered. One may see that the coefficient by Zahn corresponds to about a value  $t_{\text{diff}} \sim r/V_2$ , where  $V_2$  is defined in Eq. (30), where one has accounted that  $V_2 \sim U_2/3$ . The coefficient by Mathis et al. corresponds to a value  $t_{\text{diff}} \sim 1/(\beta\Omega_2)$ , where  $\Omega_2$  is defined in Eq. (8) and  $\beta$  is a numerical coefficient of about  $1.5 \cdot 10^{-5}$ , determined empirically. The coefficient by Maeder corresponds to  $t_{\text{diff}} \sim [r/(\Omega_2 V_2)]^{1/2}$ , meaning that the timescale considered is that necessary for the differential effects of the Coriolis force to cross the radius. At present, it is still uncertain which coefficient is to be chosen, even if the last two are in numerical agreement.

#### D. Shear mixing and other instabilities

A difference of horizontal velocity  $V$  between two layers may generate a shear instability. The vertical density stratification (along axis  $z$  or  $r$ ) favors stability and the balance of the two effects has to be considered. The criterion expressing the instability is known as the Richardson criterion, it is

$$\mathcal{R}i \equiv \frac{g}{\varrho} \frac{d\varrho/dz}{(dV/dz)^2} < \mathcal{R}i_{\text{crit}}. \quad (35)$$

The critical Richardson number is often taken equal to  $1/4$ , some studies suggest a value up to  $1.0$  (Canuto, 2002). The criterion says that an instability develops if the excess of energy  $\mathcal{R}i_{\text{crit}} \varrho (\delta V)^2$  in the differential motions (with respect to an average velocity) is bigger than the work  $g \delta \varrho \delta z$  necessary to exchange the matter vertically. The criterion can be expressed in term of the Brunt–Väisälä frequency  $N$ , i.e. the frequency of oscillatory motions under the restoring force of gravity,

$$\mathcal{R}i \equiv \frac{N^2}{(dV/dz)^2} < \mathcal{R}i_{\text{crit}}, \quad \text{with} \quad N^2 = \frac{g \delta}{H_P} \left( \nabla_{\text{ad}} - \nabla + \frac{\varphi}{\delta} \nabla_{\mu} \right). \quad (36)$$

The density stratification, in particular in regions with a high  $\mu$  gradient, is generally able to prevent the shear instability. However, the thermal diffusivity of a displaced fluid element weakens the stabilizing effect of the thermal stratification and this may lead to a significant mixing. The left hand of Eq. (36) is then multiplied by  $v \ell / (6K)$ , where  $v$  and  $\ell$  are the velocity and lengthscale of the vertical motions (the factor 6 applies to a spherical fluid element).  $K$  is the thermal diffusivity  $K = 4acT^3 / (3\kappa \varrho^2 C_P)$ . The criterion is then (Maeder, 1995; Zahn, 1992)

$$\mathcal{R}i \equiv \frac{N^2}{(dV/dz)^2} \frac{v \ell}{6K} < \mathcal{R}i_{\text{crit}}. \quad (37)$$

For constant  $\mu$ , the coefficient for the vertical diffusion by shears is easily expressed. One supposes that the turbulent diffusion is dominated by the largest eddies satisfying the Richardson's criterion

$$D_{\text{shear}} = \frac{1}{3} v \ell = 2 \mathcal{R}i_{\text{crit}} K \frac{(dV/dz)^2}{N^2}. \quad (38)$$

This coefficient expresses the transport of the elements and of the angular momentum produced by shear turbulence in an homogeneous medium, with appropriate averages on isobars (Maeder, 2009). In principle, the thermal gradient is slightly modified by the turbulence due to the shears, however this effect is often ignored.

In a zone with variable  $\mu$ , the situation is different. The horizontal turbulence tends to reduce the composition difference between the turbulent eddies and their surroundings. Thus, the restoring force of buoyancy is smaller and the shear instability is favored. The resulting coefficient becomes (Talon & Zahn, 1997)

$$D_{\text{shear}} = 2 \mathcal{R}i_{\text{crit}} \frac{(dV/dz)^2}{\frac{N_{T,\text{ad}}^2}{K + D_h} + \frac{N_{\mu}^2}{D_h}}, \quad (39)$$

$$\text{with} \quad N_{T,\text{ad}}^2 = \frac{g \delta}{H_P} (\nabla_{\text{ad}} - \nabla) \quad \text{and} \quad N_{\mu}^2 = \frac{g}{H_P} \varphi \nabla_{\mu}. \quad (40)$$

The horizontal turbulence favors the diffusion by the shear, reducing the inhibiting effect of the  $\mu$ -gradient.

There are other possible instabilities, which may play a role in differentially rotating stars (baroclinic instabilities). The Goldreich-Schubert-Fricke (GSF) instability (Goldreich & Schubert, 1967) which says that instability arises if

the  $T$  gradient, with account for thermal and viscous diffusivities, is insufficient to compensate for the growth of the centrifugal force during an arbitrary small displacement. If there is a significant  $\mu$ -gradient, the instability is killed, thus it is generally not important. Another possible instability is the so-called Axisymmetric-BaroClinic-Diffusive (ABCD) instability (Knobloch & Spruit, 1983; Talon & Zahn, 1997). If a fluid element moves over an arbitrary displacement from point A to C, it is brought back to C due to the conservation of angular momentum. However, in C the fluid eddy may be hotter than the surroundings (since the lines of constant  $\Omega$  and  $T$  do not necessarily coincide in a baroclinic star). Due to thermal diffusivity, the fluid element loses some energy on its way. Thus, when back to A, the eddy is cooler and it overpasses its equilibrium position and the oscillation amplitude grows. The viscosity due to the horizontal turbulence tends to suppress this instability. On the whole, one must say that the real importance of the GSF and ABCD instabilities is still uncertain.

## V. ROTATION AND MAGNETIC FIELDS

All the way from star formation to the endpoints, rotation and magnetic fields may be interacting. From the initial molecular clouds to the present Sun, the specific angular momentum decreases by a factor  $\sim 10^6$ . During the pre-MS phase, disk locking is a major effect for this reduction (Hartmann, 1998). Fields of  $\sim 1$  kG are sufficient for coupling a solar type star with an extended accretion disk. The contracting star is bound to its disk and it keeps the same angular velocity during contraction, thus losing lots of angular momentum. In solar type stars, the magnetic field creates a strong coupling between the star and the solar wind, which leads to further losses of angular momentum during the end of the pre-MS phase and the MS phase (Kawaler, 1988; Krishnamurthi et al., 1997).

Spectropolarimetric surveys have obtained evidences for the presence of magnetic field at the surface of OB stars (see e.g. the recent review by Walder et al., 2011, and references therein). The origin of these magnetic fields is still unknown. It might be fossil fields (e.g. the spectral characteristics of Of?p stars are indicative of organized magnetic fields, most likely of a fossil origin according to Wade et al., 2010b), or fields produced through a dynamo mechanism. Recent simulations by Cantiello et al. (2010) of subsurface convective zone in massive stars show dynamo-generated magnetic fields of the order of one kG. According to these authors, these magnetic fields might reach the surface of OB stars.

A big question is whether there is a dynamo working in internal radiative zones. This could have far reaching consequences concerning the mixing of the elements and the loss of angular momentum. This question is also essential regarding the rotation periods of pulsars and the origin of GRBs (Sect. VIII.D and XI.B). It may also be important in order to explain the flat profile of the internal rotation of the Sun (Eggenberger et al., 2005). Note that an alternative process has been invoked to explain this feature, the action of internal gravity waves (Charbonnel & Talon, 2005).

### A. Some properties of a dynamo in a radiative zone

We examine some properties of a dynamo in a radiative region. A particular case is the Tayler–Spruit dynamo (Spruit, 2002) and we are using many equations of this dynamo (Maeder & Meynet, 2005a). Some numerical simulations (Braithwaite, 2006; Zahn et al., 2007) confirm the existence of a magnetic instability, however the existence of the dynamo is still controversial.

The two quantities we are mainly interested in for stellar evolution are the magnetic viscosity  $\nu$ , which expresses the mechanical coupling due to the magnetic field  $\vec{B}$ , and the magnetic diffusivity  $\eta$  which expresses the transport by a magnetic instability and thus also the damping of the instability. Some general expressions for these two quantities may be derived. Let us first examine the energy conservation. The rate of magnetic energy production  $W_B$  per unit of time and volume is of the same order of magnitude as the rate  $W_\nu$  of dissipation of the excess of rotational energy by the magnetic viscosity  $\nu$ . The differential motions in shellular rotation give velocity differences  $dv = r d\Omega$ . The amount of energy dissipated during a time  $dt$  for an element of matter  $dm$  in a volume  $dV$  is

$$W_\nu = \frac{1}{2} dm (dv)^2 \frac{1}{dV} \frac{1}{dt} = \frac{1}{2} \varrho \nu \left( \frac{dv}{dr} \right)^2 = \frac{1}{2} \varrho \nu \Omega^2 q^2 \quad \text{with} \quad q = r |\nabla \Omega| / \Omega, \quad (41)$$

because the viscous time is  $dt = (dr)^2 / \nu$ . The magnetic energy density is  $u_B = B^2 / (8\pi)$ , it is produced within the characteristic growth time of the magnetic field  $\sigma_B^{-1}$ , thus the rate  $W_B$  of magnetic energy creation by unit of volume and time is

$$W_B = \frac{B^2}{8\pi} \sigma_B = \frac{1}{2} \omega_A^2 r^2 \sigma_B \varrho, \quad (42)$$

where we have used the expression of the Alfvén frequency  $\omega_A = \frac{B}{r(4\pi\rho)^{1/2}}$ . Let us assume  $W_\nu = W_B$ , i.e. that the excess of energy in the differential rotation is converted to magnetic energy by unit of time. This gives for the viscosity coefficient of magnetic coupling

$$\nu = \frac{\omega_A^2 r^2 \sigma_B}{\Omega^2 q^2}. \quad (43)$$

This coefficient intervenes in the expression for the transport of angular momentum, in the Lagrangian form as given by Eq. (27). Compared to the energy available for the solar dynamo, the amount of energy available from differential rotation is very limited.

If due to an instability, some vertical motions with an amplitude  $l_r/2$  occur around an average position, the restoring buoyancy force produces vertical oscillations at the Brunt–Väisälä frequency  $N$ . The restoring oscillations will have an average density of kinetic energy  $u_N = f \rho l_r^2 N^2$ , where  $f$  is of the order of unity. The magnetic field must overcome the buoyancy effect, which implies  $u_B > u_N$ , otherwise the restoring force of gravity would counteract the magnetic instability at the dynamical timescale. From this condition, one obtains  $l_r^2 < \frac{1}{2f} r^2 \frac{\omega_A^2}{N^2}$ . If,  $f = \frac{1}{2}$ , we have the condition (Spruit, 2002)

$$l_r < r \frac{\omega_A}{N}. \quad (44)$$

An unstable vertical displacement of size  $l_r$  of the azimuthal field of lengthscale  $r$  and intensity  $B_\varphi$  also feeds a radial field component  $B_r$ . The relative sizes of these two field components are defined by the induction equation, which gives the following scaling over the time  $\delta t$  characteristic of the unstable displacement,  $B_r \approx \delta B \approx \frac{1}{r} \frac{l_r}{\delta t} B_\varphi \delta t$ . For the maximum displacement  $l_r$  given by Eq. (44), this gives

$$\frac{B_r}{B_\varphi} \approx \frac{l_r}{r}, \quad (45)$$

which provides an estimate of the ratio of the radial to azimuthal fields.

Let us now consider the magnetic diffusivity  $\eta$ , which damps the instability. The thermal diffusivity  $K$  produces heat losses from the unstable fluid elements and thus reduces the buoyancy forces opposed to the magnetic instability. Both effects have to be accounted for. If the radial scale of the vertical instability is small, the perturbation is quickly damped by the magnetic diffusivity  $\eta$  (in  $\text{cm}^2 \text{s}^{-1}$ ). The radial amplitude must satisfy the relation,

$$l_r^2 > \frac{\eta}{\sigma_B}, \quad (46)$$

where, as seen above,  $\sigma_B$  is the characteristic frequency for the growth of the instability. The combination of the two limits (44) and (46) gives for the case of marginal stability,

$$\eta = \frac{r^2 \omega_A^2 \sigma_B}{N^2}. \quad (47)$$

For given  $\eta$  and  $\sigma_B$ , this provides the minimum value of  $\omega_A$ , and thus of the magnetic field  $B$ , for the instability to occur. The instability is confined within a domain, limited on the large side by the stable stratification (44) and on the small scales by magnetic diffusion (46). For the case of marginal stability, which is likely reached in evolution, this equation relates the magnetic diffusivity  $\eta$  and the Alfvén frequency  $\omega_A$ .

The Brunt–Väisälä frequency  $N$  of a fluid element displaced in a medium with account of both the magnetic and thermal diffusivities  $\eta$  and  $K$  is (Maeder & Meynet, 2004),

$$N^2 = \frac{\frac{\eta}{K}}{\frac{\eta}{K} + 2} N_{T,\text{ad}}^2 + N_\mu^2, \quad (48)$$

with  $N_{T,\text{ad}}^2$  and  $N_\mu^2$  defined in Eq. (40). The ratio  $\eta/K$  of the magnetic to thermal diffusivities determines the heat losses. The factor of 2 is determined by the geometry of the instability, a factor of 2 applies to a thin slab, for a spherical element a factor of 6 is appropriate (Maeder & Meynet, 2005b). In the interior of a  $15 M_\odot$  star,  $\eta/K$  lies between  $10^{-6}$  and  $10^{-2}$ . Thus the  $T$ -stratification only has a little stabilizing effect, compared to the  $\mu$ -gradient.

Let us now examine the magnetic coupling, The momentum of force  $\vec{S}$  by volume unity due to the magnetic field is obtained by writing the momentum of the Lorentz force  $\vec{F}_L$ . The current density  $\vec{j}$  is given by the Maxwell equation  $\frac{4\pi}{c} \vec{j} = \vec{\nabla} \times \vec{B}$ . Thus, one has

$$\vec{S} = \vec{r} \times \vec{F}_L = \frac{1}{c} \vec{r} \times (\vec{j} \times \vec{B}) = \frac{1}{4\pi} \vec{r} \times ((\vec{\nabla} \times \vec{B}) \times \vec{B}), \quad (49)$$

$$\text{in modulus } S \approx \frac{1}{4\pi} B_r B_\varphi = \frac{1}{4\pi} \left( \frac{l_r}{r} \right) B_\varphi^2 = \rho r^2 \left( \frac{\omega_A^3}{N} \right). \quad (50)$$

The units of  $S$  are  $\text{g s}^{-2} \text{cm}^{-1}$ , the same as for  $B^2$  in the Gauss system. The kinematic viscosity  $\nu$  (in  $\text{cm}^2 \text{s}^{-1}$ ) for the vertical transport of angular momentum is

$$\nu = \frac{\eta}{\varrho} = \frac{1}{\varrho} F \frac{dr}{dv} = \frac{1}{\varrho} F \frac{dr}{r d\Omega} = \frac{1}{\varrho} F \frac{d \ln r}{\Omega d \ln \Omega}, \quad (51)$$

where  $F$  is a force by surface unity, which also corresponds to a momentum of force by volume unity in  $\text{g s}^{-2} \text{cm}^{-1}$ .  $\vec{F}$  is applied horizontally to a slab of velocity  $v$  in a direction perpendicular to  $r$ . Considering only positive quantities, with  $q = |d \ln \Omega / d \ln r|$ , one has

$$\nu = \frac{S}{\rho q \Omega} = \frac{\omega_A^3 r^2}{N q \Omega}. \quad (52)$$

Now, we can compare this expression for  $\nu$  to Eq. (43) and get

$$\sigma_B = \frac{\omega_A \Omega q}{N}, \quad (53)$$

which relates the growth rate of the magnetic field to its amplitude (through  $\omega_A$ ).

## B. The basic equations

Introducing the expression (53) of  $\sigma_B$  in Eq. (47), we get

$$\eta = r^2 \Omega q \left( \frac{\omega_A}{N} \right)^3. \quad (54)$$

Also, with the expression (48), we can write for  $\sigma_B^2$

$$\sigma_B^2 = \frac{\omega_A^2 \Omega^2 q^2}{\frac{\eta}{\frac{K}{K+2}} N_{T,\text{ad}}^2 + N_\mu^2}. \quad (55)$$

These equations are quite general. If the growth rate  $\sigma_B$  of the instability is known, the two equations (54) and (55) form a system of 2 equations with 2 unknowns  $\eta$  and  $\omega_A$ .

## C. The case of Tayler–Spruit dynamo

A purely toroidal field  $B_\varphi(r, \vartheta)$ , even very weak, in a stable stratified star is unstable on an Alfvén timescale  $1/\omega_A$  (Tayler, 1973). This is the first magnetic instability to appear. It is non-axisymmetric of type  $m = 1$  (Spruit, 1999, 2002), it occurs under a wide range of conditions and is characterized by a low threshold and a short growth time. For an azimuthal field consisting of concentric loops around the rotation axis, the instability appears as low-azimuthal order displacements of rings (Fig. 6). Due to the magnetic pressure, the magnetic loops move apart from the rotation axis, like a disordered heap of tires, as described by Spruit. The pressure is released by sideways motions. In a rotating star, the instability is also present (Pitts & Tayler, 1985), however the growth rate  $\sigma_B$  of the instability is, if  $\omega_A \ll \Omega$ ,

$$\sigma_B = \frac{\omega_A^2}{\Omega}, \quad (56)$$

instead of the Alfvén frequency  $\omega_A$ , because the growth rate of the instability is reduced by the Coriolis force (Spruit, 2002). One usually has the following ordering of the different frequencies,  $N \gg \Omega \gg \omega_A$ . In the Sun, one has  $N \approx 10^{-3} \text{ s}^{-1}$ ,  $\Omega = 3 \times 10^{-6} \text{ s}^{-1}$  and a field of 1 kG would give an Alfvén frequency as low as  $\omega_A = 4 \times 10^{-9} \text{ s}^{-1}$ .

The frequency  $\sigma_B$  being known, the system of Eqs. (54) and (55) is defined and the 2 unknown  $\eta$  and  $\omega_A$  can be obtained (Maeder & Meynet, 2005b). When  $N_\mu$  dominates, which occurs around the stellar core, one has

$$\frac{\omega_A}{\Omega} = q \frac{\Omega}{N_\mu} \quad \text{and} \quad \eta = r^2 \Omega q^4 \left( \frac{\Omega}{N_\mu} \right)^6. \quad (57)$$

This shows that the mixing of the elements decreases strongly for large  $\mu$  gradients and grows fast for large differential rotation. The ratio  $\omega_A/\Omega$  has to be equal or larger than the minimum value defined by (47). This leads to a condition on the minimum differential rotation for the dynamo to work (Spruit, 2002),

$$q > \left( \frac{N}{\Omega} \right)^{7/4} \left( \frac{\eta}{r^2 N} \right)^{1/4}, \quad (58)$$

When  $N^2$  is large, as for example when there is a significant  $\mu$  gradient, the differential rotation necessary for the dynamo to operate must also be large.

Fig. 7 shows the differences of the internal  $\Omega$ -profiles during the evolution of a 20  $M_\odot$  star with and without magnetic field created by the Tayler–Spruit dynamo. Without magnetic field, the star has a significant differential rotation, while  $\Omega$  is almost constant when a magnetic field created by the dynamo is present. It is not perfectly constant, otherwise there would be no dynamo. In fact, the rotation rapidly adjusts itself to the minimum differential rotation necessary to sustain the dynamo.

## VI. RECENT GRIDS OF MODELS OF MASSIVE ROTATING STARS

In the recent years, many grids of massive rotating stellar models have been computed. A non-exhaustive list is given in Table I. These models have been computed accounting for the effects of rotation in the frame of the theory exposed in the previous sections. We have indicated those models which were computed with the dynamo theory of Spruit (1999, 2002). Although the physics of rotation (and magnetic field when accounted for) is the same in all those models, the numerical implementations differ. Let us just mention here a few relevant differences. Some codes treat the transport of the angular momentum through a diffusion equation, not accounting for the advective nature of this equation. As explained above this may produce error not only on the amplitude of the effect but also on its sign! However, this statement should be tempered by the fact that for most of the MS phase, the region where the transport of angular momentum is transported efficiently, *i.e.* in the Gratton–Öpik cell, angular momentum is transported outwards as would do a diffusion mechanism. 2) Rotating models contain uncertain parameters, at least two. One is in the expression of  $D_{\text{shear}}$  and account for the uncertainties pertaining our knowledge of the critical Richardson number (see Section IV.D). The other is in the expression of  $D_h$ , whose amplitude remains difficult to obtain from first principles. This coefficient has to be much greater than the one of  $D_{\text{shear}}$  in order to allow “shellular rotation” to set in. Some models listed in Table I contain additional parameters, as a  $f_\mu$ , a factor multiplying the mean molecular weight gradient. A small value of this parameter decreases the effects of the  $\mu$ -barrier and facilitates mixing. To constrain the values of these uncertain parameters, some guidelines deduced from laboratory experiments or from multi-D dimensional simulations are used. Some authors also calibrate these uncertain parameters in order to achieve mean observed surface enrichments during the MS phase of B-type stars with models having an average rotational velocity.

A few authors have built 2D models for rotating stars (Deupree, 1990; Espinosa Lara & Rieutord, 2007; Roxburgh, 2006). For instance, ZAMS models with arbitrary rotation laws have been computed by Deupree (2001). The variation with the latitude of the effective temperature for rotationally deformed stars from a 2D stellar structure is given by Lovekin et al. (2006). Non radial oscillations are computed for 2D rotating massive models by Lovekin & Deupree (2008). Effects of rotation on the pulsation frequencies has been investigated recently by Deupree & Beslin (2010); Lovekin et al. (2009).

## VII. THE ELEMENT ABUNDANCES IN MASSIVE STARS

Both mass loss and rotational mixing affect the evolution of the chemical abundances at the stellar surface of massive stars. At solar abundances, mass loss dominates in stars initially more massive than about 30  $M_\odot$ , while rotation dominates below this mass limit. Let us first examine the effect of mass loss in the most massive stars.

### A. Model effects of mass loss on abundances

Fig. 8 shows the internal evolution of a star with an initial  $60 M_{\odot}$ . The removal of the outer layers reveals the internal composition. There are 5 typical domains of composition, which result from a progression in the exposition of nuclear products.

- 1. *The initial abundances.* Mass loss does in general not change the surface composition in OB stars during the MS phase, except for stars above  $60 M_{\odot}$ .
- 2. *Intermediate abundances.* This stage is characterized by partial CNO processing with possible dilution effects. There are N enrichments, enhancements of the  $^{13}\text{C}/^{12}\text{C}$  ratio, C depletions and modest O depletions. This is typical of blue and red supergiants.
- 3. *CNO equilibrium with H present.* CNO equilibrium is reached before H exhaustion. The C/N and O/N ratios are reduced by two orders of a magnitude with respect to cosmic abundances. This is the case of WR stars (bare cores) of types WNL.
- 4. *CNO equilibrium with H absent.* The He mass fraction is 98%, the CNO ratios are the same as before. This stage corresponds to WR stars of type WNE. The abundances are model independent, being determined mainly by nuclear cross-sections.
- 5. *Partial He burning.* The products of He burning, i.e.  $^{12}\text{C}$ ,  $^{16}\text{O}$ ,  $^{22}\text{Ne}$  are visible. The changes are abrupt (rotation make them smoother). The abundances depend strongly on the models (mass loss, mixing, etc.). This stage corresponds to WC stars and to WO stars for O/C ratios  $> 1$ .

Of course, not all stars go through this whole sequence: the smaller the initial mass and/or metallicity, the shorter the path. Rotation may accelerate and make smoother the evolution of surface composition, due to the contribution of internal mixing.

### B. The effects of rotation on the surface abundances

In the mass range below about  $30 M_{\odot}$ , mass loss has little effect during the MS phase. The changes of abundances, if any, are due to mixing. Fig. 9 shows the run of the diffusion by shear turbulence,  $D_{\text{shear}}$ , and by the net effect of both meridional currents and horizontal shear turbulence,  $D_{\text{eff}}$ , at three different stages during the MS phase of a rotating  $20 M_{\odot}$  model. The main mixing effect is the diffusion by shear turbulence, which results from the internal  $\Omega$  gradients built during evolution. To a smaller extent, meridional circulation makes some transport, however mainly of angular momentum.

Mixing brings to the surface the products of CNO burning: mainly  $^{14}\text{N}$  and  $^{13}\text{C}$  enrichments,  $^{12}\text{C}$  is depleted with limited  $^4\text{He}$  enrichment and  $^{16}\text{O}$  depletion. Fig. 10 shows the predicted variations of  $\log(N/H)$  during MS evolution as a function of the initial masses (Meynet & Maeder, 2000). ( $N/H$ ) is here the abundance ratio of N and H in numbers. Without rotational mixing, there would be no enrichment until the red supergiant stage, but rotation produces an increase (depending on velocity  $v$ ) of N/H during the MS phase. The N excesses also depend on the ages  $t$ . The increase is modest during the first third of the MS phase, because the elements need some time to reach the surface, then it is more rapid. The N enrichments are larger for larger masses  $M$ .

Fig. 11 shows, for given  $M$  at  $Z = 0.02$ , the evolution of the N excesses with age for different initial velocities. It shows that there is no single relation between  $v \sin i$  and the N/H excesses for a mixture of ages. The same is true for a mixture of different masses. Binarity may also affect the N and He enrichments due to tidal mixing and mass transfer. A binary star with low rotation may have a high N/H due to tidal mixing or due to the transfer of the enriched envelope of a red giant. At the opposite, a binary star may also have a high  $v \sin i$  and no N/H excess, in the case of the accretion of an unevolved envelope bringing a lot of angular momentum. On the whole, the N excess is a multivariate function

$$\Delta \log(N/H) = f(M, t, v \sin i, \text{multiplicity}, Z) . \quad (59)$$

Models with lower initial metallicities  $Z$  have higher N enrichments for given  $M$  and  $v$  (Maeder & Meynet, 2001a; Meynet et al., 2006). The reason is the higher  $\Omega$ -gradients, resulting from the absence of the Gratton–Öpik circulation cell (Sect. IV.B). The excesses become very strong at metallicities  $Z$  as low as  $10^{-8}$ .

### C. The observed N/H excesses

The amplitudes of the N enrichments at the end of the MS phase in massive stars form a reference point telling us the importance of mixing. The data at different  $Z$  (mean and largest values) are summarized in Table II from a number of sources (see references below the Table). In the lowest mass range considered ( $6.6\text{--}8.2 M_{\odot}$ ), small excesses

of He/H are still present (Lyubimkov et al., 2004), they are larger in the Small Magellanic Cloud (SMC,  $Z \approx 0.004$ ). We see the following facts:

- On the average, the N enrichments are larger for larger masses.
- The N enrichments are larger at lower  $Z$ .
- Away from the ZAMS, but still in the Main Sequence, the He and N enrichments are larger and they are even larger in the supergiant stages. These various features are quite consistent with the predicted properties of rotational mixing as can be seen in Fig. 12.
- Correlations between N or He excesses and the observed  $v \sin i$  have been found in the upper part of the MS band (Lyubimkov et al., 2004), in agreement with model predictions.

To find a correlation for a multivariate function like N/H with some parameter like  $v \sin i$ , it is necessary to limit as much as possible the range of the other involved parameters. Otherwise, the conclusions may be erroneous. From Fig. 13, we note that data samples limited in masses and ages support a N enrichment depending on rotational velocities. Stars beyond the end of the MS phase do not obey to such a relation, because their velocities converge toward low values (Meynet & Maeder, 2000). A fraction, which we estimate to be less than  $\sim 20\%$  of the stars, may escape to the relation as a result of binary evolution or due to some other mechanisms as for instance magnetic braking (Meynet et al., 2011). This latter mechanism might explain some magnetic stars showing large N-excesses and low  $v \sin i$  (Henrichs et al., 2003a,b).

To obtain more tight constraints on the models, very careful and accurate abundance analysis are required. Very interestingly Przybilla et al. (2010) showed that observed ratios of N/O and N/C follows a well defined relation in the N/O versus N/C plane, which does not depend on the models but just on the CNO nuclear reactions properties. In the future, this characteristic can be used to test the surface abundances obtained from spectral analysis before these abundances are used to constrain the stellar models.

According to Hunter et al. (2007) main-sequence binary objects have close to baseline nitrogen surface abundances. These systems thus do not present apparent signs of extra-mixing. In contrast several evolved binary objects have high nitrogen enhancements. These abundances are similar to those observed in apparently single stars. Thus it appears difficult to discriminate among the possible causes of the enrichments in binaries, *i.e.* between extra-mixing operating in single stars and mass-transfer events in close binary systems. The same result has been obtained by Trundle et al. (2007).

#### D. The observed He excesses

Surface enrichments in helium have been observed with the following main trends:

- He in O-type stars in the SMC: In the SMC, for 31 O-type stars, Mokiem et al. (2006) find values of  $y = n_{\text{He}}/(n_{\text{H}} + n_{\text{He}})$  between 0.09 and 0.24, where  $n_{\text{He}}$  is the density number of helium and  $n_{\text{H}}$  of hydrogen. Note that  $n_{\text{He}}/(n_{\text{H}} + n_{\text{He}}) = Y/(Y + 4X)$ , where  $Y$  and  $X$  are respectively the mass fraction of helium and of hydrogen. Setting  $Y \sim 1 - X$ , one obtains values for  $Y = 4y/(1 + 3y)$  between 0.28 and 0.56 (here 0.28 would correspond to  $y=0.09$  *i.e.* to the initial helium mass fraction). These authors conclude that while rotation can qualitatively account for such enrichments, the observed enrichments are in many cases much stronger than those predicted by the models.
- He in O-type stars in the Large Magellanic Cloud (LMC): In the LMC, for 28 O-type stars,  $y$  values between about 0.09 and 0.28 are obtained by Mokiem et al. (2007), *i.e.* helium mass fractions between 0.28 and 0.61.
- He in OB-type stars in the Milky Way (MW): Huang & Gies (2006b) determine He abundances for OB galactic stars. In their high mass range ( $8.5 M_{\odot} < M < 16 M_{\odot}$ ), the He enrichment progresses through the main sequence and is greater among the faster rotators<sup>1</sup>. On average He abundance increases of  $23\% \pm 13\%$  between ZAMS and TAMS. These authors also obtain that He enrichments are higher for higher  $v \sin i$  values. Lyubimkov et al. (2004) find an increase during the MS phase in He abundance of 26% for stars in the mass range 4-11  $M_{\odot}$  and 67% for more massive stars in the range 12-19  $M_{\odot}$ .

---

<sup>1</sup> These authors also found many helium peculiar stars (He-weak and He-strong). These stars were not used to study the process of He-enrichment.



From a theoretical point of view, one expects that the N-enrichment occurs very rapidly at the surface well before any surface helium enrichment. This is of course due to the fact that very rapidly the nitrogen abundance increases at the centre creating thus a strong chemical gradient between the core and the envelope. Since diffusive velocity is greater when the gradient of abundance is greater, the presence of such a strong gradient favors a rapid mixing. The gradient of helium in stellar interiors is built up on much longer timescales than the gradient in nitrogen. As a consequence, the diffusion of this element is expected to be much less rapid than that of nitrogen. Thus any strong He-enhancement should be accompanied by a very strong nitrogen enhancement. At the moment, the observations of both He- and N-enrichments in the same stars are too scarce to check this trend.

## VIII. EVOLUTION OF ROTATION AT THE SURFACE AND IN THE INTERIOR

### A. Initial conditions for rotating models

Ideally one would like to know the shape of the distribution of rotational velocities on the ZAMS for the whole mass and metallicity ranges spanned by the stars during the whole cosmic history. This is of course not an easy task and many difficulties have to be overcome. Let us just mention the main ones here:

- First, most observations concern non-ZAMS stars, whose surface velocity is not representative of the initial stellar velocity. In order to obtain ZAMS velocities some theoretical guidelines have to be used. For instance, using stellar models, it is possible to deduce which are the velocities needed on the ZAMS in order to achieve a given mean velocity during the MS phase.
- What is measured through Doppler broadening is  $v \sin i$  and thus a sufficiently great number of stars need to be measured in order to correct in a statistical way for the effect of the inclination angle.
- There are theoretical reasons for believing that beyond a velocity limit the line broadening due to rotation saturates, making this method inappropriate for measuring velocities near the critical limit. This is because when the velocity approaches the critical one, the equator, which has the higher linear velocities, darkens and thus contributes less to the line formation than the regions of the star near to the pole which have the smaller linear velocities.

It is also worthwhile to underline the fact that even if we knew very well the distributions of the surface velocities, this would not help in determining the initial distribution of  $\Omega$  inside the star. Hopefully asteroseismology will allow us to obtain such information, but presently the indications are still scarce (see however results presented in Aerts, 2008)<sup>2</sup>. Also interferometry, which allows us to measure the shape of fast rotating stars, can give some indications on how the interior rotate. For instance a ratio of the equatorial radius to the polar radius equal to 1.5 when the star rotates at the critical limit implies that the interior is not much deformed, in agreement with the Roche approximation.

The knowledge of the interior distribution of  $\Omega$  would be important for estimating the total angular momentum of the star on the ZAMS. At present time, stellar models make the simplifying hypothesis that the evolution starts with a flat profile of  $\Omega$ . The exact shape of the initial profile of  $\Omega$  is not so important for the further evolution of  $\Omega$  inside the star. It has been found that the initial distribution of the angular momentum inside the star is rapidly forgotten and erased by a rapid convergence of the profile of  $\Omega$  towards an equilibrium profile (Denissenkov et al., 1999). This results from two counteractive effects: on one hand meridional currents build  $\Omega$  gradient (which tends to increase  $\Omega$  in the inner layers) and on the other hand shear turbulence tends to decrease the  $\Omega$  gradient.

The mean initial angular momentum of a model star on the ZAMS,  $\mathcal{L}_{ini}$ , is estimated as the value needed for the star to rotate at the observed average rotational velocity during the MS phase. The inertia momentum of a  $10 M_{\odot}$  star on the ZAMS is of the order of  $10^{56} \text{ g cm}^2$ . Considering a radius  $R \sim 4R_{\odot}$  and a surface equatorial velocity,  $v_{eq}$ , of  $200 \text{ km s}^{-1}$  (see Fig. 1), one obtains for  $\Omega = v_{eq}/R = 0.00007 \text{ s}^{-1}$ , and a total angular momentum content of the order of  $10^{52} \text{ g cm}^2 \text{ s}^{-1}$  assuming the star rotates as a solid body on the ZAMS. These are the typical initial angular momentum which are considered in stellar models.

---

<sup>2</sup> See Table 1 in this reference. Two stars present a high contrast between the angular velocity of the core and that of the envelope, between a factor 4 and 5. One star does not show any contrast. All the three stars are slow rotators and are B2-B3 stars with class luminosity between V and III.

## B. Evolution of the surface velocities

Once the initial conditions have been chosen, models predict the evolution of the surface velocity as a function of time. The evolution of  $v$  in the HR diagram is shown in Fig. 14 ( $v_{\text{ini}} = 300 \text{ km s}^{-1}$  on the zero-age main sequence). Lines of constant  $v$  are indicated. On the MS, we notice the decrease of the surface velocity as a function of time. This trend is confirmed by the observations of Huang & Gies (2006b) who show that all OB stars of their sample experience a spin-down during the MS phase. A few relatively fast rotators are found near the end of the MS phase. According to these authors, these stars may be spun up by a short contraction phase or by mass transfer in a close binary. In Fig. 14, we see also that the decrease of the surface velocity is much faster for the most massive stars than for stars with  $M \leq 15 M_{\odot}$ , as a consequence of stronger mass losses in the higher mass range. This difference remains also present in the domain of B-supergiants. Interestingly, according to Hunter et al. (2008) there is some evidences that the most massive objects rotate slower than their less massive counterparts. Dufton et al. (2006) confirm that the mean rotational velocity of stars which have strong winds is lower than that of the lower mass stars.

A few other points can be noted: the average  $\bar{v}$  is lower for O-type stars than for the early B-type stars (Slettebak, 1970). Again this may be the consequence of the higher losses of mass and angular momentum in the most massive stars. Also, we remark that the increase of  $\bar{v}$  from O-stars to B-stars is larger for the stars of luminosity class IV than for class V (Fukuda, 1982). This is consistent with the models, which show (cf. Fig. 14) that the differences of  $\bar{v}$  between O- and B-type stars are much larger at the end of the MS phase. Another fact in the observed data is the strong decrease of  $\bar{v}$  for the massive supergiants of OB-types. Also during the crossing of the HR diagram, the rotational velocities decrease fast, to become very small, i.e. of the order of a few  $\text{km s}^{-1}$ , in the red supergiant phase. This is predicted by all stellar models (cf. also Langer, 1998) due to the growth of the stellar radii. This is also confirmed by the recent observations of Mokiem et al. (2006) and Hunter et al. (2008). These last authors find from a sample of 400 O- and early B-type stars in the Magellanic Clouds that supergiants are the slowest rotators in the sample, typically having rotational velocities less than  $80 \text{ km s}^{-1}$ .

Note that the models shown in Fig. 14 are models without magnetic fields. When magnetic fields are accounted for as in the Tayler-Spruit dynamo, the evolution of the surface velocity is different. For instance, a  $15 M_{\odot}$  model with  $v_{\text{ini}} = 300 \text{ km s}^{-1}$  on the ZAMS and computed with magnetic fields, keeps a nearly constant surface velocity around  $300 \text{ km s}^{-1}$  all along the MS phase. Without magnetic fields, the velocity decreases during the MS phase. The average velocity is around  $240 \text{ km s}^{-1}$  (see Fig. 3 in Maeder & Meynet, 2004).

Fig. 15 clearly illustrates the very different evolution of the rotational velocities of a  $60 M_{\odot}$  at various metallicities. At low  $Z$  like in the models at  $Z = 10^{-5}$ , the growth of  $\frac{\Omega}{\Omega_c}$  is possible because of the very small mass loss by stellar winds. In view of these results, it is likely that at very low  $Z$  a large fraction of the massive stars reach their break-up velocities (see right panel of Fig. 24). This question is of high importance, because if the massive stars reach their break-up velocity, most of their evolutionary and structural properties will be affected. For example, they could also lose a lot of mass and produce some Wolf-Rayet (WR) stars. They would have a relatively small remaining mass at the time of the supernova explosion, like their counterparts at solar composition. Interestingly, the trend illustrated above is supported by Hunter et al. (2008) who obtain that SMC metallicity stars rotate on average faster than galactic ones (mainly field objects) and by Martayan et al. (2007), who find that, for B and Be stars, the lower the metallicity, the higher the rotational velocities.

## C. The Be stars and the evolution towards the critical velocity

Be stars are emission line stars. Emission originates in a circumstellar outflowing disk. How do these disks form? How long are their lifetimes? Are they intermittent? Are they Keplerian? Many of these questions are still subject of a lively debate. A point however which seems well accepted is the fact that the origin of a disk might be connected to the fast rotation of the star. This view is supported by the fact that objects with Be phenomena are the fastest rotators in the sample studied by Hunter et al. (2008) (400 OB stars in the MCs). This trend has also been found by Martayan et al. (2007, 2006) who obtain that Be stars rotate faster than B stars whatever the metallicity.

Maeder et al. (1999) and Wisniewski & Bjorkman (2006) find that the fraction of Be stars with respect to the total number of B and Be stars in clusters with ages (in years) between 7.0 and 7.4 (in logarithm) increases when the metallicity decreases. This fraction passes from about 10% at solar metallicity to about 35% at the SMC metallicity. These significant proportions imply that Be stars may drastically affect the mean  $v \sin i$  obtained for a given population of B-type stars. Very interestingly there appears to be a correlation between the frequency of Be stars and that of red supergiants.

These observations indicate that metallicity plays a role in the Be phenomenon and provides hints on the way surface velocity may evolve differently for stars of different initial metallicities. The correlation of Be star populations with those of red supergiants can be seen as an indication that fast rotation not only favors the formation of Be stars

but also that of red supergiants (see Sect. X.A).

The evolution of surface velocities during the Main Sequence lifetime results from an interplay between meridional circulation (bringing angular momentum to the surface) and mass loss by stellar winds (removing it). The dependence on metallicity of these two mechanisms plays a key role in determining for each metallicity, a limiting range of initial masses (spectral types) for stars able to reach or at least approach the critical limit. Ekström et al. (2008b) computed models (with no account for the Tayler-Spruit dynamo) for initial masses between 3 and 60  $M_{\odot}$  and considered, for each initial mass, models with  $\Omega/\Omega_{\text{crit}}$  equal to 0.1, 0.3, 0.5, 0.7, 0.8, 0.9 and 0.99. The following conclusions have been obtained based on these models:

1. Meridional currents bring angular momentum inwards only at the very beginning of the core H-burning phase. During most of the MS phase, meridional currents transport angular momentum from the inner regions to the outer layers. As long as the mass loss rates are not too important, this brings the  $v/v_{\text{crit}}$  ratio close to 1 during the MS phase for stars having on the ZAMS  $\Omega/\Omega_{\text{crit}} \gtrsim 0.8$ .
2. Since the velocity of the meridional currents in the outer layers scales with the inverse of the density, the process becomes more efficient for stars of higher initial mass and/or higher initial metallicity.
3. At high metallicity however, mass loss becomes more and more important and can prevent the stars from reaching the break-up limit.
4. In stellar clusters, supposing an initial distribution of the rotational velocities as given by Huang & Gies (2006a), one expects that the fraction of stars having  $v/v_{\text{crit}} \geq 0.8$  becomes maximum for ages between 20-32 Myr at  $Z = 0.020$ . This range of ages shifts to older ages at higher metallicities and to younger ages at lower metallicities. Such a shift results from the dependence on metallicity and mass of the intensity of the mass loss rates and of the velocities of the meridional currents. If we look at stars with  $v/v_{\text{crit}} \geq 0.7$ , the maximum number will be found in clusters of ages around 10 Myr and below, and this at all non-zero metallicities.
5. Be stars might be the natural outcome of stars with an initial rotational velocity in the upper tail of the initial velocity distribution.
6. Depending on when the critical velocity is reached, one expects more or less high surface enrichments (see Fig. 12). If the limit is reached very early during the MS phase, no enrichment is expected, while if this limit is reached at the end of the MS phase, high N/C and N/O ratios are expected. However, the enrichment also depends on the initial mass. For stars originating from small initial mass stars (typically from 3  $M_{\odot}$  at standard metallicity) one expects no or small surface enrichments, at whatever time the critical velocity is reached.
7. To reproduce the higher fractions of Be stars at low metallicity, we must assume that in metal poor regions, a higher number of stars are born with high values of  $\Omega/\Omega_{\text{crit}}$ .

#### D. Evolution of the interior angular momentum content

Figure 16 shows the evolution of  $\Omega$  inside the 25  $M_{\odot}$  model from the ZAMS until the end of the core Si-burning phase (Hirschi et al., 2004). The evolution of  $\Omega$  results from many different processes: convection enforces solid body rotation, contraction and expansion respectively increases and decreases  $\Omega$  as a consequence of local conservation of the angular momentum, shear (dynamical and secular) erodes  $\Omega$ -gradients while meridional circulation may erode or build them up and finally mass loss may remove angular momentum from the surface. If during the core H-burning phase, all these processes may be important, from the end of the MS phase onwards, the evolution of  $\Omega$  is mainly determined by convection, the local conservation of the angular momentum and, for the most massive stars by mass loss.

During the MS phase,  $\Omega$  decreases in the whole star. When the star becomes a red supergiant (RSG),  $\Omega$  at the surface decreases significantly due to the expansion of the outer layers. Note that the envelope is gradually lost by winds in the 25  $M_{\odot}$  model. In the centre,  $\Omega$  significantly increases when the core contracts and then the  $\Omega$  profile flattens due to convection.  $\Omega$  reaches values of the order of  $1 \text{ s}^{-1}$  at the end of Si-burning. It never reaches the local break-up angular velocity limit,  $\Omega_c$ , although, when local conservation holds,  $\Omega/\Omega_c \propto r^{-1/2}$ .

Figure 17 shows the evolution of the specific angular momentum,  $j = 2/3 \Omega r^2$ , in the central region of a 25  $M_{\odot}$  stellar model. The specific angular momentum remains constant under the effect of pure contraction or expansion, but varies when transport mechanisms are active. One sees that the transport processes remove angular momentum from the central regions. Most of the removal occurs during the core H-burning phase. Still some decrease occurs during the core He-burning phase, then the evolution is mostly governed by convection, which transports the angular momentum from the inner part of a convective zone to the outer part. This produces the teeth seen in Fig. 17. The

angular momentum of the central regions of the star at the end of Si-burning is essentially the same as at the end of He-burning (by end of He-burning, we mean the time when the central helium mass fraction becomes less than  $10^{-5}$ ). As a numerical example, we calculated, for the  $25 M_{\odot}$  model, the angular momentum of its  $3 M_{\odot}$  remnant. We obtained  $\mathcal{L}_{\text{rem}} = 2.15 \cdot 10^{50} \text{ g cm}^2 \text{ s}^{-1}$  at the end of He-burning and  $\mathcal{L}_{\text{rem}} = 1.63 \cdot 10^{50} \text{ g cm}^2 \text{ s}^{-1}$  at the end of Si-burning. This corresponds to a loss of only 24%. In comparison, the angular momentum is decreased by a factor  $\sim 5$  between the ZAMS and the end of He-burning. This shows the importance of correctly treating the transport of angular momentum during the Main Sequence phase. It means also that, in the frame of the present models, we can obtain a first order of magnitude estimate of the pre-supernova angular momentum of the core at the end of He-burning.

The present models have difficulties in accounting for the observed rotation rates of young pulsars and white dwarfs (see e.g. Heger et al., 2005; Kawaler, 1988; Suijs et al., 2008). More precisely, they predict too fast rotation of the stellar cores in the advanced phases. This may be due to different causes that could lead to additional angular momentum loss from the central regions at different evolutionary phases:

- already during the nuclear lifetime;
- at the time of the supernova explosion in the case of neutron stars, or during the Thermal Pulse Asymptotic Giant Branch (TP-AGB) phase at the time of the superwind episode in the case of white dwarfs;
- during the early evolution of the new born neutron star or white dwarf.

During the MS phase, angular momentum can be efficiently extracted from the core in case the star rotates as a solid body. Such a situation is realized in numerical simulations where the Tayler-Spruit dynamo is accounted for as can be seen in Fig. 7 (see e.g. Maeder & Meynet, 2005b). Heger et al. (2005) find that magnetic torques decrease the final rotation rate of the collapsing iron core by about a factor 30-50 when compared with the nonmagnetic counterparts, allowing to obtain rotation periods of young pulsars which better fit the observations.

## IX. EVOLUTIONARY TRACKS AND LIFETIMES

### A. The Main-Sequence phase

Figure 18 shows the evolutionary tracks of non-rotating and rotating stellar models for initial masses between 9 and  $120 M_{\odot}$  at  $Z=0.020$ . For the rotating stellar models, the initial velocity is  $v_{\text{ini}} = 300 \text{ km s}^{-1}$ . There is little difference between tracks with  $v_{\text{ini}} = 200$  or  $300 \text{ km s}^{-1}$ . If the effects behaved like  $v_{\text{ini}}^2$ , there would be larger differences. The present saturation effect occurs because outward transport of angular momentum by shears are larger when rotation is larger, also a larger rotation produces more mass loss, which makes a larger reduction of rotation during the evolution. Let us note however that for some surface abundance ratios as N/C or N/O, the increase from  $v_{\text{ini}} = 200$  to  $300 \text{ km s}^{-1}$  produces significant changes. Thus, the similarity of the evolutionary tracks does not necessarily imply the similarity of the surface abundances for these elements.

On and near the ZAMS, rotation produces a small shift of the tracks towards lower luminosities and  $T_{\text{eff}}$ . This effect is due to both atmospheric distortions and to the lowering of the effective gravity (see e.g. Collins & Sonneborn, 1977; Kippenhahn & Thomas, 1970; Maeder & Peytremann, 1970). At this stage the star is still nearly homogeneous. When evolution proceeds, the tracks with rotation become more luminous than for no rotation. This results from essentially two effects. On one side, rotational mixing brings fresh H-fuel into the convective core, slowing down its decrease in mass during the MS. For a given value of the central H-content, the mass of the convective core in the rotating model is therefore larger than in the non-rotating one and thus the stellar luminosity is higher (Heger et al., 2000; Maeder, 1987b; Talon & Zahn, 1997).

Rotation reduces the MS width in the high mass range ( $M \sim 40 M_{\odot}$ ). Let us recall that when the mass increases, the ratio of the diffusion timescale for the chemical elements to the MS lifetime decreases. This can be shown in the following way: let us call  $\tau_{\text{diff}}$  the diffusion timescale which is proportional to  $R^2/D$  where  $R$  is the radius and  $D$  the diffusion coefficient. For shear mixing,  $D$  is proportional to  $K = 4acT^3/(3\kappa\rho^2c_P)$ , the thermal diffusivity. Using homology relations, it can be shown that  $\tau_{\text{diff}}$  varies as  $1/M^{1.8}$ . Now the MS lifetime,  $\tau_{\text{MS}}$ , for stars with initial masses greater than  $15 M_{\odot}$  varies as  $1/M^{0.8}$ , therefore the ratio  $\tau_{\text{diff}}/\tau_{\text{MS}}$  varies as  $M^{-1.1}$ . As a consequence, starting with the same  $v_{\text{ini}}$  on the ZAMS, massive stars will be more mixed than low mass stars at an identical stage of their evolution. This reduces the MS width since greater chemical homogeneity makes the star bluer. Moreover, due to both rotational mixing and mass loss, their surface will be rapidly enriched in H-burning products. These stars will therefore enter the Wolf-Rayet phase while they are still burning their hydrogen in their core. This again reduces the MS width. For initial masses between 9 and  $25 M_{\odot}$ , the MS shape can be widened by rotation mimicking the effect of overshooting (Talon et al., 1997).

## B. The post- Main-Sequence evolution

The post-MS evolution of the most massive stars ( $M \geq 40 M_{\odot}$ ) which become WR stars will be discussed in Sect. X.B below. We mention here some points of general interest. For low or moderate rotation, the convective core shrinks as usual during MS evolution, while for high masses ( $M \sim 40 M_{\odot}$ ) and large initial rotations ( $\frac{\Omega}{\Omega_{\text{crit}}} \geq 0.5$ ), the convective core grows in mass during evolution. This latter situation occurs in the fast rotating  $60 M_{\odot}$  model shown on Fig. 18. These behaviours, i.e. reduction or growth of the core, determine whether the star will follow respectively the usual redwards MS tracks in the HR diagram, or whether it will bifurcate to the blue (Maeder, 1987b) towards the classical tracks of homogeneous evolution (Schwarzschild, 1958).

The stars with initial masses between 15 and  $25 M_{\odot}$  become red supergiants (RSG). Rotation does not change qualitatively this behaviour but accelerates the redwards evolution, especially for the 15 and  $20 M_{\odot}$  models. As a numerical example, for an initial  $v_{\text{ini}} = 300 \text{ km s}^{-1}$ , the model stars burn all their helium as red supergiants at  $T_{\text{eff}}$  below 4000 K, while the non-rotating models spend a significant part of the He-burning phase in the blue part of the HR diagram: for the non-rotating 15 and  $20 M_{\odot}$  models, respectively 25 and 20% of the total He-burning lifetime is spent at  $\log T_{\text{eff}} \geq 4.0$ . Note that rotation is not the only factor able to affect the blue-red supergiant lifetimes. Mass loss, convection, overshooting, semiconvection, are, among others, all important factors in that respect. The above behaviour of the rotating models results mainly from the enhancement of the mass loss rates. This effect prevents the formation of a big intermediate convective zone and therefore favours a rapid evolution toward the RSG phase (Maeder, 1981; Stothers & Chin, 1979). Let us note that the dispersion of the initial rotational velocities produces a mixing of the above behaviours. As we shall see below (see Sect. X.A), a redwards evolution is also favored at low metallicity. But in that case, this is mainly due to rotational mixing and not to a mass loss effect.

The problem of the mass discrepancy (Herrero et al., 1992), *i.e.* of the difference obtained between spectroscopic and evolutionary masses, has been significantly reduced thanks to improvements brought to stellar atmosphere models. However still some discrepancies are reported in general linked with strong helium surface enrichments:

- In SMC: Mokiem et al. (2006) find a mild mass discrepancy for stars with spectroscopic masses inferior to about  $20 M_{\odot}$ , which correlates with the surface helium abundance. These authors find that the discrepancies are consistent with the predictions of chemically homogeneous evolution. Most of the stars observed by Heap et al. (2006) exhibit the mass discrepancy problem although no surface He enrichment.
- In LMC: Mokiem et al. (2007) from the analysis of O-type stars in the LMC find that bright giants and supergiants do not show any mass discrepancy, regardless of the surface helium abundance. In contrast they find that the spectroscopically determined masses of the dwarfs and giants are systematically smaller than those derived from non-rotating evolutionary tracks. All dwarfs and giants having  $y > 0.11$  ( $Y > 0.33$ ) show this mass discrepancy.

These mass discrepancies may arise from the use of stellar models with too small convective cores. Convective overshooting and rotation produce larger convective cores and thus can help in explaining this mass discrepancy.

## C. Lifetimes

Generally we can say that the MS lifetime duration is affected by rotation at least through three effects:

1. Rotation increases the quantity of hydrogen burnt in the core. This increases the MS lifetime.
2. The hydrostatic effects of rotation make a star of a given initial mass to behave as a non-rotating star of a smaller initial mass. This tends to increase the MS lifetime.
3. Rotation increases the helium abundance in the outer radiative envelope. This tends to make the star overluminescent with respect to its non-rotating counterpart and thus to reduce the MS lifetime.

Depending on the initial mass and metallicity, rotation can either increase or decrease the MS lifetimes with respect to the durations obtained from non-rotating stellar models. For  $Z = 0.020$ , the effect number 1 dominates and rotation increases the lifetimes. For instance, from the models by Meynet & Maeder (2000), one can deduce a nearly linear relation between the relative enhancement of the MS lifetime,  $\Delta t_{\text{H}}$  and  $\bar{v}$ , where

$$\Delta t_{\text{H}}(\bar{v}) = [t_{\text{H}}(\bar{v}) - t_{\text{H}}(0)]/t_{\text{H}}(0).$$

One obtains,

$$\frac{\Delta t_{\text{H}}(\bar{v})}{t_{\text{H}}(0)} = 0.0013 \cdot \bar{v},$$

where  $\bar{v}$  is in  $\text{km s}^{-1}$ . When the metallicity decreases, the effect number 3 tends to become the most important one. Typically at  $Z = 10^{-5}$ , the MS lifetimes are decreased by about 4–14% for the mass range between 3 and 60  $M_{\odot}$  when  $v_{\text{ini}}$  increases from 0 to 300  $\text{km s}^{-1}$  (Meynet & Maeder, 2002a). The rotating 2  $M_{\odot}$  model of the same grid has a longer MS phase than its non-rotating counterparts, in contrast with what happens for higher initial mass stars. This is because, when the initial mass decreases, the hydrostatic effects (effect number 2) become more and more important.

The He-burning lifetimes are less affected by rotation than the MS lifetimes. The changes are less than 10%. The ratios  $t_{\text{He}}/t_{\text{H}}$  of the He to H-burning lifetimes are only slightly decreased by rotation and remain around 10–15%.

## X. MASSIVE STAR POPULATIONS AND THE CASE OF FIRST STARS

### A. The ratio of blue to red supergiants

As noted by Langer & Maeder (1995), the current models (without rotation) with Schwarzschild’s criterion predict no red supergiants in the SMC. This is also seen in Fig. 19 which illustrates for models of 20  $M_{\odot}$  at  $Z = 0.004$  the variations of the  $T_{\text{eff}}$  as a function of the fractional lifetime in the He-burning phase for different rotation velocities (Maeder & Meynet, 2001b). For zero rotation, we see that the star only moves to the red supergiants at the very end of the He-burning phase, so that the blue to red supergiant ratio  $B/R$  is  $\simeq 47$ . This is 50–100 times greater than the observed ratio in the SMC cluster NGC 330 which lies between 0.5 and 0.8, according to the various sources discussed in Langer & Maeder (1995) and Eggenberger et al. (2002).

This disagreement implies that no reliable predictions can be made concerning the nature of the supernova progenitors in different environments, or the populations of supergiants in galaxies. The  $B/R$  ratio also constitutes an important and sensitive test for stellar evolution models, because it is very sensitive to mass loss, convection and mixing processes (Langer & Maeder, 1995). Thus, the problem of the blue to red supergiant ratio ( $B/R$  ratio) remains one of the most severe problems in stellar evolution.

Looking at Fig. 19, we see that for average rotational velocities  $\bar{v}$  during the MS,  $\bar{v} = 152, 229$  and  $311 \text{ km s}^{-1}$ , one has respectively  $B/R = 1.11, 0.43$  and  $0.28$ . Thus, *the  $B/R$  ratios are much smaller for higher initial rotation velocities*, as rotation favours the formation of red supergiants and reduce the lifetime in the blue. We notice in particular that for  $\bar{v} = 200 \text{ km s}^{-1}$ , we have a  $B/R$  ratio of about 0.6 well corresponding to the range of the observed values.

The reason for this variation of the  $B/R$  ratio when the rotation velocity changes is discussed in details in Maeder & Meynet (2001b). Let us just mention here that when an extended intermediate convective zone is associated to the H-burning shell, the star tends to stay in the blue part of the HR diagram. Rotational mixing tends to reduce the extension of this intermediate convective zone and thus to accelerate the redwards evolution in the HR diagram. How rotation limits the convective zone associated to the H-burning shell can be understood looking at Fig. 20. The larger He-core in the rotating models means that a larger fraction of the total luminosity is made in the core (0.42 instead of 0.31 for the models of Fig. 20). This means that the H-burning shell in the rotating model produces a smaller fraction of the total luminosity and this contributes to reduce the importance of the convective zone above the H-burning shell. Simultaneously, the higher He-content near the shell in the rotating case leads to a decrease of its H-content and opacity, and this also contributes to reduce the importance of the convective zone associated with the H-burning shell.

Thus models with rotation well account for the long standing problem of the large numbers of red supergiants observed in low  $Z$  galaxies, while current models with mass loss were predicting no red supergiants.

### B. Current problems with Wolf-Rayet stars

Wolf-Rayet stars are the bare cores of initially massive stars, whose H-rich envelope has been removed by strong stellar winds or through Roche lobe overflow in a close binary system (see e.g. the review by Crowther, 2007). Wolf-Rayet stars play a very important role in Astrophysics, as signatures of star formation in galaxies and starbursts, as injectors of chemical elements, as sources of kinetic energy into the interstellar medium and as progenitors of supernovae and, likely, as progenitors of long soft  $\gamma$ -ray bursts.

Evolutionary scenarios, at solar metallicity, for Wolf-rayet stars follow the sequences shown below

$M > 90 M_{\odot}$ :	O - Of - WNL - (WNE) - WCL - WCE - SN (Hypernova low Z )
$60 - 90 M_{\odot}$ :	O - Of/WNL $\leftrightarrow$ LBV - WNL(H poor)- WCL-E - SN(SNIIn?)
$40 - 60 M_{\odot}$ :	O - BSG - LBV $\leftrightarrow$ WNL -(WNE) - WCL-E - SN(SNIb) - WCL-E - WO SN (SNIc)
$30 - 40 M_{\odot}$ :	O - BSG - RSG - LBV ? - WNE - WCE - SN(SNIb)
$25 - 30 M_{\odot}$ :	O -(BSG)- RSG - BSG (blue loop) - RSG - SN(SNIb, SNIIL)
$10 - 25 M_{\odot}$ :	O - RSG - (Cepheid loop, $M < 15 M_{\odot}$ ) RSG - SN (SNIIL, SNIIP)

Of-stars are O-type stars showing emission lines. WN stars present emission lines from nitrogen and helium. Depending on the line ratios between N III-IV and He I-II, they are classified as WNE (WN2-WN5) or WNL (WN7-WN9), with WN6 being early (E) or late (L) type. WC spectral type depend on the line ratios of C III and C IV (WC4-WC6 are early, WC7-WC9 are late). Oxygen-rich WO stars extend the WCE sequence, exhibiting strong O VI emission lines (see the review by Crowther, 2007, and references therein). LBV stands for Luminous Blue Variables (see the review by Vink, 2009, and references therein). BSG and RSG for blue and red supergiants respectively. The sign  $\leftrightarrow$  means back and forth motions between the two stages. The various types of supernovae are tentatively indicated (see the review by Smartt, 2009, for the core-collapse supernova classification). The limits between the various scenarios depend on metallicity  $Z$  and rotation. The limiting masses indicated corresponds to the standard metallicity case, *i.e.*  $Z = 0.020$ .

From the above evolutionary scenarios, we see that at the standard metallicity, the minimum initial mass for a star to enter the WR phase is between 25 and 30  $M_{\odot}$ . This inferior limit is however dependent on the stellar models considered and in particular on the mass loss rates used and the mixing processes (size of the convective zone and other mixing processes in radiative zones as for instance those induced by rotation). These processes, mass loss and mixing, also affect the durations of the WR phases.

Let us recall some difficulties faced by standard stellar models concerning the WR stars. A good agreement between the predictions of the stellar models for the WR/O number ratios and the observed ones at different metallicities in regions of constant star formation was achieved provided the mass loss rates were enhanced by about a factor of two during the MS and WNL phases (Maeder & Meynet, 1994). This solution, which at that time appeared reasonable in view of the uncertainties pertaining the mass loss rates, is no longer applicable at present, at least if we take for granted the fact that the mass loss rates during the WR phase are reduced by a factor 2 to 3, when account is given to the clumping effects in the wind (Nugis & Lamers, 2000). Also, the mass loss rates for O-type stars have been substantially revised (and in general reduced) by the results of Vink et al. (2001). With these revised mass loss rates the predicted numbers of WR stars by the standard non-rotating models of Meynet & Maeder (2003) are much too low with respect to the observations.

A second difficulty of the standard models with mass loss concerns the observed number of transition WN/WC stars. These stars show simultaneously some nitrogen characteristic of WN stars and some carbon of the further WC stage. The observed frequency of WN/WC stars among WR stars turns around 4.4 % (van der Hucht, 2001), while the frequency predicted by the standard models without extra-mixing processes are lower by 1–2 orders of magnitude (Maeder & Meynet, 1994). This feature cannot be accounted for by a change of the mass loss rates and indicates that mixing is not adequately incorporated in the standard stellar models. A third difficulty of the standard models as far as WR stars were concerned was that there were relatively too many WC stars with respect to WN stars predicted at low metallicity (see the review by Massey, 2003). These difficulties are the signs that some process is missing in standard models.

### C. Solutions of WR problems in terms of rotation?

What could be missing? Binarity, changes of the mass loss history, mixing processes can be invoked and there is little doubt that playing with these different features, a given observational feature can be reproduced. We think however that good stellar models have to reproduce all the main observed features exhibited by massive stars simultaneously (as the MS width, the changes of the surface abundances during the MS phase, the variation with the metallicity of the of blue to red supergiant ratio, or of the WR/O number ratio to just cite a few of them) without having to change the physics included in order to adapt it to resolve a particular question. This makes the problem much more constrained and discard some solutions. As discussed previously, there are some evidences that some extra mixing process is still missing in stellar models and that this extra-mixing is probably driven by rotation. Thus in the following we shall focus on the consequences for the WR population of rotational mixing. We first indicate some general trends induced by rotation and then illustrate the consequences obtained in some specific stellar models.

Rotational mixing favours the entry into the WR phase in two ways, firstly by allowing chemical species produced in the core to diffuse in the radiative envelope and, secondly, by making the mass of the convective core larger. In the

non-rotating model, mass loss by stellar winds is the key physical ingredient which allows internal chemical products to appear at the surface and thus the formation of a WR star. The star becomes a WR star only when sufficiently deep layers are uncovered. In rotating models, the characteristic surface abundances of WR stars can be obtained through the effects of mass loss by stellar winds and of rotational mixing. The action of rotation allow WR stars to appear through the single star scenario even when the mass loss rates are reduced. To realize that, imagine a star rotating so fast that it would follow a homogenous evolution. Such a star can become a WR star, i.e. being a star with a  $\log T_{\text{eff}}$  greater than about 4 and a mass fraction of hydrogen at the surface below  $\sim 0.4$  without losing mass!

When models with a time-averaged rotation velocity during the MS phase in the range of the observed values are considered, then a reasonable number of WR stars can be produced through the single star scenario even using low mass loss rates. This is illustrated in Fig. 21. Also the rotational models well reproduce the WN/WC ratio at low metallicity, the observed fraction of WR stars in the transition stage WN/WC and the variation with the metallicity of the number ratios of type Ibc to type II supernovae (see more detailed discussion in Meynet & Maeder, 2003, 2005, and in Sect. XI.A).

The number of WC to WN stars increases with the metallicity (see Fig. 22<sup>3</sup>). Many attempts have been performed to reproduce the observed trend: for instance the enhanced mass loss rate models of Meynet et al. (1994) provided a good agreement for solar and higher than solar metallicity but produced too few WN stars in metal-poor regions. The inclusion of rotation together with reduced mass loss rates accounting for the effects of clumping improved the situation in the metal poor region, but produced too many WN stars at solar and higher metallicities (Meynet & Maeder, 2005). Eldridge & Vink (2006) show that models that include the mass-loss metallicity scaling during the WR phase closely reproduce the observed decrease of the relative population of WC over WN stars at low metallicities. However such models severely underestimate the fraction of WR to O-type stars. In that case, to improve the situation, a high proportion of Wolf-Rayet stars originating from mass transfer in close binaries would have to be assumed at all metallicities. For instance at solar metallicity about 75% of the WR stars should be produced in close binary systems (see Fig. 5 in Eldridge et al., 2008). This is clearly in contradiction with the results of Foellmi et al. (2003a,b) that locally in the Milky Way only 24% of the WR stars are binaries. Thus, as shown below, another explanation has to be found.

The WN/WC number ratio depends also on other factors, in particular on the evolutionary scenario. In Meynet & Maeder (2003, 2005), the most massive rotating stars enter into the WR regime already during the MS phase. This feature has good and bad effects. On one hand, it allows these models to well reproduce the variation of the number fraction of WR to O-type stars since it significantly increases the WR lifetimes. On the other hand, it produces very long WN phases since the star enters into the WR phase having still a huge H-rich envelope. As a consequence, too low values for the WC/WN ratio are obtained at solar and higher metallicities.

In Meynet & Maeder (2003, 2005), the hypothesis has been made that when a star enters into the WR stage during the MS phase, it avoids the Luminous Blue Variable phase. Actually, stars may behave differently. It may well be that a star which becomes a WR star during the MS phase, enters a LBV phase after the core H-burning phase, before evolving back into the WR regime. When this evolutionary scenario is followed, reasonable values for both the WR/O and the WC/WN ratios are obtained. Indeed the ratios of WR/O and of WC/WN given by these models at the solar metallicity are 0.06 and 0.9 which compare reasonably well with the observed values of 0.1 and 0.9 respectively. Both ratios are not reproduced by the non-rotating models to which a similar scenario is applied. This discussion illustrates the possible key role that the LBV phase may play in shaping the WC/WN ratio.

#### D. Pop III star models with rotation

Understanding the evolution of massive stars at low and very low metallicity is a requirement to address questions such as the nature of the sources of the reionization in the early Universe, the evolution of the interstellar abundances during the early phases of the evolution of galaxies, for finding possible signatures of primordial stellar populations in the integrated light of very distant galaxies and for discovering which objects are the progenitors of the long soft Gamma Ray Bursts. At present, the most “iron” poor objects known in the Universe are not very far from us since they are galactic halo field stars. Provided these stars are trustworthy very metal poor stars (a view recently challenged by Venn & Lambert, 2008), these objects offer a unique opportunity to study the yields of the first generations of stars.

In this section, we focus the discussion on Pop III stars, i.e. on stars which were made up of material having

---

<sup>3</sup> We consider here regions having reached a stationary situation, *i.e.* regions where the star formation rate can be considered to have remained constant for the last twenty million years.



been processed only by primordial nucleosynthesis. In an environment with primordial composition, one expects the following differences with respect to the more classical evolution at higher metallicity:

- At strictly  $Z = 0$ , the cooling processes, so important for allowing the evacuation of the energy produced when the molecular clouds collapse and thus its fragmentation, are not so efficient than when metals are present. This favors the formation of more massive stars. The initial mass function is probably different depending on the mass of the “minihaloes” (see Greif & Bromm, 2006). In minihaloes with masses between  $10^6$  and  $10^8 M_\odot$ , virial temperature is between  $10^3$  and  $10^4$  K and the cooling is due mainly to the molecules  $H_2$ . This allows the formation of stars with characteristic masses  $\geq 100 M_\odot$ . In minihaloes where ionization occurs prior to the late stages of the protostellar accretion process, namely those with a virial temperature superior to  $10^4$  K and thus with masses above  $10^8 M_\odot$ <sup>4</sup>, the hydrogen deuteride (HD) molecule provides an additional cooling channel. In those minihaloes, metal-free gas can cool more efficiently. This leads to the formation of stars with masses superior to  $10 M_\odot$ . Thus at the very beginning, we would have first, during a quite short period, only very massive Pop III stars and, when gas assembles in more massive haloes (or is reionized by the first stars), a second Pop III star generation appears with smaller characteristic masses (about  $10 M_\odot$  and above). When the metallicity becomes higher than  $10^{-3.5} Z_\odot$ , *i.e.* for  $Z$  above about  $5 \cdot 10^{-6}$  a normal IMF governs the mass distribution of newly born stars<sup>5</sup>. According to Greif & Bromm (2006) the very massive Pop III stars only contribute marginally to feed the reservoir of ionizing photons and to the chemical enrichment of the interstellar medium. Much more important are on this respect the less massive Pop III stars born in more massive haloes or in relic HII regions.
- The (nearly) absence of heavy elements implies that massive stars cannot begin burning hydrogen through the CNO cycle but through the pp chains. However the energy output extracted from the pp chains is not sufficient to compensate for the high luminosity of these stars. The stars must compensate the deficit of nuclear energy by extracting energy from the gravitational reservoir, *i.e.* they contract. At a given point however, due to this contraction, the central temperature becomes high enough for activating triple  $\alpha$  reactions. Some carbon is then produced. When the mass fraction of carbon is of the order of  $10^{-12}$ , the CN cycle becomes the main source of energy and the evolution then proceeds as in a more metal rich massive stars. For stars above about  $20 M_\odot$ , activation of the CN cycle intervenes very early during the core H-burning (typically before five percents of the hydrogen at the centre is consumed, see Marigo et al., 2003).
- Pop III stars are more compact due to the contraction they undergo at the beginning of the core H-burning phase (see above) and to the fact that the opacity of primordial material is smaller than that of metal rich one. Typically a Pop III  $20 M_\odot$  star on the ZAMS has a radius reduced by a factor 3.5 with respect to the radius of the corresponding star with  $Z = 0.020$ . Even passing from the very low metallicity  $Z = 10^{-5}$  to 0 already produces a decrease of the radius by a factor 2! Smaller radius favors more efficient mixing in two ways: first, for a given value of the diffusion coefficient,  $D$ , the mixing timescale decreases with the square of the radius as  $\sim R^2/D$ , second as can be seen from Fig. 23, in pop III models, the meridional currents have smaller amplitudes and present a very different configuration than at higher metallicities. Typically at high metallicity (look at the curve for  $Z = 0.020$ ), there is an extended outer cell which tends to reduce the  $\Omega$ -gradient. This is no longer the case in metal poor models.

Recently Ekström et al. (2008a) presented a grid of Pop III stellar models including the effects of rotation. Evolutionary tracks of non-rotating and rotating Pop III stellar models are shown in Fig. 24 (left panel). The models are computed until the end of the core Si-burning, except the  $9 M_\odot$  that has developed a degenerate core before carbon ignition and has thus been stopped then, and the  $15 M_\odot$  model that has been stopped at the end of O-burning also because of a too degenerate core at that time. An initial velocity of  $800 \text{ km s}^{-1}$  on the ZAMS was chosen. For the  $60 M_\odot$  model, this corresponds to a value of  $v/v_{\text{crit}} = 0.52$  on the ZAMS, which is slightly superior to 0.4, the value required at solar metallicity to obtain averaged velocities during the MS phase corresponding to observed values.

We notice that the ZAMS is shifted toward lower effective temperature and luminosity with respect to the non-rotating case as was the case at higher metallicities<sup>6</sup>. Then, when the evolution proceeds, the tracks become more luminous, and the main-sequence turn-off is shifted to cooler temperature: the core of the rotating models is refueled by fresh H brought by the mixing. It thus grows, leading to an enhancement of the luminosity.

<sup>4</sup> This may also happen in relic HII regions left by the first stars, (see Johnson & Bromm, 2006).

<sup>5</sup> Some authors argue that star formation switches to more classical mode already when  $Z = 10^{-6}$  due to dust production in the early Universe, (see Schneider et al., 2006).

<sup>6</sup> We recall that this shift is due to the sustaining effect of the rotation: the gravity is counter-balanced both by the gas pressure and the centrifugal force in such a way that the star behaves like a lower mass one.

The onset of the CNO cycle described above can be seen in the HRD: the tracks evolve toward the blue side of the diagram, until the energy provided by the CNO cycle stops the contraction and bends the tracks back in the usual MS feature. In the rotating  $9 M_{\odot}$  model, this happens at an age of 12.2 Myr (when the central H mass fraction is  $X_c = 0.439$ ) while in the non-rotating one it happens a little earlier, at an age of 10.9 Myr (but at a similar burning stage:  $X_c = 0.439$ ). In the case of the non-rotating  $15 M_{\odot}$  model, it happens after merely 1.5 Myr ( $X_c = 0.695$ ), while it takes 2 Myr ( $X_c = 0.677$ ) in the case of the rotating one.

After central H exhaustion, the core He-burning phase (CHeB) starts right away: the core was already hot enough to burn a little He during the MS and does not need to contract much further. This prevents the models to start a redward evolution, so they remain in the blue part of the HRD at the beginning of CHeB. Then, something particular happens to the rotating models: because of rotational mixing, some carbon produced in the core is diffused toward the H-burning shell, allowing a sudden ignition of the CNO-cycle in the shell. This boost of the shell leads to a retraction of the convective core and a decrease of the luminosity. At the same time, it transforms the quiet radiative H-burning shell into an active convective one. Some primary nitrogen is produced (see more on that point in the next section).

All the models, except the  $9 M_{\odot}$ , reach the critical velocity during the MS phase (see the right panel of Fig. 24). Once at critical limit, all the models remain at the critical limit until the end of the Main-Sequence phase. On the right panel of Fig. 24, the 85 and especially the  $200 M_{\odot}$  seem to depart from  $\Omega/\Omega_{\text{crit}} = 1$ , but this is due to the limit shown here being only the  $\Omega$ -limit, where the centrifugal force alone is taken into account to counterbalance the gravity. In the two above models however, the radiative acceleration is strong and the models reach the so-called  $\Omega\Gamma$ -limit, that is the second root of the equation giving the critical velocity:  $g_{\text{eff}} [1 - \Gamma] = \vec{0}$  (Maeder & Meynet, 2000b). The true critical velocity is lowered by the radiative acceleration, and though the  $\Omega/\Omega_{\text{crit}}$  ratio plotted becomes lower than 1, these models are actually at the  $\Omega\Gamma$  critical limit and remain at this limit till the end of the MS phase. At central H exhaustion, the moderate inflation of the radius brings the surface back to sub-critical velocities. The mass which is lost by the mechanical winds amounts only to a few percents of the initial stellar mass and thus does not much affect neither their evolution, nor their nucleosynthetic outputs. Much more mass can be lost by mechanical mass loss (see next subsection) when the effects of magnetic fields are accounted for as prescribed in the Tayler-Spruit dynamo theory (Spruit, 2002), or when the metallicity is non-zero.

### E. Strong mass loss in Pop III stars?

According to Heger et al. (2003), the fate of single stars depends on their He-core mass ( $M_{\alpha}$ ) at the end of the evolution. They have shown that at very low metallicity, the stars having  $64 M_{\odot} < M_{\alpha} < 133 M_{\odot}$  will undergo pair-instability and be entirely disrupted by the subsequent supernova. This mass range in  $M_{\alpha}$  has been related to the initial mass the star must have on the main sequence (MS) through standard evolution models:  $140 M_{\odot} < M_{\text{ini}} < 260 M_{\odot}$ . However the link between the masses of the He-core mass and the initial mass can be very different depending on the physics considered. Ekström et al. (2008a) showed that a  $Z=0$ ,  $150 M_{\odot}$  stellar model, having an initial ratio between the equatorial velocity and the critical one equal to  $v_{\text{ini}}/v_{\text{crit}} = 0.56$ , computed accounting for the Tayler-Spruit dynamo mechanism (Spruit, 2002) and the effects of wind anisotropy (Maeder, 1999) will lose such great amount of mass that it will reach the end of the core He-burning phase with a mass of  $M_{\alpha}$  too small to go through a pair-instability process.

In Fig. 25, we present the evolution in the HR diagram (left panel) and the evolution of mass with time (right panel) for the  $150 M_{\odot}$  stellar model of Ekström et al. (2008a). The grey line shows a non-rotating model computed with the same physics for comparison. During its whole evolution up to the end of core He-burning, the non-rotating model loses only  $1.37 M_{\odot}$ . This illustrates the weakness of radiative winds at  $Z = 0$ . The evolution of the rotating model (black line) can be described by four distinct stages:

1. (*continuous part*, lower left corner) The model starts its evolution on the MS with only radiative winds, losing only a little more than  $0.002 M_{\odot}$ . During this stage, the ratio of the surface velocity to the critical one increases quickly, mainly because of the strong coupling exerted by the magnetic fields.
2. (*dashed part*) When the central content of hydrogen is still about 0.58 in mass fraction, the star reaches the critical velocity and starts losing mass by mechanical mass loss. It remains at the critical limit through the whole MS, but the mechanical wind removes only the most superficial layers that have become unbound, and less than 10% of the initial mass is lost at that stage ( $11.44 M_{\odot}$ ). The model becomes also extremely luminous, and reaches the Eddington limit when 10% of hydrogen remains in the core. Precisely, it is the so-called  $\Omega\Gamma$ -limit that is reached here.
3. (*dotted part*) The combustion of helium begins as soon as the hydrogen is exhausted in the core, then the radiative H-burning shell undergoes a CNO flash, setting the model on its redward journey. The model remains at the

$\Omega\Gamma$ -limit and loses a huge amount of mass. The strong magnetic coupling keeps bringing angular momentum to the surface and even the heavy mass loss is not able to let the model evolve away from the critical limit. The mass lost during that stage amounts to  $53.46 M_{\odot}$ . When the model starts a blue hook in the HR diagram, its surface conditions become those of a WR star ( $X_{surf} < 0.4$  and  $T_{eff} > 10^4 000$  K). The luminosity drops and takes the model away from the  $\Gamma$ -limit, marking the end of that stage.

4. (*continuous part*) The rest of the core He-burning is spent in the WR conditions. The mass loss is strong but less than in the previous stage: another  $26.34 M_{\odot}$  are lost.

At the end of core He-burning, the final mass of the model is only  $M_{fin} = 58 M_{\odot}$ , already below the minimum  $M_{\alpha}$  needed for PISN ( $M_{\alpha} \geq 64 M_{\odot}$ ). Note that the contraction of the core after helium exhaustion brings the model back to critical velocity, so this value for  $M_{fin}$  must be considered as an upper limit.

This result shows that a fast rotating Pop III  $150 M_{\odot}$  may avoid to explode as a PISN. Of course it is by far not certain that the conditions required for such a scenario to occur are met in the first stellar generations but it underlines the fact that fast rotation may drastically change the picture.

The yields of PISN is discussed by Heger & Woosley (2005) and are dominated by alpha nuclei. The iron-to-oxygen ratio show a strong increase with the initial mass. The PISN yields show a strong decrease beyond the iron group, have essentially no s-process and r-process element production. These nucleosynthetic signatures of PISN are not observed in the most metal poor halo stars. Is this due to the above scenario? To the fact that the signature was very quickly erased by the next generations of stars?<sup>7</sup> Or were such high mass stars not formed? These various hypotheses cannot be disentangled at the present time, but the observation of more and more metal-deficient stars will probably provide elements of response to these questions.

## XI. SUPERNOVAE AND GAMMA RAY BURSTS

### A. The type Ib and Ic supernovae

Type Ib supernovae are core-collapse supernovae whose spectrum shows no hydrogen lines. The spectra of type Ic show no hydrogen and helium lines (see e.g. Nomoto et al., 1994; Wheeler et al., 1987). The progenitors of these core collapse supernovae are thus believed to be stars stripped of their original H-rich envelope for type Ib's and also of their He-rich envelope for type Ic's. Progenitors are therefore naked stellar cores as e.g. Wolf-Rayet stars. The observed frequency at solar metallicity of type Ibc supernovae is about 20% the frequency of type II supernovae (see e.g. Cappellaro et al., 1999), which represents a significant fraction of all core collapse supernovae. In four cases, the typical spectrum of a type Ic supernova has been observed associated with a long soft gamma ray burst (GRB) event (Woosley & Bloom, 2006), indicating a privileged link between type Ic's and the most powerful supernova explosions observed in the Universe.

Fig. 26 shows the different supernova types expected for various initial masses and metallicities as given from rotating models by Georgy et al. (2009). Type Ic SNe cover a much broader range of initial masses than type Ib. This trend reflects that most stars which, at a given stage, in their evolution have peeled off their H-rich envelope do not stop at that stage. Their evolution drives them beyond, up to the stage where most of their He-rich layers have been peeled off.

One immediately sees that the number fraction of type Ibc to type II supernovae should increase with metallicity. This is an effect of the stronger winds at higher metallicities, which favor the formation of H-free stars at the end of their evolution. Very interestingly, this expected increase of the Ibc/II ratio has been put in evidence by Prantzos & Boissier (2003). When one compares the theoretical ratios obtained from single stars with the observed ones, a good fit is obtained only for the rotating models (Georgy et al., 2009; Meynet & Maeder, 2005).

However such an observed trend can also be reproduced invoking close binary-star evolution (see for example Eldridge et al., 2008; Podsiadlowski et al., 1992; Vanbeveren et al., 2007). In this scenario, the hydrogen-rich envelope is removed either through a Roche lobe overflow process or during a common envelope phase, producing a WR star. Thus we face here the situation where two very different models (single stars with rotation/close binary evolution with mass transfer) are both able to give a reasonable fit to the data. Actually both scenarios probably contribute to the observed populations of type Ibc supernovae. However, it would be interesting to know their relative importance and how their relative importance changes with the metallicity. It might be that both scenarios predict different behaviors

---

<sup>7</sup> Maybe the metal-poor stars we observe are enriched by more SNe than we actually think, and the later contributions are masking the primordial ones.

for the way the frequencies of the type Ib and type Ic SNe vary as a function of the metallicity. Predictions of single star models for the variations with the metallicity of the separate ratios of type Ib/II and of Ic/II are discussed in Georgy et al. (2009).

## B. The progenitors of long soft Gamma Ray Bursts

One of the most promising model for the progenitors of the long soft Gamma Ray Bursts (GRB) is the collapsar model by Woosley (1993). In this model, GRB are the product of the evolution of massive stars which, at the end of their evolution, produces a fast rotating black hole. In addition, for the GRB to be visible, the massive star should have lost its envelope. This model received a strong support when observations showed that there is a connection between so-called long-soft GRB events and type Ic supernovae (Woosley & Bloom, 2006). This kind of supernova can be produced by both WC or WO stars. In this way, WC and WO stars are natural candidates to be GRB progenitors. However, GRBs are primarily found in metal-poor environments (Modjaz et al., 2008), while type Ic's SNe appear mainly at high metallicity. Many physical reasons have been invoked to explain why GRBs seem to occur only at low metallicities. Among them are the following (see the review by Woosley & Bloom, 2006):

- At low metallicity, stellar winds (even during the WR phases) are weaker, thus bringing away small quantities of angular momentum. Black holes are also more easily formed since higher final masses are obtained.
- As already emphasized previously, in absence of any magnetic coupling, the transport of the angular momentum is mainly due to meridional currents, while the mixing of the elements is mainly driven by shear instabilities. At low metallicity the transport of angular momentum between the core and the envelope is less efficient than at high metallicities (see Fig. 23), because of slower meridional currents in metal poor stars. This favors a higher angular momentum content of the core when the star is at the end of its nuclear lifetime, it also favors steeper  $\Omega$ -gradient in the interior triggering more efficient shear instabilities and thus chemical mixing.
- Since the chemical mixing due to rotation is more efficient at low  $Z$ , homogeneous evolution is more easily obtained in metal-poor regions. Homogeneous evolution allows massive stars to produce a type Ic SN event without having to lose large amounts of mass (and thus of angular momentum). Indeed, a perfectly homogeneous evolution (actually never realized) would allow the formation of a pure CO core (and then lead to a type Ic SN event) at the end of the core He-burning phase without the need for the star to lose any mass! Note that such homogeneous evolution allows massive stars to produce much more ionizing photons than standard one (see e.g. Meynet et al., 2008).
- The distribution of initial velocities at low metallicity might contain more fast rotators than at high metallicities (see Fig. 9 in Martayan et al., 2007).

It is interesting to compare the observed GRB frequency with the observed frequency of potential candidates. First, as mentioned above, type Ic supernovae at low metallicity do appear interesting candidates. From Fig. 27, one can see that the observed rate of type Ic supernovae from single star models is still above the estimated number ratio GRB / core collapse supernovae (CCSNe) even when one only considers low-metallicity, type Ic SNe. Here it is supposed that the formation of a BH does not prevent a SN event. In case, only rare circumstances would allow a SN to occur when a black hole is formed, then the situation might be very different.

Other interesting candidates are the WO stars that primarily occur at low metallicity. These stars will explode as a type Ic SN. The frequency of type Ic's SNe with WO star progenitors is shown in Fig. 27. The expected rate is only marginally compatible with the observed GRB rate (assuming that the aperture angle of the bipolar jet is very small, typically around  $1^\circ$ ). This conclusion has been obtained by Hirschi et al. (2005a), so even restraining the progenitors of GRB to WO stars would still not match the observed frequency of GRBs.

From the above discussion, it can be deduced that exploding as a type Ic SN in metal-poor regions (or having a WO progenitor) is not a sufficient condition for obtaining a GRB. Physical characteristics shared by a subsample of the metal poor type Ic events exists that are needed to obtain a GRB event. Probably this physical characteristic is the high angular momentum in the core (Woosley & Heger, 2006; Yoon et al., 2006).

If GRB would only occur for initially very fast-rotating stars, rotating so fast that these stars would follow a homogeneous evolution (Maeder, 1987a; Meynet & Maeder, 2007; Woosley & Heger, 2006; Yoon et al., 2006), can we expect to find any peculiar feature in the chemical composition of the ejecta testifying this previous homogeneous evolution? Or in other words, is there any difference in the chemical composition of the ejecta between a type Ic having “normal WC or WO” progenitors and those arising from a model that followed a homogeneous evolution during the MS phase? The answer is probably no. It has been shown by Georgy et al. (2009) that the differences

in the masses of He, CNO elements, and  $Z$  are very small. Thus there is little chance from the observations of the composition of the ejecta in CNO elements to be able to distinguish between a normal and a homogeneous evolution.

A point that would be interesting to check is the following: since the star rotates very fast during a great part of its evolution, it will produce anisotropic stellar winds (see Fig. 28), typically bipolar winds and probably equatorial mass loss when the critical limit is reached (Maeder, 1999). These anisotropic winds will shape the circumstellar environment of the star (van Marle et al., 2008, and see also Fig. 28) and it might be that some traces of the resulting particular morphology will still be present at the time of the SN event (for instance, equatorial mass loss probably gives rise to a slow equatorial expanding disk whose traces might still be present when the star explodes). In that case the circumstellar environment of GRBs may be peculiar. This can in turn have an impact on some features in the spectrum. More generally, the circumstellar environment of stars that have been in a not too remote past very fast rotators may also be characterized by such features.

## XII. STELLAR NUCLEOSYNTHESIS

### A. Rotation and stellar yields at $Z=0.020$

Figure 29 displays the total stellar yields (i.e. the mass of an element newly synthesized by the star and ejected into the interstellar medium) divided by the initial mass of the star,  $p_{im}^{\text{tot}}$ , as a function of its initial mass,  $m$ , for the non-rotating (left) and rotating (right) models (Hirschi et al., 2005b). The different shaded areas correspond from top to bottom to  $p_{im}^{\text{tot}}$  for  $^4\text{He}$ ,  $^{12}\text{C}$ ,  $^{16}\text{O}$  and the rest of the heavy elements. The fraction of the stars locked in the remnant as well as the expected explosion type are shown at the bottom. The dotted areas show the wind contribution for  $^4\text{He}$ ,  $^{12}\text{C}$  and  $^{16}\text{O}$ .

The remnant masses have been estimated using the relation between the mass of the carbon-oxygen core and the mass of the remnant given by Maeder (1992) (see details in Hirschi et al., 2004, 2005b). This value is quite uncertain and may affect the yields, especially those of the iron-group elements and heavier. The yields shown in Fig. 29 are those obtained before explosive nucleosynthesis occurs.

For  $^4\text{He}$  (and other H-burning products like  $^{14}\text{N}$ ), the wind contribution increases with mass and dominates for  $M \gtrsim 22 M_{\odot}$  for rotating stars and  $M \gtrsim 35 M_{\odot}$  for non-rotating stars, i. e. for the stars which enter the WR stage. For very massive stars, the SN contribution is negative and this is why  $p_{4\text{Hem}}^{\text{tot}}$  is smaller than  $p_{4\text{Hem}}^{\text{wind}}$ . In order to eject He-burning products, a star must not only become a WR star but must also become a WC star. Therefore for  $^{12}\text{C}$ , the wind contributions only start to be significant above the following approximative mass limits: 30 and 45  $M_{\odot}$  for rotating and non-rotating models respectively. Above these mass limits, the contribution from the wind and the pre-SN are of similar importance. Since at solar metallicity, no WO star is produced, for  $^{16}\text{O}$ , as for heavier elements, the wind contribution remains very small in the whole mass range.

So we see that, below  $\sim 30 M_{\odot}$ , rotation increases the total metal yields,  $Z$ , and in particular the yields of carbon and oxygen by a factor of 1.5–2.5. As a rule of thumb, the yields of a rotating 20  $M_{\odot}$  star are similar to the yields of a non-rotating 30  $M_{\odot}$  star, at least for the light elements shown in Fig. 29. We see therefore that at  $Z = 0.020$ , the effects of rotation are qualitatively similar to those obtained by models with larger convective cores as for instance those computed with an overshoot. This is of course not surprising since rotational mixing tends also to increase the core size at a given evolutionary phase. For very massive stars ( $\sim 60 M_{\odot}$ ), rotation increases the yield of helium but does not significantly affect the yields of heavy elements. The similarities of the results between the rotating and non-rotating models for the 60  $M_{\odot}$  model comes from the fact that, although the mass is not lost at the same stages in both series of models, the total mass loss is nevertheless not very different. The non-rotating model goes through an LBV phase after the MS phase where a significant fraction of the mass is lost. The rotating model enters into the WR phase already during the MS phase and no LBV phase has been accounted.

Figure 30 presents the stellar yields convolved with the Salpeter initial mass function (IMF) ( $dN/dM \propto M^{-2.35}$ ). This reduces the importance of the very massive stars. Nevertheless, the differences between rotating and non-rotating models remain significant, especially around 20  $M_{\odot}$ . Despite these differences, it will be difficult to discriminate between these two series of yields from observations of the evolution of the abundances as a function of the increasing metallicity, because in such comparisons, the yields are only one of the ingredients of the chemical evolution models. Other factors as the star formation history, the initial mass function, the rate of infall and outflow etc... will blur the picture. More constraining are the early phases of the chemical evolution of the galaxies during which only massive stars had time to contribute.

## B. Impact on the early chemical evolution of galaxies

Very metal poor halo stars have formed (at least in part) from matter ejected by very metal poor massive stars (see e.g. Chiappini et al., 2008, 2006). By very metal poor stars we mean here Pop III stars and/or stars with an initial metal abundance lower or equal to that of the metal poor halo considered. Their surface compositions thus reflect the nucleosynthesis occurring in the first generations of massive stars (provided of course that no other processes as accretion or in-situ mixing mechanism has changed their surface composition).

Interestingly, many observations of these stars show puzzling features. Among them let us cite the two following ones shown in Fig. 32: spectroscopic observations (e.g. Spite et al., 2005) indicate a primary production of nitrogen over a large metallicity range; Halo stars with  $\log(\text{O}/\text{H})+12$  inferior to about 6.5 present higher C/O ratios than halo stars with  $\log(\text{O}/\text{H})+12$  between 6.5 and 8.2 (Akerman et al., 2004; Spite et al., 2005).

Fast rotating massive stars are very interesting candidates for producing primary nitrogen at low metallicity and in a very short time delay as is required by the observations of the N/O plateau shown in the upper panel of Fig. 32. Primary nitrogen production occurs in both high mass and intermediate mass stars provided they rotate and have a metallicity below about 0.001 (Meynet & Maeder, 2002a,b). The initial rotation needed to obtain sufficient primary nitrogen production corresponds to values between 50 and 70% of the critical rotation on the ZAMS. These values are above the usual ratio adopted for solar metallicity models, which is 40%, but are still far from extreme values near the critical limit. Let us note that recent models of Pop III star formation seem to support very high initial rotational velocities (Stacy et al., 2010).

For a given initial velocity, primary nitrogen production is more efficient when a small amount of metals is present than in stars made of primordial material. Indeed, although rotational mixing in Pop III stars is by far not a negligible effect, it remains at a relatively modest level due to the absence of strong contraction at the end of the core H-burning phase. On the contrary, when  $Z \gtrsim 10^{-10}$ , the physical conditions during the core H-burning phase and the core He-burning phase are so different that a strong contraction occurs at the end of the core H-burning phase leading to steep  $\Omega$ -gradient, strong mixing and important primary nitrogen production. For metallicities higher than about 0.001, rotational mixing is not efficient enough for triggering important primary nitrogen production (at least for the rotational velocities corresponding to the observed ones at this metallicity) and thus rotational mixing, although still important for explaining the surface enrichments, does not change the stellar yields as much as at very low metallicity.

A comparison of various yields for CNO elements for Pop III stars and very metal poor stars is shown in Fig. 31. For  $^{12}\text{C}$  (*left*) and  $^{16}\text{O}$  (*right*), our non-rotating 15 and 25  $M_{\odot}$  yields compare within a factor 2 or 3 with those of Chieffi & Limongi (2004). Their 25  $M_{\odot}$  produces also a huge amount of  $^{14}\text{N}$  (*centre*), even a factor  $\sim 10$  higher than ours. Recent non-rotating models by Heger & Woosley (2010) predict also important quantities of primary nitrogen in some mass range, indicating that primary nitrogen production in  $Z=0$  star models may not be linked to rotation. However, according to chemical evolution model of Chiappini et al. (2006), the production of primary nitrogen only by Pop III stars may not be sufficient to account for the observed N/O plateau shown by halo stars. Primary nitrogen production over a metallicity range is needed. At the moment, rotating models can provide a mechanism which operates over a sufficient extended metallicity range to account for the observations.

When the yields of rotating massive star models are included in chemical evolution model for the halo, nice agreement can be obtained with the observations. It is possible to account for the high observed N/O ratio at very low  $\log(\text{O}/\text{H})+12$  values and to reproduce the observed C/O upturn mentioned just above. This is illustrated in Fig. 32, where predictions for the evolution of N/O and C/O of chemical evolution models using different sets of yields are compared (Chiappini et al. 2006a<sup>8</sup>). We see that the observed N/O ratio is much higher than what is predicted by a chemical evolution model using the yields of the slow-rotating  $Z = 10^{-5}$  models from Meynet & Maeder (2002a) down to  $Z = 0$ . When adding the yields of the fast-rotating  $Z = 10^{-8}$  models from Hirschi (2007); Meynet et al. (2006)<sup>9</sup> the fit is much improved. The same improvement is found for the C/O ratio, which presents an upturn at low metallicity. These comparisons support fast rotating massive stars as the sources of primary nitrogen in the most metal poor galactic halo stars.

High N/O and the C/O upturn of the low-metallicity stars are also observed in low-metallicity DLAs (Pettini et al., 2008, see the crosses in Fig. 32). We note that the observed points are below the points for the halo stars in the N/O versus O/H plane. This may be attributed to two causes: either the observed N/O ratios observed in halo stars are somewhat overestimated or the difference is real and might be due to different star formation histories in the halo and in DLAs. Let us just discuss these two possibilities.

<sup>8</sup> The details of the chemical evolution models can be found in Chiappini et al. (2006b), where they show that such a model reproduces nicely the metallicity distribution of the Galactic halo. This means that the timescale for the enrichment of the medium is well fitted.

<sup>9</sup> These models use the same physics as the models of Meynet & Maeder (2002a), simply the initial rotation velocities considered are higher.

Measures of nitrogen abundances at the surface of very metal poor stars is quite challenging, much more than the measure of nitrogen in the interstellar medium as is done for the DLAs, therefore one expects that the data for DLAs suffer much smaller uncertainties than those for halo stars. In that respect the observed N/O ratios in DLAs should be preferred to compare with the chemical evolution models. In case both DLAs and the galactic halo had the same star formation history, *i.e.* are the result of an intense and rapid star formation episode, then the chemical evolution models presented in Fig. 32 can also apply to DLAs. We see that the DLA data still require models with fast rotation to be fitted (the shift of the DLA data towards lower N/O ratios is by far not sufficient to discard fast rotating models).

Probably the star formation history in DLAs is not the same as in the halo. While in the halo we see the result of strong and rapid star formation episodes, in DLAs one might see the result of much slower and weaker star formation episodes. In that case, both massive stars and intermediate mass stars contributed to the build up of the chemical abundances and the chemical evolution models presented in Fig. 32 do no longer apply to these systems. It will be very interesting to study the results of chemical evolution models adapted to this situation and accounting for stellar yields from both massive and intermediate mass stars. Let us just mention at this stage that primary nitrogen production in metal poor intermediate mass stars is also strongly favoured when rotational mixing is accounted for (Meynet & Maeder, 2002a,b)<sup>10</sup>. Thus also in that case, rotation may play a key role.

The primary nitrogen production is accompanied by other interesting features such as the production of primary <sup>13</sup>C (see Chiappini et al., 2008), and of primary <sup>22</sup>Ne. Primary <sup>22</sup>Ne is produced by diffusion of primary nitrogen from the H-burning shell into the core He-burning zone, or by the engulfment of part of the H-burning shell by the growing He-burning core. These processes occur in rotating massive star models (Hirschi, 2007; Meynet & Maeder, 2002a). In the He-burning zone, <sup>14</sup>N is transformed into <sup>22</sup>Ne through the classical reaction chain <sup>14</sup>N( $\alpha,\gamma$ )<sup>18</sup>F( $\beta^+\nu$ )<sup>18</sup>O( $\alpha,\gamma$ )<sup>22</sup>Ne.

In the He-burning zones (either in the core at the end of the core He-burning phase or in the He-burning shell during the core C-burning phase), neutrons are released through the reaction <sup>22</sup>Ne( $\alpha,n$ )<sup>25</sup>Mg. These neutrons then can either be captured by iron seeds (or elements with atomic numbers near the one of the iron called iron peak elements) and produce s-process elements or be captured by neutron poisons and thus removed from the flux of neutrons which is useful for s-process element nucleosynthesis. From what precedes one can easily conceive that the final outputs of s-process elements will depend on at least three factors: the amounts of 1.- <sup>22</sup>Ne, 2.- neutron poisons and 3.- iron seeds. In standard models, when the metallicity decreases, the amount of <sup>22</sup>Ne decreases (less neutrons produced), the amount of neutron poison becomes relatively more important because for [Fe/H] <sup>11</sup> < -2 main neutron poisons are primary elements and the amount of iron seeds decreases also. Thus very small quantities of s-process elements are expected (see the triangles in Fig. 33). When primary nitrogen and therefore primary <sup>22</sup>Ne is present as given by rotating models which can reproduce the observed trends for the N/O and C/O ratios observed in the halo stars, then a very different output is obtained. One can see that globally the abundances of the s-process elements are increased by many order of magnitudes, and that the elements produced in the greatest quantities are no longer in the iron-nickel region as is the case in standard models but cover an extended region from strontium up to baryum (Pignatari et al., 2008).

These first results need to be extended for other masses, rotation and metallicities. However they already show that some heavy s-process elements, not produced in standard models, might be produced in significant quantities in metal poor rotating stellar models. It will be very interesting in the future to find some non ambiguous signature of the occurrence of this process in the abundance pattern of very metal poor halo stars.

### C. The Carbon-Enhanced- Metal- Poor stars

At least 1 star out of 4, with [Fe/H]  $\leq$  -2.5, exhibits [C/Fe]  $\geq$  +1.0 (see the review by Beers & Christlieb, 2005). These stars are known as C-enhanced metal poor stars (CEMP). The two most iron poor stars presently known ([Fe/H] equal to -5.96 and -5.4) are C-rich, they are called C-rich Ultra-Metal Poor Stars (CRUMPS). The origin of their peculiar surface abundances is not known. The high nitrogen abundances observed in some CEMP stars implies that the material which is responsible for their peculiar abundance pattern must be heavily loaded in primary nitrogen. As seen above, rotating stars (both massive and intermediate mass stars) can produce large amounts of

<sup>10</sup> In that paper, the evolution was stopped in the E-AGB phase and was not pursued in the TP-AGB stars, however the quantity of primary nitrogen obtained at that stage will be a lower limit of what will be found at the end of the TP-AGB phase and thus represents some lower limit value.

<sup>11</sup> [Fe/H] =  $\lg(n(\text{Fe})_*/n(\text{H})_*) - \lg(n(\text{Fe})_\odot/n(\text{H})_\odot)$ , where  $n(\text{Fe})_*$  is the number density of iron nuclei in the considered star and  $n(\text{Fe})_\odot$  in the Sun,  $n(\text{H})_*$  and  $n(\text{H})_\odot$  the number of hydrogen nuclei in the star and in the Sun.

primary nitrogen. Rotating models can account also for the observed enhancements in C, O, Na, Mg and Al, thus Meynet et al. (2006) and Hirschi (2007) have proposed that CEMP stars may be formed from material ejected by fast rotating stars (massive or intermediate mass stars). Different chemical signatures are expected depending on the fact that the CEMP stars are formed from wind ejecta, from wind ejecta together with supernova ejecta or from the envelope of an AGB star. For instance CEMP stars formed from wind material of massive rotating stars mixed with small amount of pristine interstellar medium produce stars which are He-rich, Li-depleted and with low  $^{12}\text{C}/^{13}\text{C}$  ratios Meynet et al. (2010). By He-rich we mean stars that, at very low  $[\text{Fe}/\text{H}]$ , present a helium mass fraction between 0.30 and 0.60.

Rotation is probably a key ingredient to explain the abundance patterns of CEMP stars. Similar non-rotating models, without any other extra-mixing, do not succeed to simultaneously explain the enhancements in the three CNO elements.

#### D. The chemical anomalies in globular clusters

The finding of a double sequence in the globular cluster  $\omega$  Cen, as well as in many other globulars, and the further interpretation of the bluer sequence by a strong excess of helium constitutes a major enigma for stellar and galactic evolution (Norris, 2004). The bluer sequence with a metallicity  $[\text{Fe}/\text{H}] = -1.2$  or  $Z = 2 \cdot 10^{-3}$  implies an He-content  $Y = 0.38$  (0.35-0.45), i.e. an helium enrichment  $\Delta Y = 0.14$  (see also Norris, 2004). In turn, this demands a relative helium to metal enrichment  $\Delta Y/\Delta Z$  of the order of 70 (Piotto et al., 2005). This is enormous and more than one order of magnitude larger than the current value of  $\Delta Y/\Delta Z = 4 - 5$  (Pagel et al., 1992) obtained from extragalactic HII regions. A value of 4-5 is consistent with the chemical yields from supernovae (Maeder, 1992) forming black holes above about  $20-25 M_{\odot}$ . Maeder & Meynet (2006) showed that the wind contributions of low  $Z$  rotating stars are able to produce the high  $\Delta Y/\Delta Z$  observed in the blue Main Sequence in  $\omega$  Cen.

Recent observations show that He-rich stars in globular clusters might be a common feature. For instance, clusters like NGC 2808, M13 and NGC 6441 (Caloi & D’Antona, 2007) show a well-developed blue horizontal branch, and a strong slope upward from the red clump to the blue of the RR Lyrae regions. Both features could be explained if He-rich stars are present in these clusters. Kaviraj et al. (2007) studied the UV and optical properties of 38 massive globular clusters in M87 (elliptical galaxy in virgo cluster). A majority of these clusters appear extremely bright in the far-UV. Canonical models (i.e. models without any super He-rich stars) would imply ages for these clusters about 3 - 5 Gyr larger than the age of the Universe according to the WMAP data! This difficulty is removed when a super-He-rich ( $\Delta Y/\Delta Z > \sim 90$ ) stellar component is supposed to be present in these clusters.

It has also long been known that globular cluster stars present some striking anomalies in their content in other light elements<sup>12</sup>: while in all the Galactic globular clusters studied so far one finds “normal” stars with detailed chemical composition similar to that of field stars of same metallicity (i.e., same  $[\text{Fe}/\text{H}]$ ), one also observes numerous “anomalous” main sequence and red giant stars that are simultaneously deficient (to various degrees) in C, O, and Mg, and enriched in N, Na, and Al (see the review by Gratton et al., 2004).

It is clear now that these chemical peculiarities have been inherited at birth by the low-mass stars we observe today in globular clusters. The observed abundance pattern indicates that the material from which these stars formed was nuclearily processed by CNO burning and the NeNa- and MgAl-chains that occurred in an early generation of more massive and faster evolving globular cluster stars. Therefore, there were at least two generations of stars in Galactic globular clusters. The first one corresponds to the bulk of “normal” stars born with the pristine composition of the protocluster gas; these objects are those with the highest O and Mg and the lowest He and Na and Al abundances also found in their field contemporaries. The second generation contains the stars born out of material polluted to various degrees by the ejecta of more massive stars, and which present lower O and Mg and higher He, Na and Al abundances than their first generation counterparts.

Any model aiming at explaining the chemical properties of globular cluster stars should at least give an answer to the following questions: (1) Which type of stars did produce the material enriched in H-burning products? (2) What is the physical mechanism responsible for selecting only material bearing the signatures of H-processing? (3) Why does this process occur only in globular clusters?<sup>13</sup> Models for explaining the chemical anomalies in globular clusters invoke either TP-AGB stars (Ventura & D’Antona, 2008), massive binaries (de Mink et al., 2009) and massive rotating stars (Decressin et al., 2007b). These last authors propose that the matter from which the stars rich in H-burning products

<sup>12</sup> On the contrary, the content in heavy elements is fairly constant from star to star in any well-studied individual Galactic globular cluster (with the notable exception of  $\omega$  Cen).

<sup>13</sup> Indeed up to now the peculiar chemical patterns observed in globular clusters, i.e., the O-Na and Mg-Al anticorrelations, have not been found in field stars.



are formed, has been released by slow winds of fast rotating massive stars. Of course, part of the needed material can also be released by AGB stars. The massive star origin presents however some advantages: first a massive star can induce star formation in its surrounding, thus two effects, the enrichment and the star formation can be triggered by the same cause. Second, the massive star scenario allows to use a less flat IMF than the scenario invoking AGB stars (Prantzos & Charbonnel, 2006). The slope of the IMF might be even a Salpeter's one in case the globular cluster lost a great part of its first generation stars by tidal stripping (Decressin et al., 2007a). Finally the material released through the mechanism invoked above presents the property that the sum of the C+N+O elements remain constant. Interestingly, the sum  $[(C+N+O)/Fe]$  for individual globular cluster stars presenting otherwise very different chemical features is constant to within experimental errors in all the clusters studied so far with the exception of NGC 1851 (see references in Decressin et al., 2009). These last authors show also that rotating AGB models lead to a large increase of the total C+N+O value, which disfavors these models for explaining the origin of the chemical anomalies in most of the globular clusters.

### XIII. CONCLUSIONS

The evolution of massive stars depends sensitively on the metallicity which has an impact on the intensity of the line driven stellar winds and on rotational mixing. We can distinguish four metallicity regimes: 1.- the very metal poor regime  $0 \leq Z < \sim 10^{-10}$ ; 2.- The low metallicity regime  $10^{-10} \leq Z < 0.001$ ; 3.- The near solar metallicity regime  $0.001 \leq Z < 0.020$ ; 4.- The high metallicity regime  $0.020 \leq Z$ . In each of these metallicity ranges, some specific physical processes occur.

In the (likely rare) Pop III regime, Ekström et al. (2008a) find that models rotate with an internal profile  $\Omega(r)$  close to local angular momentum conservation, because of a very weak core-envelope coupling. Rotational mixing drives a H-shell boost due to a sudden onset of CNO cycle in the shell. This boost leads to a high  $^{14}N$  production, which can be as much as  $10^6$  times higher than the production of the non-rotating models. Due to the low mass loss and the weak coupling, the core retains a high angular momentum at the end of the evolution. The high rotation rate at death probably leads to a much stronger explosion than previously expected, changing the fate of the models.

In the low metallicity regime, rotating models produce large amounts of primary  $^{13}C$ ,  $^{14}N$  and  $^{22}Ne$ . Rotation has also probably a strong impact on the s-process elements nucleosynthesis. Rotational mixing, by increasing the CNO surface abundances, might trigger important mass losses through radiatively driven stellar winds. Stars may also lose some mass by mechanical mass loss when rotating at the critical limit. For all these reasons, rotation may play an important role in explaining the CEMP stars and the chemical anomalies in globular clusters.

In the near solar metallicity regime, rotation and mass loss by stellar winds are of similar importance, however the balance of the two effects varies with mass. Neither of the two aspects can be neglected. This metallicity range is also the one in which models can be checked and calibrated by comparisons with well observed features either of individual stars or of stellar populations. Among these observed features let us cite

- The observed changes of the surface abundances.
- The observed changes of the surface velocities.
- The width of the Main Sequence band.
- The shape of fast rotating stars measured by interferometric technics, the shape of the nebulosities around high mass losing stars, the anisotropies of the stellar winds.
- In a near future, the size of the convective core as deduced from asteroseismic analysis, as well as the variation with depth of the angular velocity as obtained from asteroseismic observations. Note that simultaneous observations in asteroseismology and interferometry (Cunha et al., 2007), together with estimate of the surface magnetic field (Wade et al., 2010a) will provide new and important clues on massive star evolution.
- The existence and variation with  $Z$  of the populations of Be stars.
- The variation with  $Z$  of the blue to red supergiant ratios.
- The variation with  $Z$  of the Wolf-Rayet populations.
- The rotation rates of young pulsars.
- The variation with  $Z$  of different core collapse supernova types.

As a general statement, it does appear that models including the effects of rotation provide a much better fit to most of the above observed features. Other aspects, not discussed in the present review as the synthesis of  $^{26}\text{Al}$ , the origin of the isotopic anomalies in the galactic cosmic rays and in meteorites can also be affected by rotation (Arnould et al., 2006; Binns et al., 2005; Palacios et al., 2005).

Above solar metallicities, radiative line driven winds become the dominant factor affecting the evolution of massive stars. In models with moderate rotation, we note however that the effects of rotational mixing are still important but their impact is less apparent being somewhat mixed with those of the stellar winds. An interesting difference which occurs at high metallicity is the evolution of the angular momentum. One expects that at high metallicity, angular momentum is more easily transported from the core to the surface, due to faster meridional currents, and more easily ejected at the surface by the stellar winds. Thus, everything being equal, one would expect that the angular momentum of the central regions will be lower when the metallicity is higher. Together with the fact that Black-Hole formation is probably more difficult at high  $Z$  (also because of the strong stellar winds), this makes the formation of collapsars which are considered as a serious candidate for long soft gamma ray burst much less favorable at high metallicity. In case the rotation rate of young pulsar depends to some extent to the rotation rate of the core at the presupernova stage, the above line of reasoning would lead to the conclusion that the rotation rate of young pulsars should be slower in metal rich regions than in metal poor ones.

As we can see, rotation and mass loss are two key physical processes which have a strong impact on the evolution of the massive stars during the whole cosmic history. These two processes, which interact with each other, are responsible for a great diversity of outputs, going from the shape of the nebulae, to the evolution of the abundances in the interstellar medium, passing through the origin of the Gamma Ray Bursts. It is interesting to note that the energy in form of rotational energy in stars is quite small, at most of the order of the percent of the gravitational energy. Similarly, metallicity or heavy elements, which shape the intensity of the line driven winds, represent only at most two percents of the mass of all chemical elements. Nevertheless, the impacts of both rotation and metallicity are very important. It reminds us that sometimes a pinch is sufficient for creating new worlds!

## References

- Aerts, C. 2008, in IAU Symposium, Vol. 250, IAU Symposium, ed. F. Bresolin, P. A. Crowther, & J. Puls, 237–244
- Akerman, C. J., Carigi, L., Nissen, P. E., Pettini, M., & Asplund, M. 2004, *A&A*, 414, 931
- Arnould, M., Goriely, S., & Meynet, G. 2006, *A&A*, 453, 653
- Asplund, M., Grevesse, N., & Sauval, A. J. 2005, in Astronomical Society of the Pacific Conference Series, Vol. 336, Cosmic Abundances as Records of Stellar Evolution and Nucleosynthesis, ed. T. G. Barnes, III & F. N. Bash, 25
- Beers, T. C. & Christlieb, N. 2005, *ARA&A*, 43, 531
- Binns, W. R., Wiedenbeck, M. E., Arnould, M., et al. 2005, *ApJ*, 634, 351
- Braithwaite, J. 2006, *A&A*, 449, 451
- Brott, I., de Mink, S. E., Cantiello, M., et al. 2011, *ArXiv e-prints*
- Caloi, V. & D’Antona, F. 2007, *A&A*, 463, 949
- Cantiello, M., Braithwaite, J., Brandenburg, A., et al. 2010, *ArXiv e-prints*
- Canuto, V. M. 2002, *A&A*, 384, 1119
- Cappellaro, E., Evans, R., & Turatto, M. 1999, *A&A*, 351, 459
- Carciofi, A. C., Domiciano de Souza, A., Magalhães, A. M., Bjorkman, J. E., & Vakili, F. 2008, *ApJ*, 676, L41
- Chaboyer, B. & Zahn, J.-P. 1992, *A&A*, 253, 173
- Charbonneau, P. 1992, *A&A*, 259, 134
- Charbonnel, C. & Talon, S. 2005, *Science*, 309, 2189
- Chiappini, C., Ekström, S., Meynet, G., et al. 2008, *A&A*, 479, L9
- Chiappini, C., Hirschi, R., Meynet, G., et al. 2006, *A&A*, 449, L27
- Chieffi, A. & Limongi, M. 2004, *ApJ*, 608, 405
- Collins, II, G. W. & Sonneborn, G. H. 1977, *ApJS*, 34, 41
- Crowther, P. A. 2007, *ARA&A*, 45, 177
- Crowther, P. A., Dessart, L., Hillier, D. J., Abbott, J. B., & Fullerton, A. W. 2002, *A&A*, 392, 653
- Crowther, P. A., Lennon, D. J., & Walborn, N. R. 2006, *A&A*, 446, 279
- Cunha, M. S., Aerts, C., Christensen-Dalsgaard, J., et al. 2007, *A&A Rev.*, 14, 217
- de Mink, S. E., Pols, O. R., Langer, N., & Izzard, R. G. 2009, *A&A*, 507, L1
- Decressin, T., Charbonnel, C., & Meynet, G. 2007a, *A&A*, 475, 859
- Decressin, T., Charbonnel, C., Siess, L., et al. 2009, *ArXiv e-prints*
- Decressin, T., Meynet, G., Charbonnel, C., Prantzos, N., & Ekström, S. 2007b, *A&A*, 464, 1029
- Denissenkov, P. A., Ivanova, N. S., & Weiss, A. 1999, *A&A*, 341, 181
- Deupree, R. G. 1990, *ApJ*, 357, 175
- Deupree, R. G. 2001, *ApJ*, 552, 268
- Deupree, R. G. & Beslin, W. 2010, *ApJ*, 721, 1900

- Domiciano de Souza, A., Kervella, P., Jankov, S., et al. 2003, *A&A*, 407, L47
- Domiciano de Souza, A., Kervella, P., Jankov, S., et al. 2005, *A&A*, 442, 567
- Dufton, P. L., Smartt, S. J., Lee, J. K., et al. 2006, *A&A*, 457, 265
- Eggenberger, P., Maeder, A., & Meynet, G. 2005, *A&A*, 440, L9
- Eggenberger, P., Meynet, G., & Maeder, A. 2002, *A&A*, 386, 576
- Ekström, S., Meynet, G., Chiappini, C., Hirschi, R., & Maeder, A. 2008a, *A&A*, 489, 685
- Ekström, S., Meynet, G., Maeder, A., & Barblan, F. 2008b, *A&A*, 478, 467
- Eldridge, J. J., Izzard, R. G., & Tout, C. A. 2008, *MNRAS*, 384, 1109
- Eldridge, J. J. & Vink, J. S. 2006, *A&A*, 452, 295
- Espinosa Lara, F. & Rieutord, M. 2007, *A&A*, 470, 1013
- Foellmi, C., Moffat, A. F. J., & Guerrero, M. A. 2003a, *MNRAS*, 338, 360
- Foellmi, C., Moffat, A. F. J., & Guerrero, M. A. 2003b, *MNRAS*, 338, 1025
- Fukuda, I. 1982, *PASP*, 94, 271
- Georgy, C., Meynet, G., & Maeder, A. 2011, *A&A*, 527, A52+
- Georgy, C., Meynet, G., Walder, R., Folini, D., & Maeder, A. 2009, *A&A*, 502, 611
- Gies, D. R. & Lambert, D. L. 1992, *ApJ*, 387, 673
- Goldreich, P. & Schubert, G. 1967, *ApJ*, 150, 571
- Gräfenr, G. & Hamann, W.-R. 2008, *A&A*, 482, 945
- Gratton, R., Sneden, C., & Carretta, E. 2004, *ARA&A*, 42, 385
- Greif, T. H. & Bromm, V. 2006, *MNRAS*, 373, 128
- Hartmann, L. 1998, *Accretion Processes in Star Formation*, ed. L. Hartmann
- Heap, S. R., Lanz, T., & Hubeny, I. 2006, *ApJ*, 638, 409
- Heger, A., Fryer, C. L., Woosley, S. E., Langer, N., & Hartmann, D. H. 2003, *ApJ*, 591, 288
- Heger, A. & Langer, N. 2000, *ApJ*, 544, 1016
- Heger, A., Langer, N., & Woosley, S. E. 2000, *ApJ*, 528, 368
- Heger, A. & Woosley, S. 2005, in *IAU Symposium*, Vol. 228, *From Lithium to Uranium: Elemental Tracers of Early Cosmic Evolution*, ed. V. Hill, P. François, & F. Primas, 297–302
- Heger, A. & Woosley, S. E. 2010, *ApJ*, 724, 341
- Heger, A., Woosley, S. E., & Spruit, H. C. 2005, *ApJ*, 626, 350
- Henrichs, H. F., Neiner, C., & Geers, V. C. 2003a, in *IAU Symposium*, Vol. 212, *A Massive Star Odyssey: From Main Sequence to Supernova*, ed. K. van der Hucht, A. Herrero, & C. Esteban, 202
- Henrichs, H. F., Neiner, C., & Geers, V. C. 2003b, in *Astronomical Society of the Pacific Conference Series*, Vol. 305, *Astronomical Society of the Pacific Conference Series*, ed. L. A. Balona, H. F. Henrichs, & R. Medupe, 301
- Herrero, A., Kudritzki, R. P., Vilchez, J. M., et al. 1992, *A&A*, 261, 209
- Hirschi, R. 2007, *A&A*, 461, 571
- Hirschi, R., Meynet, G., & Maeder, A. 2004, *A&A*, 425, 649
- Hirschi, R., Meynet, G., & Maeder, A. 2005a, *A&A*, 443, 581
- Hirschi, R., Meynet, G., & Maeder, A. 2005b, *A&A*, 433, 1013
- Huang, W. & Gies, D. R. 2006a, *ApJ*, 648, 580
- Huang, W. & Gies, D. R. 2006b, *ApJ*, 648, 591
- Hunter, I., Brott, I., Langer, N., et al. 2009, *A&A*, 496, 841
- Hunter, I., Dufton, P. L., Smartt, S. J., et al. 2007, *A&A*, 466, 277
- Hunter, I., Lennon, D. J., Dufton, P. L., et al. 2008, *A&A*, 479, 541
- Israelian, G., Ecuillon, A., Rebolo, R., et al. 2004, *A&A*, 421, 649
- Johnson, J. L. & Bromm, V. 2006, *MNRAS*, 366, 247
- Kaviraj, S., Sohn, S. T., O’Connell, R. W., et al. 2007, *MNRAS*, 377, 987
- Kawaler, S. D. 1988, *ApJ*, 333, 236
- Kilian, J. 1992, *A&A*, 262, 171
- Kippenhahn, R. & Thomas, H.-C. 1970, in *IAU Colloq. 4: Stellar Rotation*, 20–
- Knobloch, E. & Spruit, H. C. 1983, *A&A*, 125, 59
- Krishnamurthi, A., Pinsonneault, M. H., Barnes, S., & Sofia, S. 1997, *ApJ*, 480, 303
- Kudritzki, R.-P. & Puls, J. 2000, *ARA&A*, 38, 613
- Lamers, H. J. G. L. M. & Cassinelli, J. P. 1999, *Introduction to Stellar Winds* (Cambridge University Press)
- Langer, N. 1998, *A&A*, 329, 551
- Langer, N. & Maeder, A. 1995, *A&A*, 295, 685
- Lebovitz, N. R. 1967, *ARA&A*, 5, 465
- Lovekin, C. C. & Deupree, R. G. 2008, *ApJ*, 679, 1499
- Lovekin, C. C., Deupree, R. G., & Clement, M. J. 2009, *ApJ*, 693, 677
- Lovekin, C. C., Deupree, R. G., & Short, C. I. 2006, *ApJ*, 643, 460
- Lyubimkov, L. S., Rostopchin, S. I., & Lambert, D. L. 2004, *MNRAS*, 351, 745
- Maeder, A. 1981, *A&A*, 102, 401
- Maeder, A. 1987a, *A&A*, 173, 247
- Maeder, A. 1987b, *A&A*, 178, 159
- Maeder, A. 1992, *A&A*, 264, 105

- Maeder, A. 1995, *A&A*, 299, 84
- Maeder, A. 1999, *A&A*, 347, 185
- Maeder, A. 2003, *A&A*, 399, 263
- Maeder, A. 2009, *Physics, Formation and Evolution of Rotating Stars* (Springer Verlag)
- Maeder, A. & Desjacques, V. 2001, *A&A*, 372, L9
- Maeder, A. & Eenens, P., eds. 2004, *IAU Symposium*, Vol. 215, *Stellar Rotation*
- Maeder, A., Grebel, E. K., & Mermilliod, J.-C. 1999, *A&A*, 346, 459
- Maeder, A. & Meynet, G. 1994, *A&A*, 287, 803
- Maeder, A. & Meynet, G. 2000a, *A&A*, 361, 159
- Maeder, A. & Meynet, G. 2000b, *A&A*, 361, 159
- Maeder, A. & Meynet, G. 2001a, *A&A*, 373, 555
- Maeder, A. & Meynet, G. 2001b, *A&A*, 373, 555
- Maeder, A. & Meynet, G. 2004, *A&A*, 422, 225
- Maeder, A. & Meynet, G. 2005a, *A&A*, 440, 1041
- Maeder, A. & Meynet, G. 2005b, *A&A*, 440, 1041
- Maeder, A. & Meynet, G. 2006, *A&A*, 448, L37
- Maeder, A., Meynet, G., Ekstrom, S., & Georgy, C. 2008, *ArXiv e-prints*
- Maeder, A. & Peytremann, E. 1970, *A&A*, 7, 120
- Maeder, A. & Zahn, J.-P. 1998, *A&A*, 334, 1000
- Marigo, P., Chiosi, C., & Kudritzki, R.-P. 2003, *A&A*, 399, 617
- Martayan, C., Floquet, M., Hubert, A. M., et al. 2007, *A&A*, 472, 577
- Martayan, C., Frémat, Y., Hubert, A.-M., et al. 2006, *A&A*, 452, 273
- Massey, P. 2003, *ARA&A*, 41, 15
- Mathis, S., Palacios, A., & Zahn, J.-P. 2004, *A&A*, 425, 243
- Meynet, G., Eggenberger, P., & Maeder, A. 2011, *A&A*, 525, L11+
- Meynet, G., Ekström, S., & Maeder, A. 2006, *A&A*, 447, 623
- Meynet, G., Ekström, S., Maeder, A., et al. 2008, in *IAU Symposium*, Vol. 250, *IAU Symposium*, ed. F. Bresolin, P. A. Crowther, & J. Puls, 147–160
- Meynet, G., Hirschi, R., Ekstrom, S., et al. 2010, *A&A*, 521, A30+
- Meynet, G. & Maeder, A. 1997, *A&A*, 321, 465
- Meynet, G. & Maeder, A. 2000, *A&A*, 361, 101
- Meynet, G. & Maeder, A. 2002a, *A&A*, 390, 561
- Meynet, G. & Maeder, A. 2002b, *A&A*, 381, L25
- Meynet, G. & Maeder, A. 2003, *A&A*, 404, 975, paper X
- Meynet, G. & Maeder, A. 2005, *A&A*, 429, 581, paper XI
- Meynet, G. & Maeder, A. 2007, *A&A*, 464, L11
- Meynet, G., Maeder, A., & Mowlavi, N. 2004, *A&A*, 416, 1023
- Meynet, G., Maeder, A., Schaller, G., Schaerer, D., & Charbonnel, C. 1994, *A&AS*, 103, 97
- Modjaz, M., Kewley, L., Kirshner, R. P., et al. 2008, *AJ*, 135, 1136
- Mokiem, M. R., de Koter, A., Evans, C. J., et al. 2007, *A&A*, 465, 1003
- Mokiem, M. R., de Koter, A., Evans, C. J., et al. 2006, *A&A*, 456, 1131
- Monnier, J. D., Zhao, M., Pedretti, E., et al. 2007, *Science*, 317, 342
- Morel, T., Hubrig, S., & Briquet, M. 2008, *A&A*, 481, 453
- Nomoto, K., Yamaoka, H., Pols, O. R., et al. 1994, *Nature*, 371, 227
- Norris, J. E. 2004, *ApJ*, 612, L25
- Nota, A. 1999, in *Lecture Notes in Physics*, Berlin Springer Verlag, Vol. 523, *IAU Colloq. 169: Variable and Non-spherical Stellar Winds in Luminous Hot Stars*, ed. B. Wolf, O. Stahl, & A. W. Fullerton, 62
- Nugis, T. & Lamers, H. J. G. L. M. 2000, *A&A*, 360, 227
- Nugis, T. & Lamers, H. J. G. L. M. 2002, *A&A*, 389, 162
- Pagel, B. E. J., Simonson, E. A., Terlevich, R. J., & Edmunds, M. G. 1992, *MNRAS*, 255, 325
- Palacios, A., Meynet, G., Vuissoz, C., et al. 2005, *A&A*, 429, 613
- Peterson, D. M., Hummel, C. A., Pauls, T. A., et al. 2008, in *The Power of Optical/IR Interferometry: Recent Scientific Results and 2nd Generation*, ed. A. Richichi, F. Delplancke, F. Paresce, & A. Chelli, 43
- Peterson, D. M., Hummel, C. A., Pauls, T. A., et al. 2006, *ApJ*, 636, 1087
- Pettini, M., Zych, B. J., Steidel, C. C., & Chaffee, F. H. 2008, *MNRAS*, 385, 2011
- Pignatari, M., Gallino, R., Meynet, G., et al. 2008, *ApJ*, 687, L95
- Piotto, G., Villanova, S., Bedin, L. R., et al. 2005, *ApJ*, 621, 777
- Pitts, E. & Tayler, R. J. 1985, *MNRAS*, 216, 139
- Podsiadlowski, P., Joss, P. C., & Hsu, J. J. L. 1992, *ApJ*, 391, 246
- Podsiadlowski, P., Mazzali, P. A., Nomoto, K., Lazzati, D., & Cappellaro, E. 2004, *ApJ*, 607, L17
- Prantzos, N. & Boissier, S. 2003, *A&A*, 406, 259
- Prantzos, N. & Charbonnel, C. 2006, *A&A*, 458, 135
- Przybilla, N., Farnstein, M., Nieva, M. F., Meynet, G., & Maeder, A. 2010, *A&A*, 517, A38+
- Roxburgh, I. W. 2006, *A&A*, 454, 883

- Schneider, R., Omukai, K., Inoue, A. K., & Ferrara, A. 2006, MNRAS, 369, 1437
- Schwarzschild, M. 1958, Structure and evolution of the stars., ed. M. Schwarzschild
- Searle, S. C., Prinja, R. K., Massa, D., & Ryans, R. 2008, A&A, 481, 777
- Slettebak, A. 1970, in IAU Colloq. 4: Stellar Rotation, 3
- Smartt, S. J. 2009, ARA&A, 47, 63
- Spite, M., Cayrel, R., Plez, B., et al. 2005, A&A, 430, 655
- Spruit, H. C. 1999, A&A, 349, 189
- Spruit, H. C. 2002, A&A, 381, 923
- Stacy, A., Bromm, V., & Loeb, A. 2010, ArXiv e-prints
- Stothers, R. & Chin, C.-W. 1979, ApJ, 233, 267
- Suijs, M. P. L., Langer, N., Poelarends, A.-J., et al. 2008, A&A, 481, L87
- Talon, S., Zahn, J., Maeder, A., & Meynet, G. 1997, A&A, 322, 209
- Talon, S. & Zahn, J.-P. 1997, A&A, 317, 749
- Tayler, R. J. 1973, MNRAS, 161, 365
- Trundle, C., Dufton, P. L., Hunter, I., et al. 2007, A&A, 471, 625
- van Belle, G. T., Ciardi, D. R., ten Brummelaar, T., et al. 2006, ApJ, 637, 494
- van der Hucht, K. A. 2001, VizieR Online Data Catalog, 3215, 0
- van Loon, J. T., Cioni, M.-R. L., Zijlstra, A. A., & Loup, C. 2005, A&A, 438, 273
- van Marle, A. J., Langer, N., Yoon, S.-C., & García-Segura, G. 2008, A&A, 478, 769
- Vanbeveren, D., Van Bever, J., & Belkus, H. 2007, ApJ, 662, L107
- Venn, K. A. & Lambert, D. L. 2008, ApJ, 677, 572
- Ventura, P. & D'Antona, F. 2008, MNRAS, 385, 2034
- Villamariz, M. R. & Herrero, A. 2005, A&A, 442, 263
- Villamariz, M. R., Herrero, A., Becker, S. R., & Butler, K. 2002, A&A, 388, 940
- Vink, J. S. 2009, ArXiv e-prints
- Vink, J. S., de Koter, A., & Lamers, H. J. G. L. M. 2000, A&A, 362, 295
- Vink, J. S., de Koter, A., & Lamers, H. J. G. L. M. 2001, A&A, 369, 574
- Wade, G. A., Alecian, E., Bohlender, D. A., et al. 2010a, ArXiv e-prints
- Wade, G. A., Grunhut, J. H., Marcolino, W. L. F., et al. 2010b, ArXiv e-prints
- Walder, R. & Folini, D. 2000, in Astronomical Society of the Pacific Conference Series, Vol. 204, Thermal and Ionization Aspects of Flows from Hot Stars, ed. H. Lamers & A. Sagar, 281–+
- Walder, R., Folini, D., & Meynet, G. 2011, Space Sci. Rev., 57
- Wheeler, J. C., Harkness, R. P., Barker, E. S., Cochran, A. L., & Wills, D. 1987, ApJ, 313, L69
- Wisniewski, J. P. & Bjorkman, K. S. 2006, ApJ, 652, 458
- Woosley, S. E. 1993, ApJ, 405, 273
- Woosley, S. E. & Bloom, J. S. 2006, ARA&A, 44, 507
- Woosley, S. E. & Heger, A. 2006, ApJ, 637, 914
- Yoon, S.-C. & Langer, N. 2005, A&A, 443, 643
- Yoon, S.-C., Langer, N., & Norman, C. 2006, A&A, 460, 199
- Zahn, J.-P. 1992, A&A, 265, 115
- Zahn, J.-P., Brun, A. S., & Mathis, S. 2007, A&A, 474, 145

## Figures

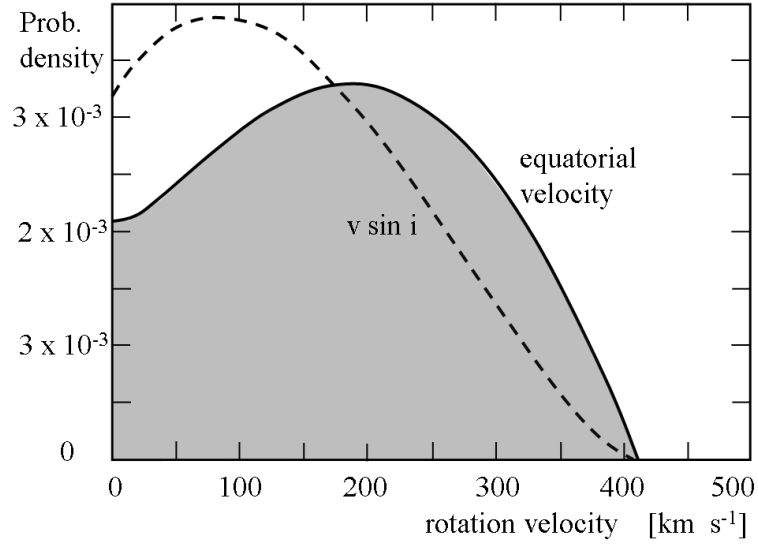


FIG. 1 Probability density by  $\text{km s}^{-1}$  of rotation velocities for 496 stars with types O9.5 to B8, i.e. masses between about 3 and  $20 M_{\odot}$  (Huang & Gies, 2006a).

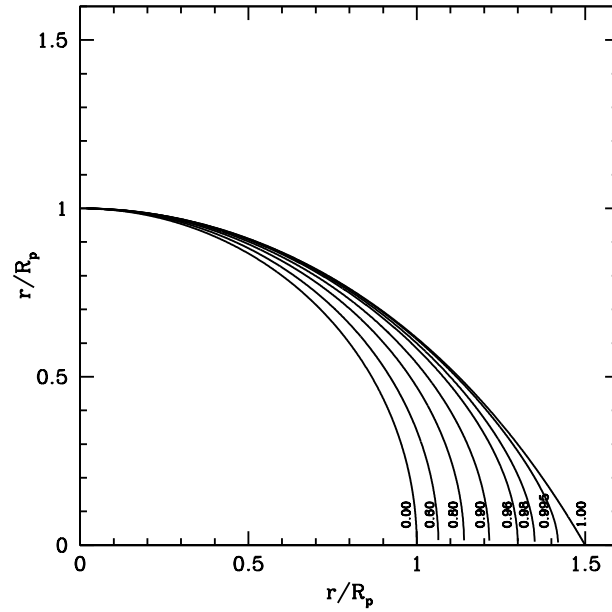


FIG. 2 Shape of the surface for various values of  $\omega = \frac{\Omega}{\Omega_{\text{crit}}}$  (labelled at the bottom of each curve). The x-axis is the equatorial radius, and the y-axis the polar one. Hence this is how we would see the star equator-on.  $R_p$  is the polar radius. Figure taken from Georgy et al. (2011).

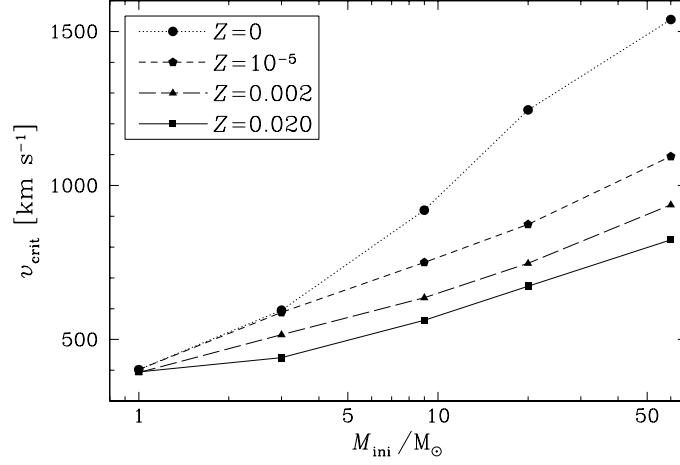


FIG. 3 The critical velocities  $v_{\text{crit}}$  as a function of stellar masses for different metallicities  $Z$  for stars on the ZAMS. The effects of the changes of the polar radius with rotation are accounted for. Figure taken from Ekström et al. (2008b).

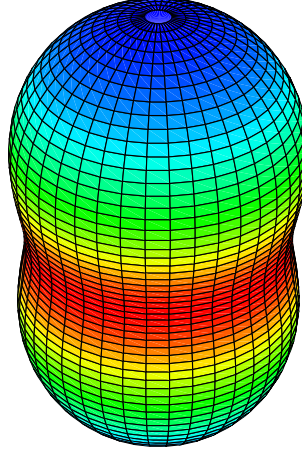


FIG. 4 The mass fluxes around a rotating star of  $100 M_{\odot}$  with  $10^{6.5} L_{\odot}$  and a ratio of the angular velocity to the break-up angular velocity  $\omega = 0.80$ , assuming a polar  $T_{\text{eff}} = 30000 \text{ K}$  (Maeder & Desjacques, 2001).

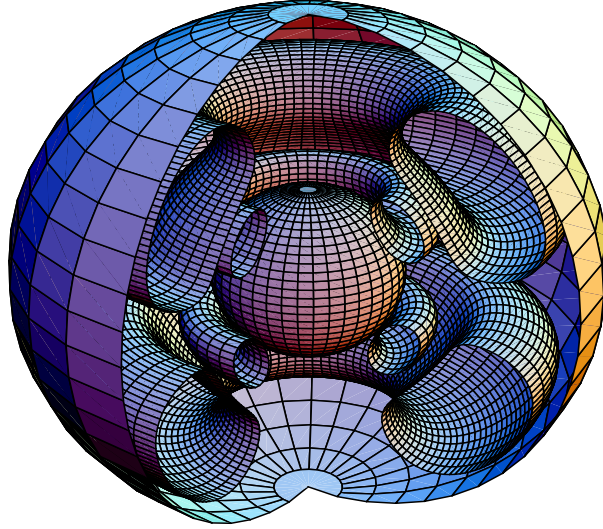


FIG. 5 Schematic structure with stream lines of meridional circulation in a rotating  $20 M_{\odot}$  model of  $5.2 R_{\odot}$  with  $Y = 0.30$ ,  $Z = 0.02$  and  $v_{\text{ini}} = 300 \text{ km s}^{-1}$  at the beginning of the MS phase. The figure is made as a function of  $M_r$ . In the upper hemisphere on the right section, matter is turning counterclockwise along the outer stream line and clockwise along the inner one. The inner sphere is the convective core. It has a radius of  $1.7 R_{\odot}$  (Meynet & Maeder, 2002a).

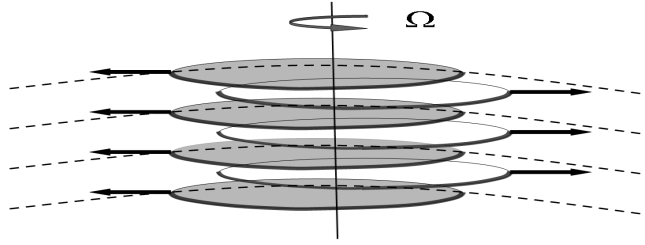


FIG. 6 Unstable displacements with  $m = 1$  of the azimuthal magnetic field in the polar region. The large arcs (thin broken lines) indicate the horizontal stellar surfaces. Adapted from Spruit (1999).

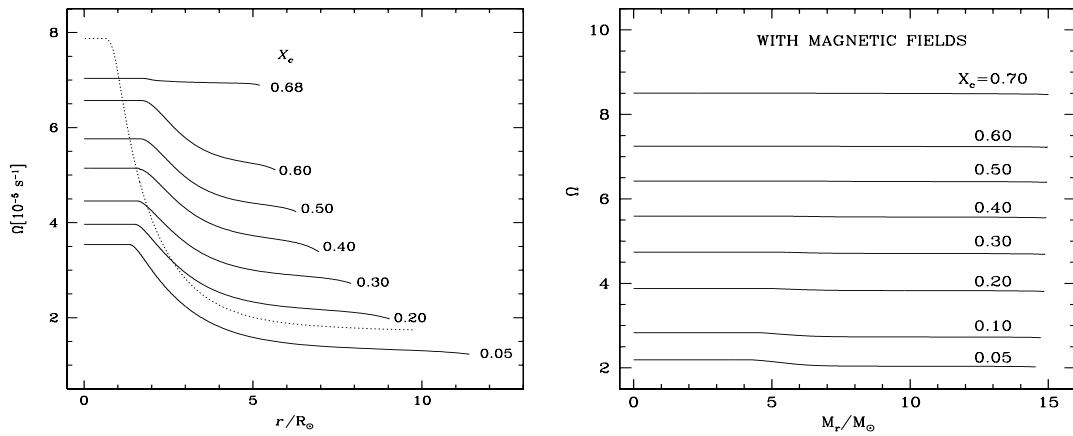


FIG. 7 Left: evolution of the angular velocity  $\Omega$  as a function of the distance to the center in a  $20 M_{\odot}$  star with  $v_{\text{ini}} = 300 \text{ km s}^{-1}$ .  $X_c$  is the hydrogen mass fraction at the center. The dotted line shows the profile when the He-core contracts at the end of the H-burning phase (Meynet & Maeder, 2000). Right: rotation profiles at various stages of evolution (labeled by the central H content  $X_c$ ) of a  $15 M_{\odot}$  model with  $X = 0.705$ ,  $Z = 0.02$ , an initial velocity of  $300 \text{ km s}^{-1}$  and magnetic field from the Tayler-Spruit dynamo (Maeder & Meynet, 2005b).



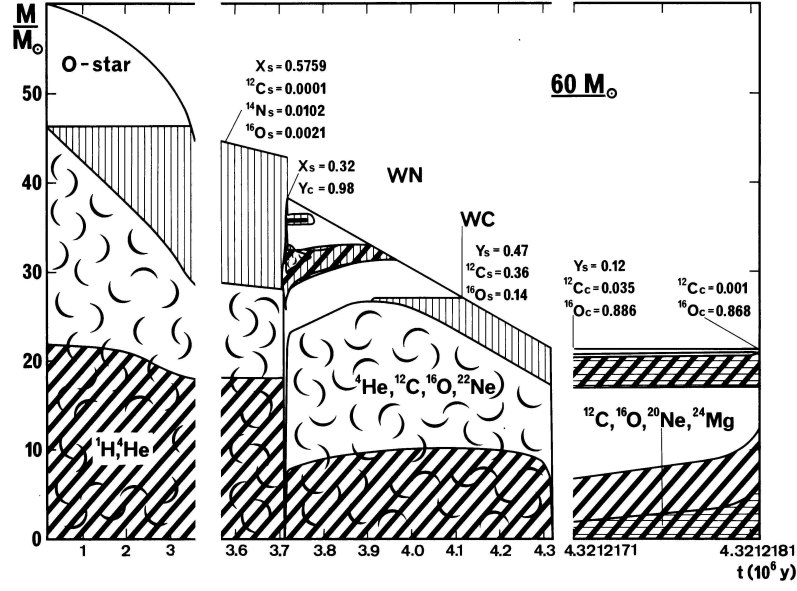


FIG. 8 Evolution with mass loss (only) of the total mass and internal structure as a function of time for a star with an initial mass of  $60 M_{\odot}$  (Maeder, 1987a). The cloudy regions indicate convection, the heavy diagonal hatching the regions of high nuclear production, the light vertical hatching regions of variable composition.

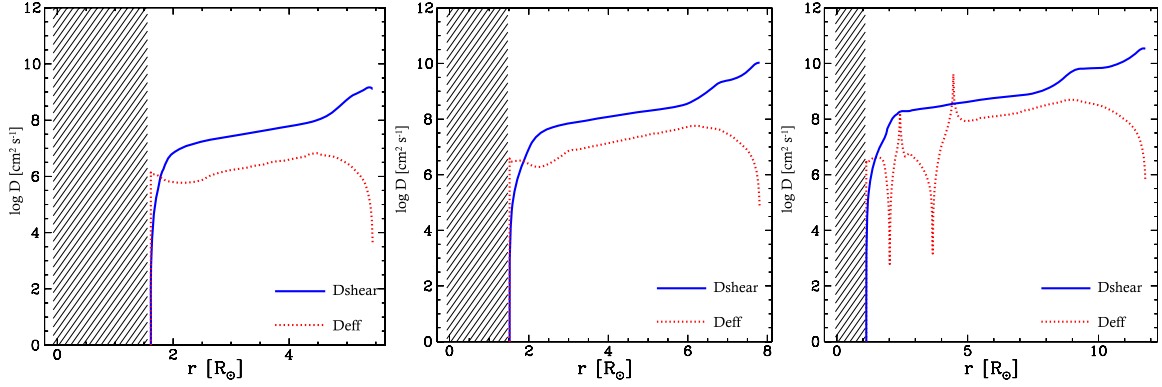


FIG. 9 Variation of the diffusion coefficients as a function of the radius inside a  $20 M_{\odot}$  model with an initial metallicity  $Z=0.014$  and an initial velocity on the ZAMS equal to 40% the critical velocity. From left to right, is shown the situation corresponding to central mass fraction of hydrogen equal to 0.60, 0.30 and 0.01 respectively. Courtesy of S. Ekstrom.

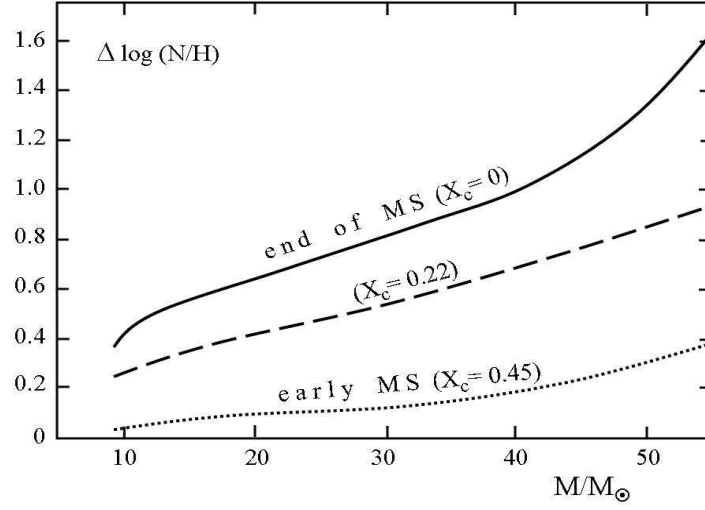


FIG. 10 The differences in  $\log(N/H)$  as a function of the initial masses at 3 stages during the MS phase for models at  $Z = 0.02$  with the average rotation velocities (i.e. 217, 209, 197, 183, 172, 168  $\text{km s}^{-1}$  for respectively 12, 15, 20, 25 40 and 60  $M_{\odot}$ ). The 3 stages are indicated by the value of the central H-content  $X_c$  (Maeder et al., 2008).

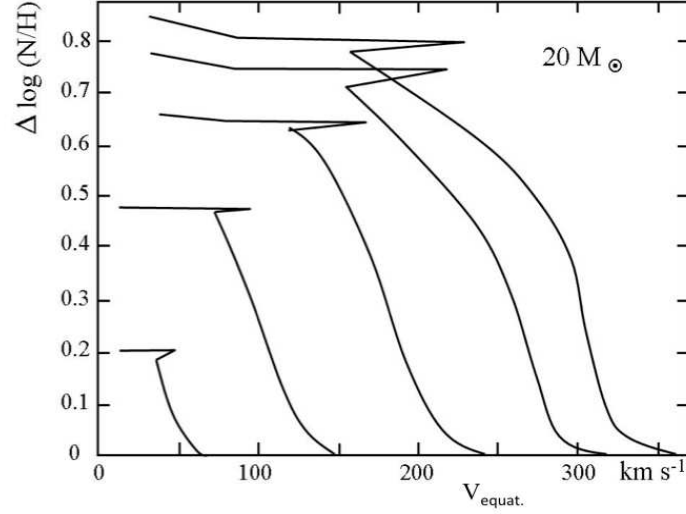


FIG. 11 The evolution of the differences in  $\log(N/H)$  during the MS phase as a function of the actual rotation velocities ( $\sin i$  being equal to 1 here) for models of 20  $M_{\odot}$  with  $Z = 0.02$  and different initial velocities (Maeder et al., 2008).

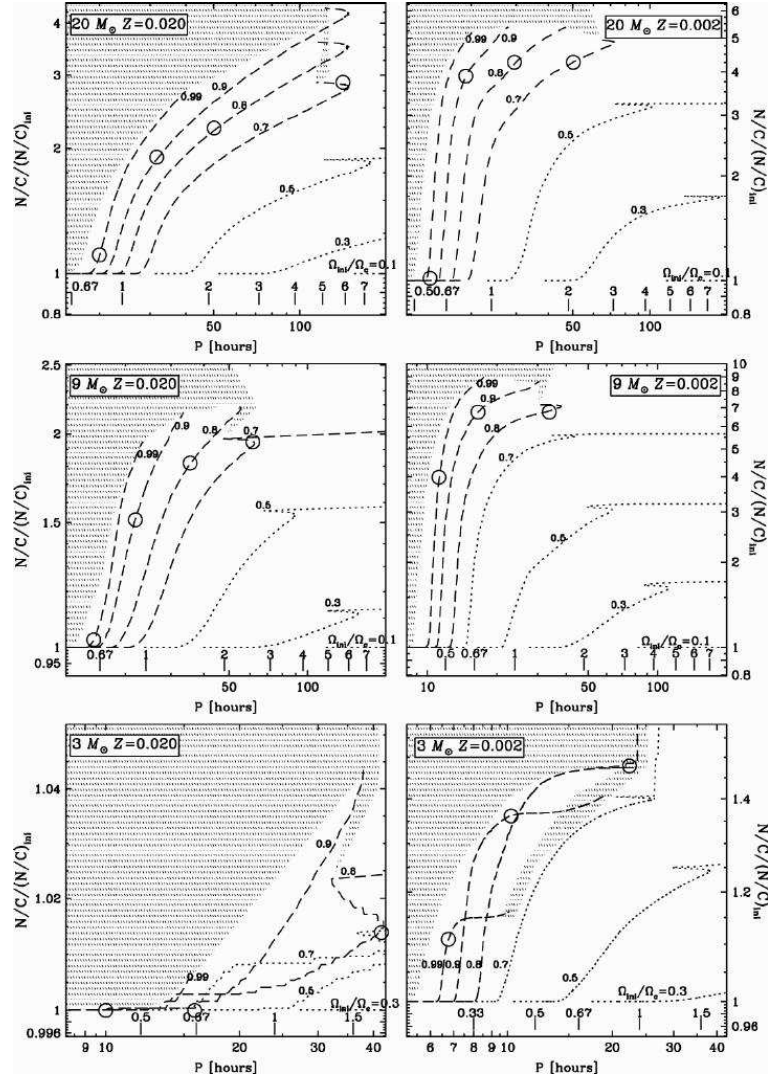


FIG. 12 Evolutionary tracks in the plane surface N/C ratio, normalized to its initial value, versus the rotational period in hours for different initial mass stars, various initial velocities and for the metallicities  $Z=0.02$  and  $0.002$ . Positions of some periods in days are indicated at the bottom of the figure. The dotted tracks never reach the critical limit during the MS phase. The short dashed tracks reach the critical limit during the MS phase. The dividing line between the shaded and non-shaded areas corresponds to the entrance into the stage when the star is at the critical limit during the MS evolution. Big circles along some tracks indicate the stage when  $v/v_{\text{crit}}$  becomes superior to 0.7. If Be stars are rotating at velocities superior to 70% of the critical velocity, present models would predict that they would lie in the region comprised between the big circles and the dividing line. Beware the different vertical scales used when comparing similar masses at different metallicities. Figure taken from Ekström et al. (2008b).

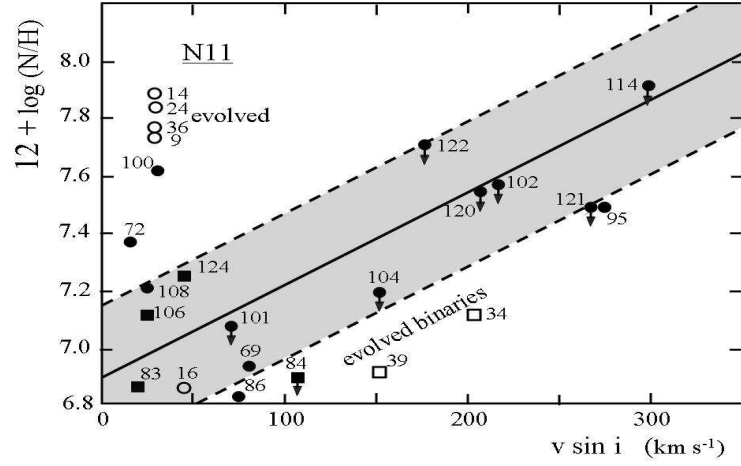


FIG. 13 The N abundance (in a scale where  $\log H = 12.0$ ) as a function of  $v \sin i$  for the MS stars (black dots) in N11 with masses between 14 and 20  $M_{\odot}$  according to Hunter et al. (2008). The downward arrows indicate abundance upper limits. The binaries are shown by a square. The evolved stars in a band of 0.1 dex in  $\log T_{\text{eff}}$  beyond the end of the MS are shown with open symbols. The grey band indicates uncertainties of  $\pm 0.25$  dex (Maeder et al., 2008).

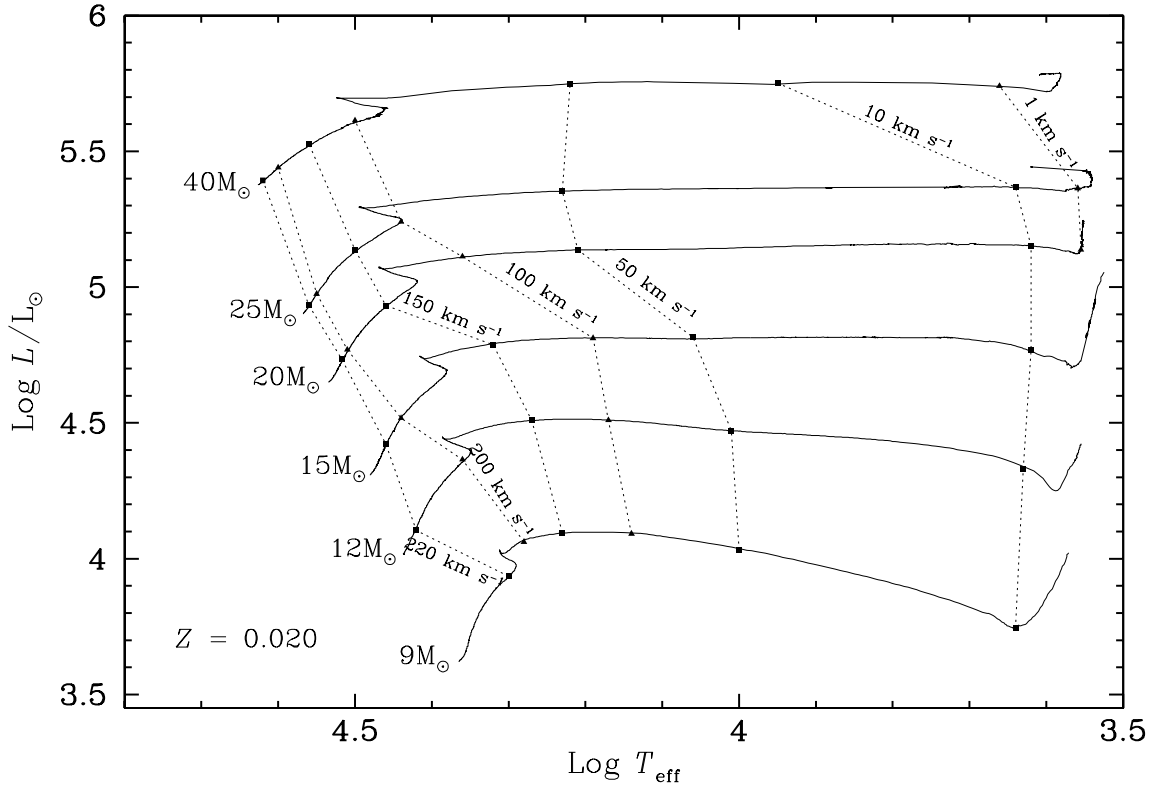


FIG. 14 Evolution of the equatorial surface velocities along the evolutionary tracks in the HR diagram starting from  $v_{\text{ini}} = 300$   $\text{km s}^{-1}$ . For purpose of clarity, only the first part of the 40  $M_{\odot}$  track is shown. Figure taken from Meynet & Maeder (2000).

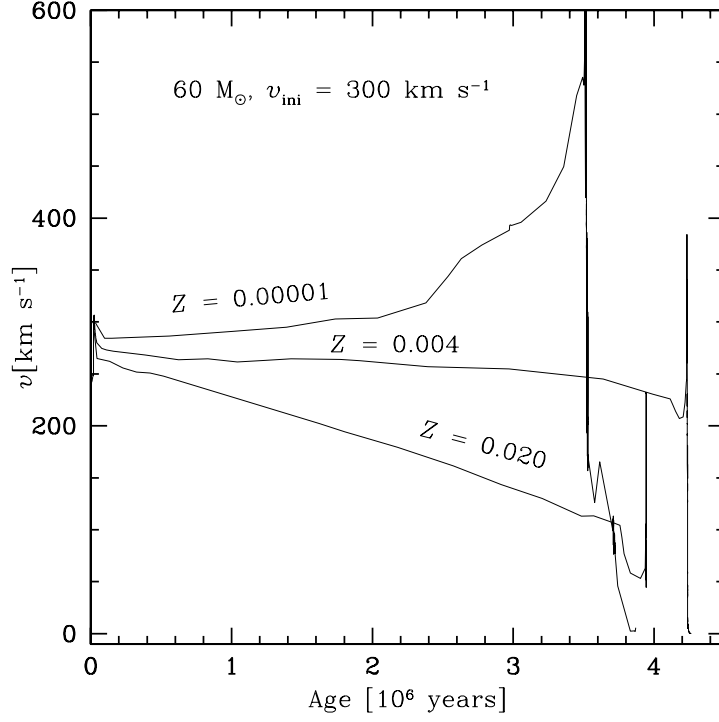


FIG. 15 Evolution of the surface equatorial velocity as a function of time for  $60 M_{\odot}$  stars with  $v_{\text{ini}} = 300 \text{ km s}^{-1}$  at different initial metallicities. Figure taken from Meynet & Maeder (2002a).

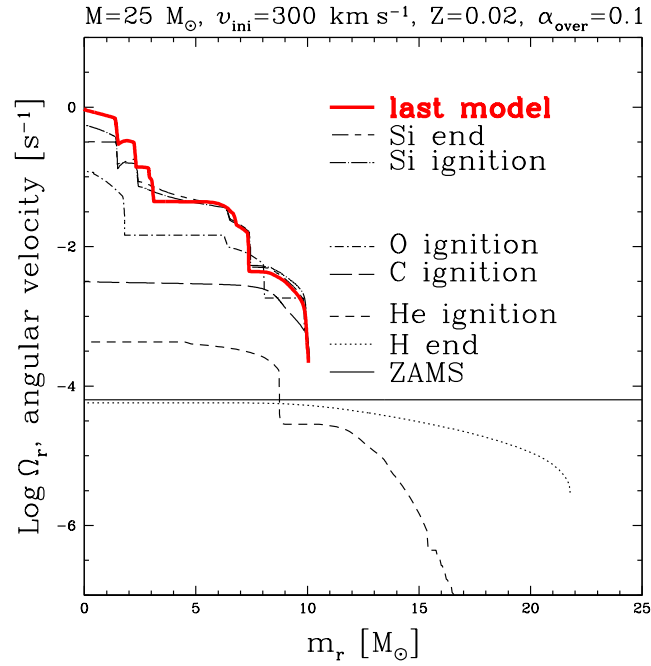


FIG. 16 Angular velocity as a function of the lagrangian mass coordinate,  $m_r$  inside the  $25 M_{\odot}$  model ( $v_{\text{ini}} = 300 \text{ km s}^{-1}$ ) at various evolutionary stages (Hirschi et al., 2004).

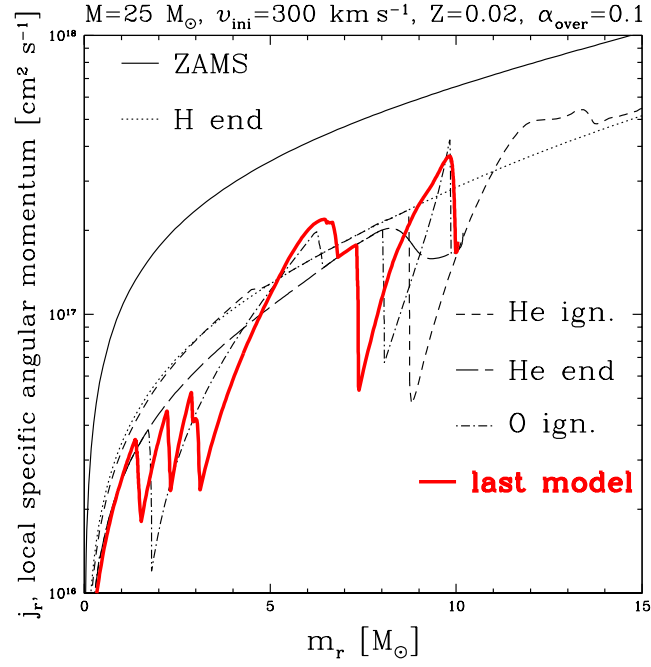


FIG. 17 Local specific angular momentum profiles for the  $25\ M_{\odot}$  model ( $v_{\text{ini}}=300\ \text{km s}^{-1}$ ) at different evolutionary stages (Hirschi et al., 2004).

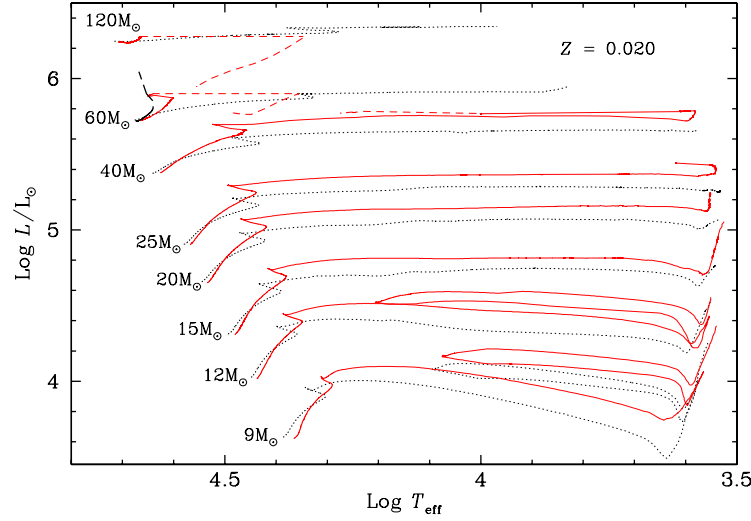


FIG. 18 Evolutionary tracks for non-rotating (dotted lines) and rotating (continuous lines) models with solar metallicity. The rotating models have an initial velocity  $v_{\text{ini}}$  of  $300\ \text{km s}^{-1}$ . For purpose of clarity, only the first part of the tracks for the most massive stars ( $M \geq 40\ M_{\odot}$ ) is shown. Portions of the evolution during the WR phase for the rotating massive stars are indicated by short-dashed lines. The long-dashed track for the  $60\ M_{\odot}$  model corresponds to a very fast rotating star ( $v_{\text{ini}} \sim 400\ \text{km s}^{-1}$ ), which follows a nearly homogeneous evolution. Only the beginning of its evolution is shown. Figure taken from Meynet & Maeder (2000).

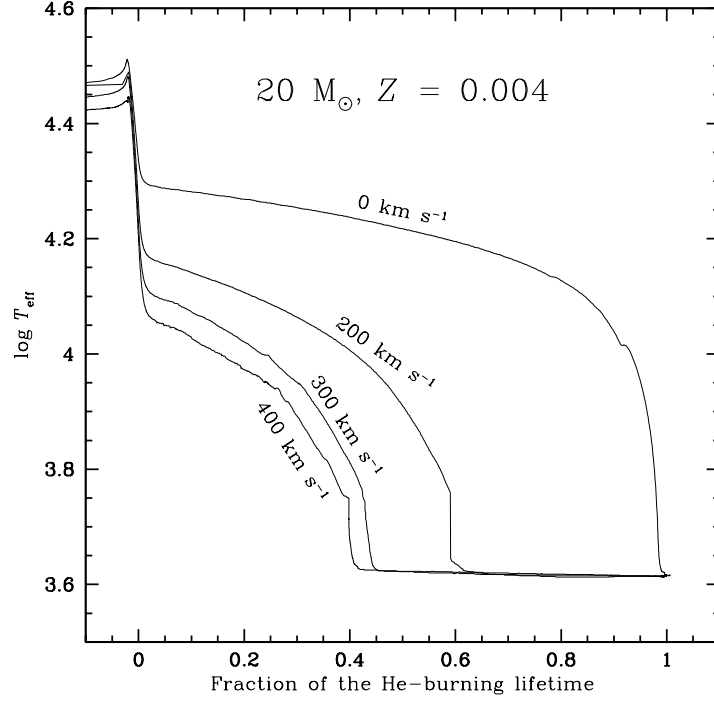


FIG. 19 Evolution of the  $T_{\text{eff}}$  as a function of the fraction of the lifetime spent in the He-burning phase for  $20 M_{\odot}$  stars with different initial velocities. Figure taken from Maeder & Meynet (2001b).

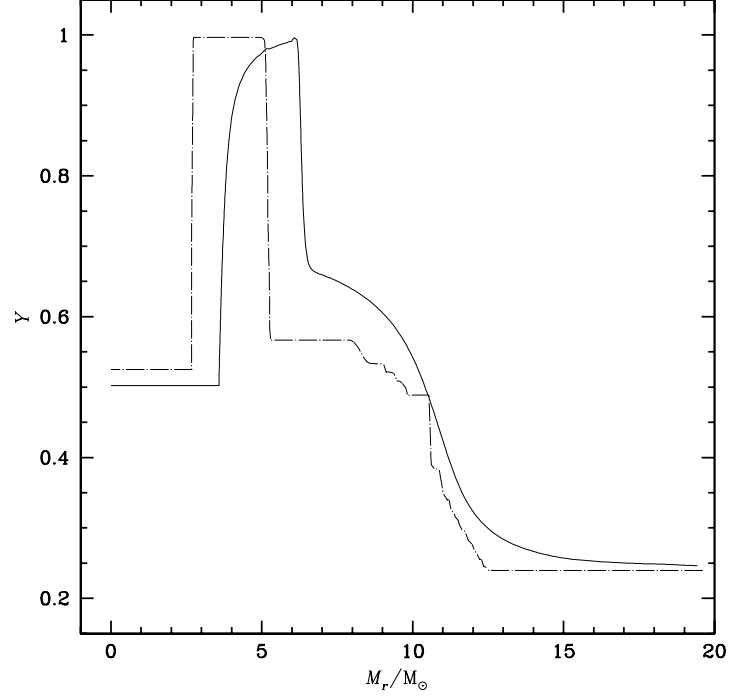


FIG. 20 Comparison of the internal distribution of helium in two models of  $20 M_{\odot}$  at the middle of the He-burning phase. The dashed-dot line concerns the models with zero rotation and the continuous line represents the case with  $v_{\text{ini}} = 300 \text{ km s}^{-1}$ . Figure taken from Maeder & Meynet (2001b).

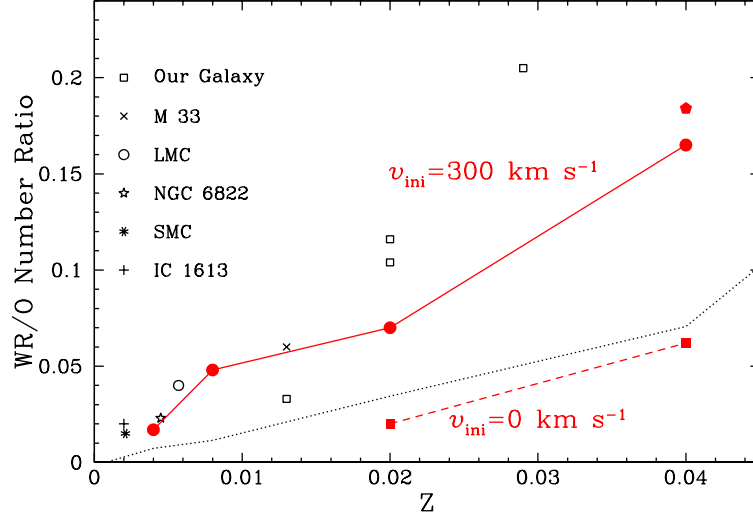


FIG. 21 Variation of the number ratios of Wolf-Rayet stars to O-type stars as a function of the metallicity. The observed points are taken as in Maeder & Meynet (1994). The dotted line shows the predictions of the models of Meynet et al. (1994) with normal mass loss rates. The continuous and the dashed lines show the predictions of the rotating and non-rotating stellar models respectively of Meynet & Maeder (2003, 2005). The black pentagon shows the ratio predicted by  $Z=0.040$  models computed with the metallicity dependence of the mass loss rates during the WR phase proposed by Crowther et al. (2002).

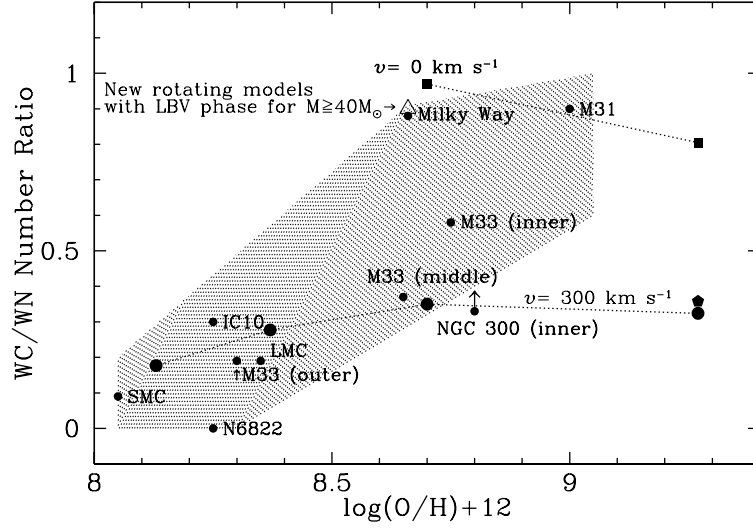


FIG. 22 Variation of the number ratios of WN to WC stars as a function of metallicity. The grey area encompasses the observed ratios. Individual measures are indicated by black circles labeled with the name of the Galaxy (see references in Meynet & Maeder, 2005). Solar (O/H) value is taken from Asplund et al. (2005), the (O/H) values for the SMC and LMC are taken from (Hunter et al., 2007). The dotted lines show the predictions of the rotating and non-rotating stellar models of Meynet & Maeder (2003, 2005). The black pentagon shows the ratio predicted by  $Z=0.040$  models computed with the metallicity dependence of the mass loss rates during the WR phase. The open triangle shows the WC/WN ratio obtained from the rotating models allowing an LBV phase during the WR phase (Meynet et al., 2008).



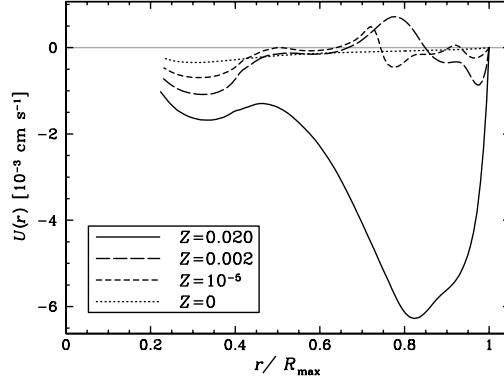


FIG. 23 Internal profile of  $U(r)$  in models of  $20 M_{\odot}$  at various metallicities, with  $\Omega_{\text{ini}}/\Omega_{\text{crit}} = 0.5$ , where  $u(r, \theta)$  the vertical component of the velocity of the meridional circulation is  $u(r, \theta) = U(r) P_2(\cos \theta)$  with  $P_2$  the second Legendre polynomial. The radius is normalized to the outer one. All the models are at the same evolutionary stage, when the central H mass fraction is about 0.40. Figures taken from Ekström et al. (2008a).

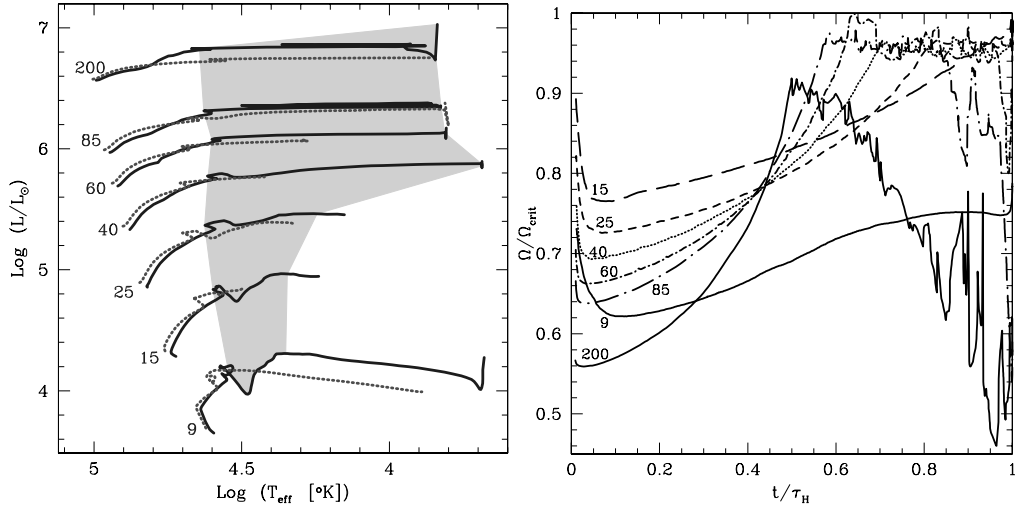


FIG. 24 *Left panels:* Evolution of  $Z = 0$  models (with rotation: continuous lines; without rotation: dotted lines) in the Hertzsprung Russell diagram. The grey area shows the zone of the diagram where He burns in the core of the rotating models. *Right panel:* Evolution of the  $\Omega/\Omega_{\text{crit}}$  ratio during the MS. All the models start the MS with  $v_{\text{eq}} = 800 \text{ km s}^{-1}$ , except the  $9 M_{\odot}$  which starts the MS with  $500 \text{ km s}^{-1}$ . Figures taken from Ekström et al. (2008a).

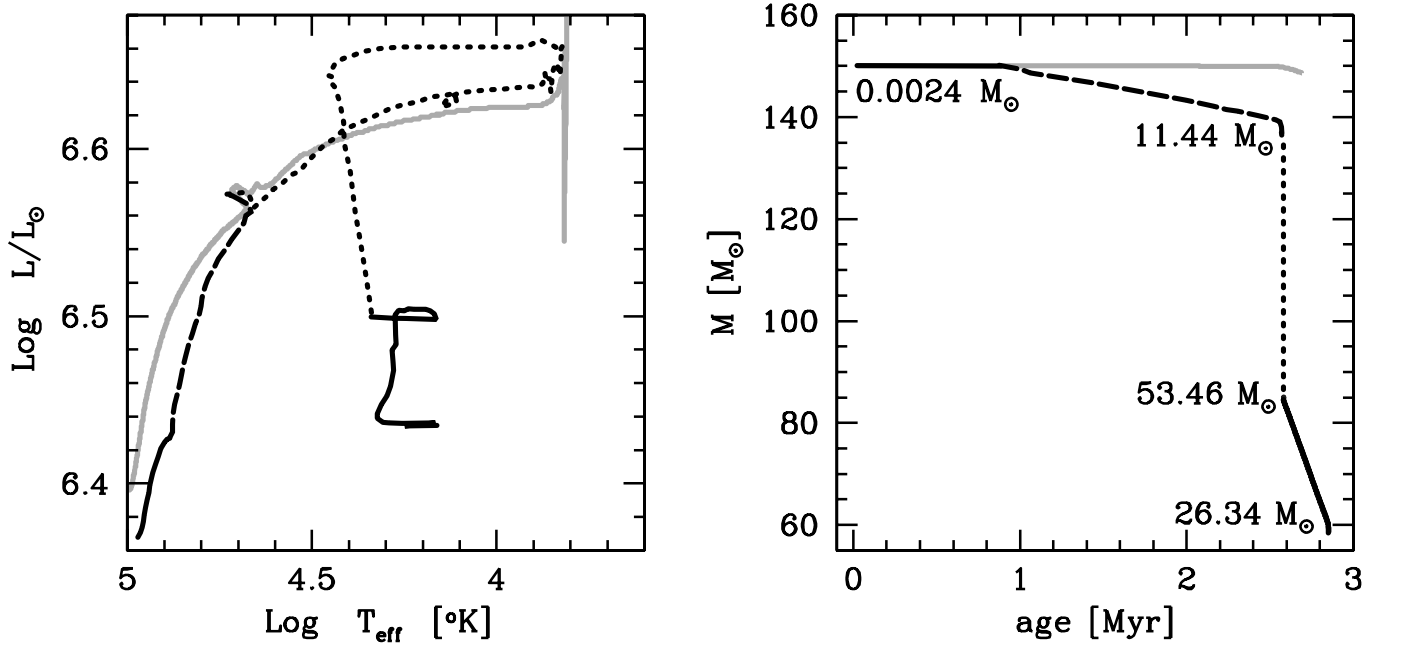


FIG. 25 *Left panel*: evolution in the Hertzsprung-Russell diagram; *Right panel*: evolution of the mass of the model. The mass indicated is the mass lost at each stage, not a summation. Black line: rotating model; *continuous part*: beginning of MS ( $X_c = 0.753$  down to 0.58; *dashed part*: rest of the MS; *dotted part*: beginning of core He-burning phase ( $Y_c = 1.00$  down to 0.96); *continuous part*: rest of the He-burning. Grey line: non-rotating model for comparison. Figures taken from Ekström et al. (2008a).

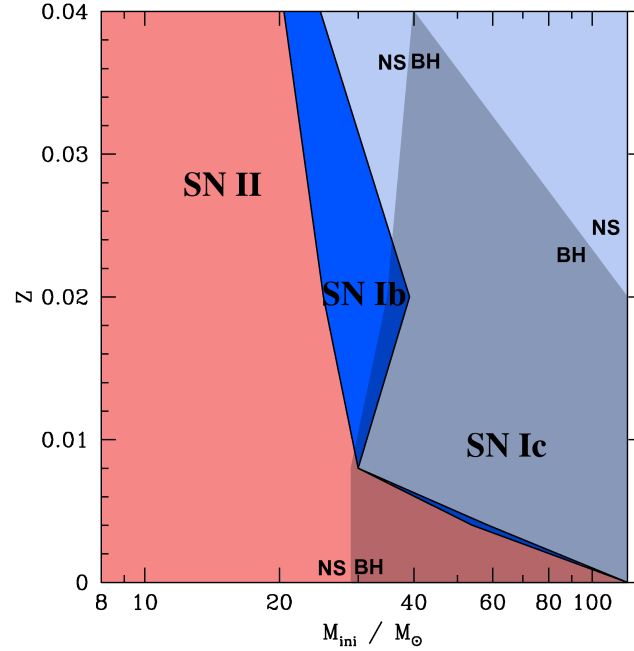


FIG. 26 Ranges of masses of different types of supernovae at different metallicities. The shading on the right indicates the area where formation of a black hole (BH) is expected; elsewhere, the remnant is a neutron star (NS). Figure taken from Georgy et al. (2009).

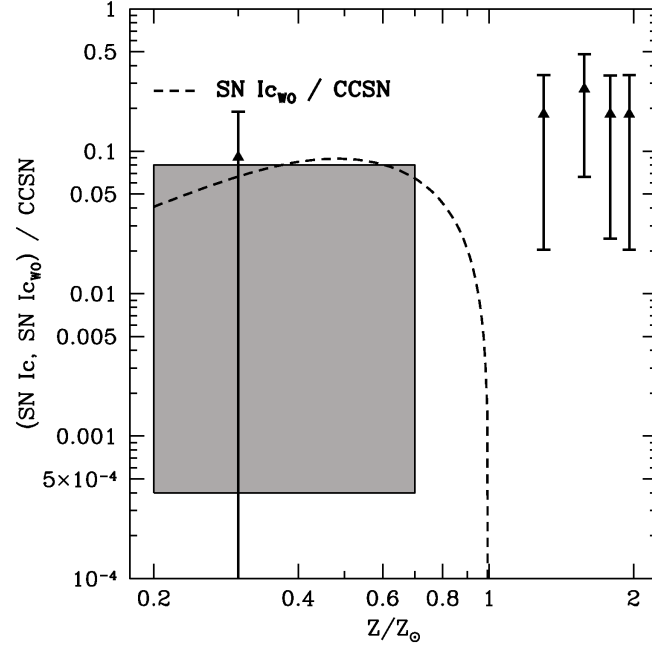


FIG. 27 Observed rate of type Ic SNe (triangles with error bars) and predicted rate of type Ic SNe whose progenitor is a WO star (dashed line) with respect to the total number of core collapse SNe (CCSN). The grey rectangle represents the extension in metallicity (Modjaz et al., 2008) and rate (Podsiadlowski et al., 2004) of GRB events. Figure taken from Georgy et al. (2009).

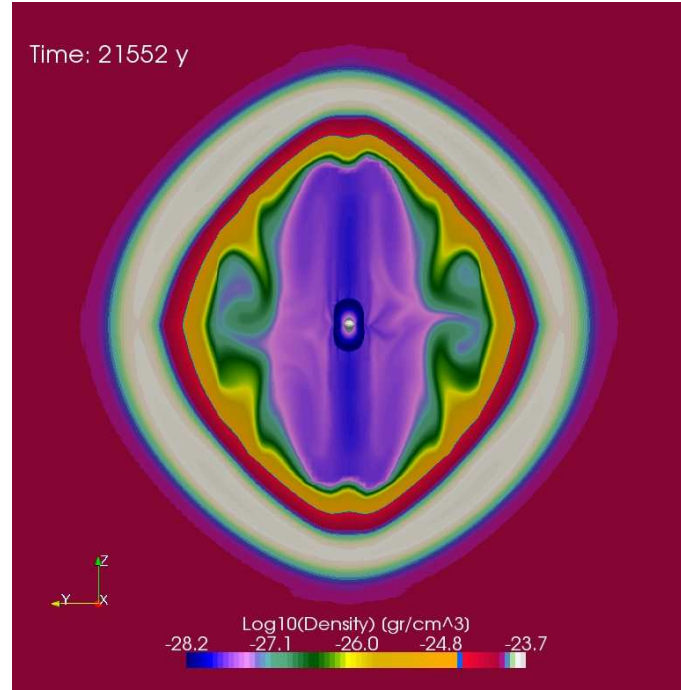


FIG. 28 Young bi-modal shaped nebula blown from the highly aspherical, polar dominated winds around a  $20 M_{\odot}$  star at  $Z = 10^{-5}$ . The star has evolved during 21552 yr since it has left the ZAMS. The maximal extension of the wind is  $\sim 1.5 \cdot 10^{18}$  cm. This model was computed by the A-Maze code (Walder & Folini, 2000). Figure taken from Georgy et al. (2009).

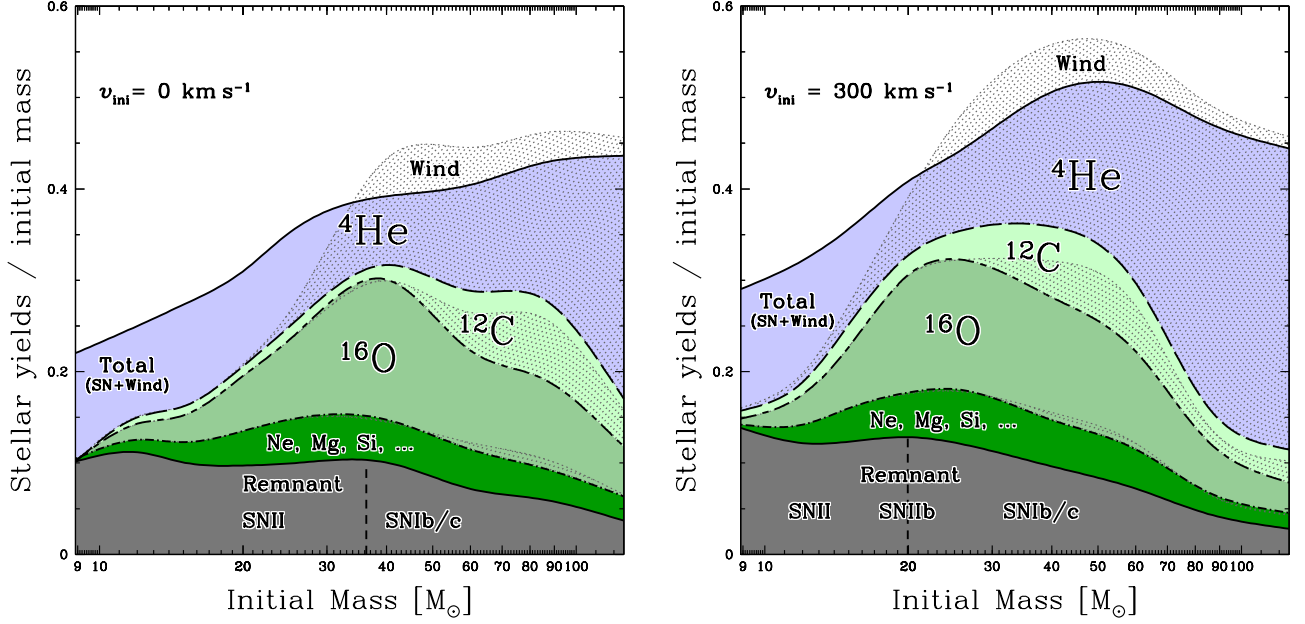


FIG. 29 Stellar yields divided by the initial mass,  $p_{im}^{\text{tot}}$ , as a function of the initial mass for the non-rotating (left) and rotating (right) models at solar metallicity. The different total yields (divided by  $m$ ) are shown as piled up on top of each other and are not overlapping.  $^4\text{He}$  yields are delimited by the top solid and long dashed lines (top shaded area),  $^{12}\text{C}$  yields by the long dashed and short-long dashed lines,  $^{16}\text{O}$  yields by the short-long dashed and dotted-dashed lines and the rest of metals by the dotted-dashed and bottom solid lines. The bottom solid line also represents the mass of the remnant ( $M_{\text{rem}}^{\text{int}}/m$ ). The corresponding SN explosion type is also given. The wind contributions are superimposed on these total yields for the same elements between their bottom limit and the dotted line above it. Dotted areas help quantify the fraction of the total yields due to winds. Note that for  $^4\text{He}$ , the total yields is smaller than the wind yields due to negative SN yields. Figure taken from Hirschi et al. (2005b).

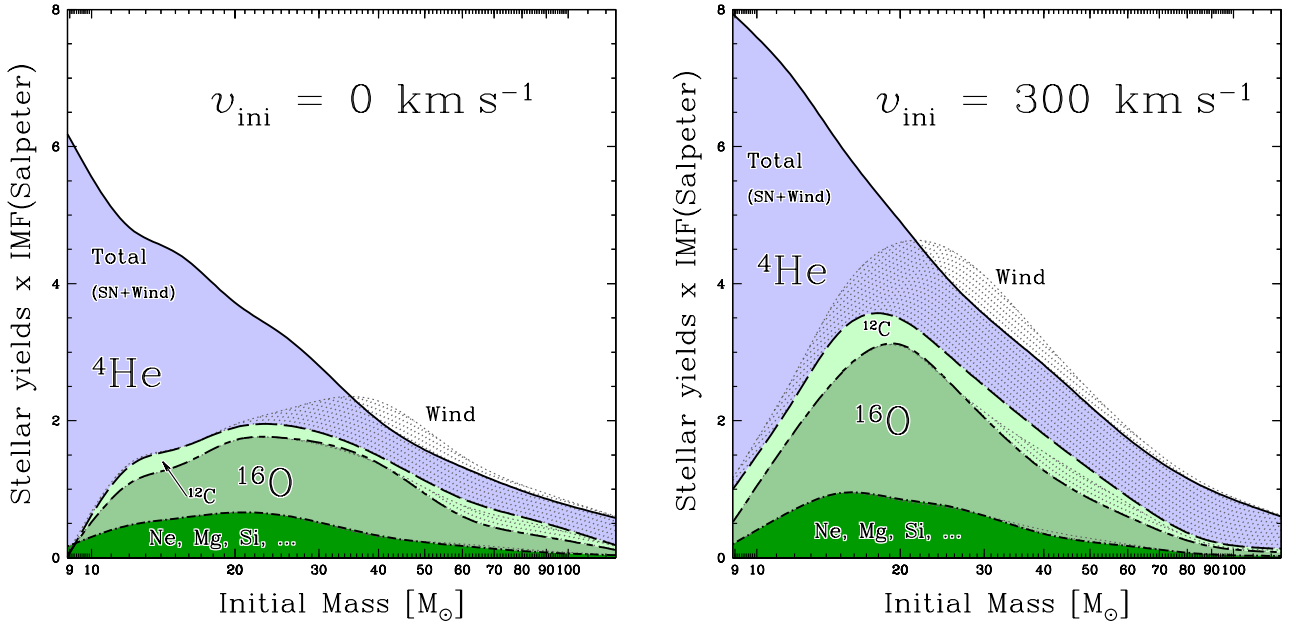


FIG. 30 Product of the stellar yields,  $mp_{im}^{\text{tot}}$  by Salpeter's IMF (multiplied by an arbitrary constant:  $1000 \times M^{-2.35}$ ), as a function of the initial mass for the non-rotating (left) and rotating (right) models at solar metallicity. The different shaded areas correspond from top to bottom to  $mp_{im}^{\text{tot}} \times 1000 \times M^{-2.35}$  for  $^4\text{He}$ ,  $^{12}\text{C}$ ,  $^{16}\text{O}$  and the rest of the heavy elements. The dotted areas show for  $^4\text{He}$ ,  $^{12}\text{C}$  and  $^{16}\text{O}$  the wind contribution. Figure taken from Hirschi et al. (2005b).

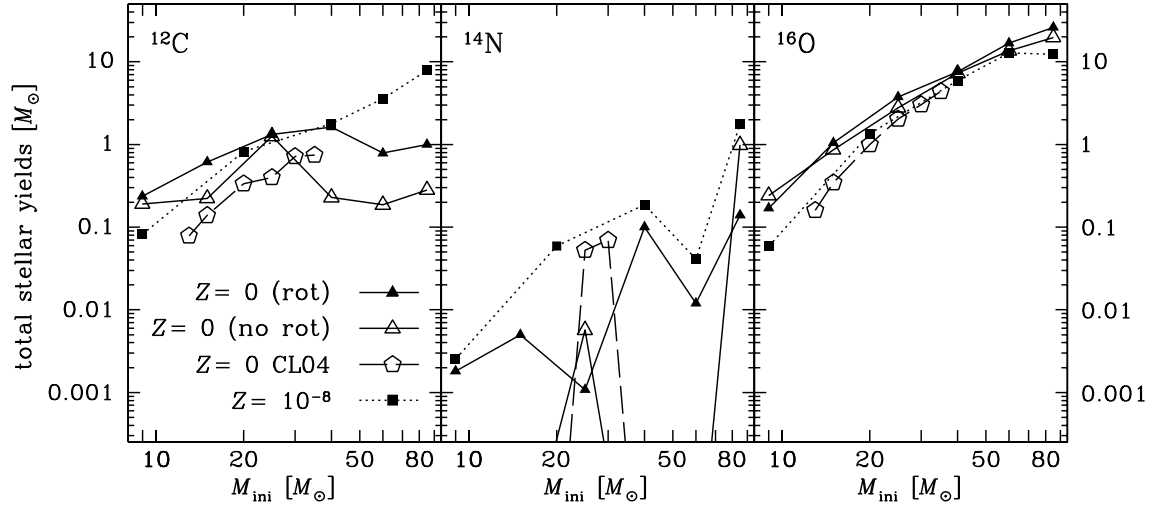


FIG. 31 Yields comparison between the non-rotating  $Z = 0$  models from Chieffi & Limongi (2004, CL04, open pentagons), the rotating  $Z = 10^{-8}$  models from Hirschi (2007, filled squares) and the rotating (filled triangles) and non-rotating (open triangles)  $Z = 0$  models from Ekström et al. (2008a). *Left:*  $^{12}\text{C}$ ; *centre:*  $^{14}\text{N}$ ; *right:*  $^{16}\text{O}$ . Figure taken from Ekström et al. (2008a).

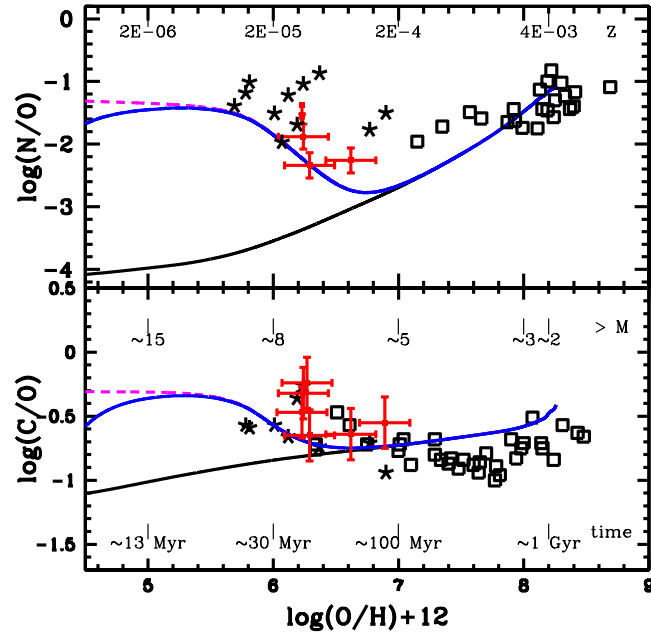


FIG. 32 Evolution of the N/O and C/O ratios. Data points for halo stars are from Israelian et al. (2004, open squares) and of Spite et al. (2005, stars). The points with error bars are for DLA systems from Pettini et al. (2008). The (black) continuous curve is the chemical evolution model obtained with the stellar yields of slow rotating  $Z = 10^{-5}$  models from Meynet & Maeder (2002a) and Hirschi et al. (2005b). The (magenta) dashed line includes the yields of fast rotating  $Z = 10^{-8}$  models from Hirschi (2007) at very low metallicity. The (blue) dotted curve is obtained using the yields of the  $Z = 0$  models presented in Ekström et al. (2008a) up to  $Z = 10^{-10}$ . The chemical evolution models are from Chiappini et al. (2006).

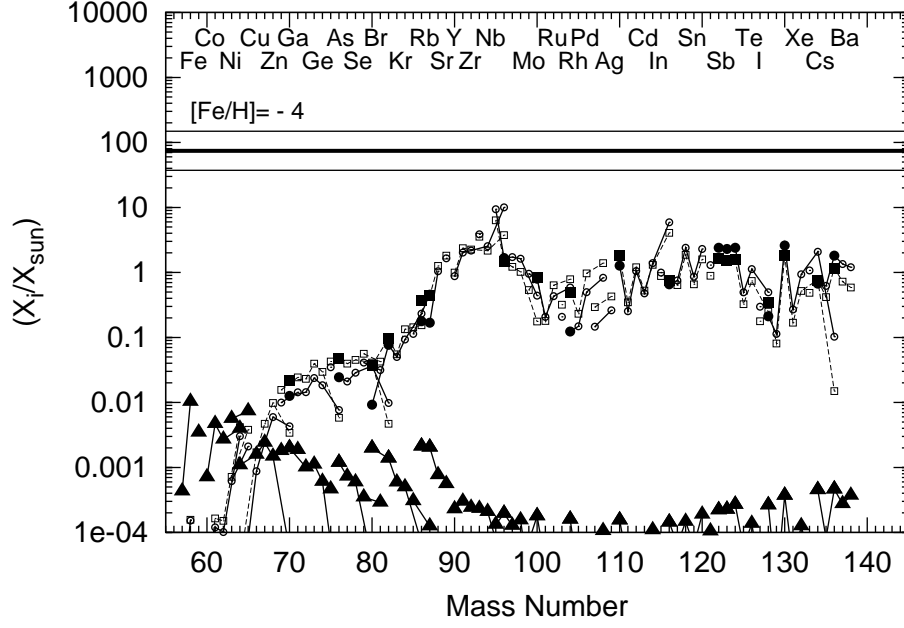


FIG. 33 s-process distributions between  $^{57}\text{Fe}$  and  $^{138}\text{Ba}$  normalized to solar for the  $25 M_{\odot}$  and  $[\text{Fe}/\text{H}]=-4$  at the end of the convective C-burning shell. The horizontal line corresponds to the  $^{16}\text{O}$  overabundance in the C shell (thick line), multiplied and divided by two (thin lines). Isotopes of the same element are connected by a line. The cases presented are the following: *i*) case without additional  $^{22}\text{Ne}$  (black triangles) and  $X(^{22}\text{Ne})_{\text{ini}} = 5.21 \times 10^{-5}$ ; *ii*) case with additional  $^{22}\text{Ne}$  (open squares, full squares for the s-only isotopes) and  $X(^{22}\text{Ne})_{\text{ini}} = 5.0 \times 10^{-3}$ ; *iii*) case with additional  $^{22}\text{Ne}$  (open circles, full circles for the s-only isotopes) and  $X(^{22}\text{Ne})_{\text{ini}} = 1.0 \times 10^{-2}$ . Figure from Pignatari et al. (2008).

## Tables

TABLE I Grids of rotating massive star models (starting from 2000).

Masses $M_{\odot}$	$Z$	Initial rotation km/s	Magnetic field (interior)	Ref.
9- 200	0	0-800	no	Ekström et al. (2008a)
3-60	0	39-1423	no	Ekström et al. (2008b)
9-85	0.00000001	800	no	Hirschi (2007)
2-60	0.00001	0-400	no	Meynet & Maeder (2002a)
20-60	0.00001	230-605	yes	Yoon & Langer (2005)
12-60	0.00001	0 - 936	yes	Yoon et al. (2006)
3-60	0.0001	39-1017	no	Ekström et al. (2008b)
20-200	0.0005	0-800	no	Decressin et al. (2007b)
20-60	0.001	230-605	yes	Yoon & Langer (2005)
12-60	0.001	0-747	yes	Yoon et al. (2006)
3-60	0.002	32-879	no	Ekström et al. (2008b)
12-60	0.002	0-653	yes	Yoon et al. (2006)
5-60	0.0021	0-600	yes	Brott et al. (2011)
9-60	0.004	0-300	no	Maeder & Meynet (2001b)
30-120	0.004	300	no	Meynet & Maeder (2005)
12-60	0.004	0-507	yes	Yoon et al. (2006)
5-60	0.0047	0-600	yes	Brott et al. (2011)

30-120	0.008	300	no	Meynet & Maeder (2005)
5-60	0.0088	0-600	yes	Brott et al. (2011)
8-25	0.020	0-474	no	Heger & Langer (2000)
8-25	0.020	200	no	Heger et al. (2000)
9-120	0.020	0-300	no	Meynet & Maeder (2000)
9-120	0.020	0-300-500	no	Meynet & Maeder (2003)
12-60	0.020	0-300	no	Hirschi et al. (2004)
12-35	0.020	200	yes & no	Heger et al. (2005)
16-40	0.020	210-556	yes	Yoon et al. (2006)
3-60	0.020	28-732	no	Ekström et al. (2008b)
20,25,40,60,85,120	0.040	0-300	no	Meynet & Maeder (2005)

TABLE II Values of the average and largest  $[N/H]$  excesses observed for different types of stars in the Galaxy, LMC and SMC. The number of stars used to obtain the quoted values are indicated as well the sources for the observations.

Types of stars	[N/H] in Galaxy				[N/H] in LMC				[N/H] in SMC			
	mean	max.	N <sub>*</sub>	Ref.	mean	max.	N <sub>*</sub>	Ref.	mean	max.	N <sub>*</sub>	Ref.
O stars	0.3-0.5	0.4-0.6	3	[1]					1.0-1.2	1.3-1.5	14	[8]
B dwarfs $M < 20 M_{\odot}$	0.2-0.4	0.5-0.7	22	[2,3,4,5]	0.3-0.5	0.9-1.1	35	[5]	0.5-0.8	1.3-1.5	34	[5]
B giants, super. $M < 20 M_{\odot}$	0.4-0.6	0.7-0.9	10	[5]	0.6-0.8	1.1-1.3	21	[5]				
B giants, super. $M > 20 M_{\odot}$	0.4-0.6	0.8-1.0	38	[6,7]								

[1] Villamariz & Herrero (2005); Villamariz et al. (2002)

[2] Gies & Lambert (1992)

[3] Kilian (1992)

[4] Morel et al. (2008)

[5] Hunter et al. (2009)

[6,7] Crowther et al. (2006); Searle et al. (2008)

[8] Heap et al. (2006)